



Pilkington Library

Author/Filing Title LOVELADY

.....

Vol. No. Class Mark T

**Please note that fines are charged on ALL
overdue items.**

FOR REFERENCE ONLY

0402589629



**Materials Jetting for Advanced Optoelectronic
Interconnect : Technologies and Application**

by

Michael J Lovelady


A Master's Thesis

Submitted in partial fulfilment of the requirements for the award of

Master of Philosophy of Loughborough University

January 2001

© Michael J Lovelady (January 2001)

 Loughborough University P... Library
Date <i>Aug 02</i>
Class
Acc No. <i>040258962</i>

Abstract

This report covers the work carried out on Teaching Company Scheme No. 2275 “Materials Jetting for Advanced Interconnect ” between February 1998 and February 2000. The project was conducted at the Harlow laboratories of Nortel Networks with the support of the Department of Manufacturing Engineering of Loughborough University. Technical direction and supervision has been provided by Mr Paul Conway, Reader, at Loughborough University, Professor Ken Snowdon and Mr Chris Tanner of Nortel Networks.

The aim of the project was to produce and deposit minute and precise volumes of a range of materials, such as metallic alloys, glasses and polymers, onto a variety of substrates commonly used in the electronics and optoelectronics fields. The technology, which is analogous to ink-jet printing, firstly had to be refined to accommodate higher processing temperatures of up to 350°C. The ultimate project deliverable was to produce a specification for jetting equipment suited towards volume manufacturing.

The project was based around the technique of Continuous Mode Jetting licensed from the Massachusetts Institute of Technology (MIT). The equipment was transferred to Harlow and was subsequently re-designed, upgraded and refined to produce a series of lead-free solder spheres from 100 to 1000 microns in diameter. Lead-free interconnect is likely to be necessary to meet draft environmental legislation being prepared in Europe and possibly Japan.

Experience of jetting technology also enabled a second mode of application, the drop-on-demand variant to be investigated via collaboration with the US company Microfab. This enabled both a world first in the deposition of a lead-free tin-copper solder pre-form and the investigation of the potential for optoelectronic applications of polymeric lenses on fibres and adhesives dispensing. Volumes as small as 50 picolitres can be dispensed rapidly and repeatably using this equipment. This work

has lead to the ordering of a drop-on-demand machine for further exploitation in optoelectronic automation within Nortel Networks.

The performance of lead-free solder and adhesives deposition illustrate the potential for drop on demand printing to be included in the production environment in the near future. Further testing of real applications and problems in manufacturing will allow for specific devices and solutions to be identified and novel ones being developed to enable this disruptive technology solution.

Table of Contents

<i>Abstract</i>	<i>iii</i>
<i>Definitions and Abbreviations</i>	<i>viii</i>
<i>List of Figures</i>	<i>xii</i>
<i>List of Tables</i>	<i>xvii</i>
<u>1 Introduction</u>	<i>1</i>
<u>1.1 Background and Technology</u>	<i>1</i>
<u>1.2 Continuous-mode materials jetting</u>	<i>2</i>
<u>1.3 Drop-on-demand mode materials jetting</u>	<i>4</i>
<u>1.4 Technological issues</u>	<i>5</i>
<u>1.5 Applications in electronics manufacturing</u>	<i>7</i>
<u>1.6 Optoelectronic applications</u>	<i>12</i>
<u>2 Physics and Hardware</u>	<i>20</i>
<u>2.1 Droplet Formation</u>	<i>20</i>
<u>2.1.1 Droplet size</u>	<i>22</i>
<u>2.1.2 Charging and deflection</u>	<i>25</i>
<u>2.2 On demand droplet formation</u>	<i>30</i>
<u>2.2.1 Drive waveform</u>	<i>32</i>
<u>2.2.2 Fluid properties</u>	<i>32</i>
<u>2.3 Modelling</u>	<i>34</i>
<u>2.4 Case studies</u>	<i>40</i>
<u>2.4.1 MIT Droplet-based Manufacturing Group</u>	<i>40</i>
<u>2.4.2 Experimental procedure</u>	<i>45</i>

2.4.3	<u>Microfab Technologies Inc</u>	47
2.4.4	<u>Gas Subsystem</u>	51
2.4.5	<u>Motion System</u>	51
3	<u>Process Development 1 - Software</u>	54
3.1	<u>MIT Software</u>	54
3.2	<u>Software development</u>	57
3.3	<u>Histogram Method of Droplet Size Measurement</u>	59
3.3.1	<u>Droplet-to-space ratio measurement method</u>	64
3.3.2	<u>Droplet volume control thread</u>	67
3.3.3	<u>Gas flow sensitivity</u>	75
3.4	<u>Substrate motion control</u>	81
3.4.1	<u>Manual Control</u>	84
3.5	<u>Description of Ancillary Controllers</u>	84
3.6	<u>Alternate droplet detection and measurement</u>	86
4	<u>Process Development 2 - Hardware Development and Test</u>	90
4.1	<u>Orifice redesign</u>	91
4.1.1	<u>Orifice pre-mounted in a component</u>	94
4.1.2	<u>Laser-machined holes</u>	95
4.2	<u>Lead Free Solder Sphere Production</u>	101
4.2.1	<u>Other Orifice Samples</u>	103
4.3	<u>Stream control</u>	103
5	<u>Optoelectronic Demonstrators</u>	110
5.1	<u>What Materials Jetting has to offer</u>	111
5.2	<u>Adhesives</u>	114
5.3	<u>Pre-form replacement</u>	116
5.4	<u>Passive optical components</u>	123
5.4.1	<u>Design issues</u>	123

<u>5.4.2</u>	<u><i>Lens on single-mode fibre for beam collimation</i></u>	<i>132</i>
<u>5.4.3</u>	<u><i>Lens on collar</i></u>	<i>133</i>
<u>5.4.4</u>	<u><i>Collar evolution</i></u>	<i>137</i>
<u>5.4.5</u>	<u><i>Lens on glass slide</i></u>	<i>142</i>
<u>5.4.6</u>	<u><i>Lens array characterisation</i></u>	<i>145</i>
<u>5.4.7</u>	<u><i>Microscope measurements of focal length</i></u>	<i>146</i>
<u>5.4.8</u>	<u><i>Interferometry measurements of curvature</i></u>	<i>147</i>
<u>5.5</u>	<u><i>Further Drop on Demand Work</i></u>	<i>148</i>
<u>6</u>	<u><i>Discussion and Specifications</i></u>	<i>151</i>
<u>7</u>	<u><i>Acknowledgements</i></u>	<i>154</i>
<u>8</u>	<u><i>References</i></u>	<i>155</i>
<u>9</u>	<u><i>Appendix 1 - Listing A</i></u>	<i>159</i>
<u>10</u>	<u><i>Appendix 2 - Listing B</i></u>	<i>163</i>
<u>11</u>	<u><i>Appendix 3 – Lenslet arrays data</i></u>	<i>166</i>
<u>12</u>	<u><i>Appendix 4 – Interferometer Images</i></u>	<i>167</i>

Definitions and Abbreviations

λ	<i>Wavelength</i>
ρ	<i>Fluid density (Kg/m³)</i>
τ	<i>Characteristic time (in seconds)</i>
σ	<i>Surface tension (dy/cm)</i>
Z	<i>Propagation distance (in metres)</i>
δ	<i>Displacement in direction of the field</i>
π	<i>Pi (i.e. 3.1412927)</i>
ϵ_0	<i>Permittivity of free space (Fm⁻¹)</i>
δ_{camera}	<i>Linear factor to convert number of pixels on screen to a real distance in metres.</i>
\varnothing_d	<i>Droplet diameter (in metres)</i>
\varnothing_0	<i>Orifice diameter (in metres)</i>
Δp	<i>Pressure difference</i>
δ_{sol}	<i>Solidification ratio</i>
a_i	<i>Amplitude of instability</i>
A	<i>Acceleration</i>
A_0	<i>Initial disturbance in the radius of the column</i>
AEA	<i>Atomic Energy Authority</i>
$AGRIN$	<i>Axial gradient index of refraction</i>
API	<i>Application programming interface</i>
BGA	<i>Ball grid array</i>
C	<i>Change in amount of voltage (with respect to the droplet size control software)</i>
CAD	<i>Computer aided design</i>
CCD	<i>Charge-coupled device</i>
$CCIR$	<i>International Radio Consultative Committee; a predecessor organization of the <u>ITU-T</u></i>
$CCTV$	<i>Closed circuit Television</i>
CDU	<i>Compact detecting unit</i>

<i>CMMJ</i>	<i>Continuous-mode materials jetting</i>
<i>C_{noz}</i>	<i>Discharge coefficient of nozzle</i>
<i>COM</i>	<i>Communications (serial port on a PC)</i>
<i>cp, cps, or</i>	<i>Centipoise (viscosity)</i>
<i>cPs</i>	
<i>CPU</i>	<i>Central processing unit</i>
<i>CSP</i>	<i>Chip scale package</i>
<i>d</i>	<i>Separation distance between parallel deflection plates (in metres)</i>
<i>DBM</i>	<i>Droplet based manufacturing</i>
<i>d_c</i>	<i>Diameter of circular electrode (in metres)</i>
<i>DC</i>	<i>Direct current</i>
<i>DCA</i>	<i>Direct chip attach</i>
<i>DFT</i>	<i>Discrete Fourier transform</i>
<i>DI</i>	<i>De-Ionised</i>
<i>DODJ</i>	<i>Drop-on-demand mode materials jetting</i>
<i>DWDM</i>	<i>Dense wave division multiplexing</i>
<i>DXF</i>	<i>Drawing exchange format</i>
<i>dy/cm</i>	<i>Dynes/centimetre (surface tension)</i>
<i>E</i>	<i>Electric field strength</i>
<i>e</i>	<i>Error in ball to space ratio (with respect to the droplet size control software)</i>
<i>EU</i>	<i>European Union</i>
<i>f</i>	<i>Frequency of perturbation</i>
<i>F</i>	<i>Force</i>
<i>FBGA</i>	<i>Fine pitch ball grid array</i>
<i>FFT</i>	<i>Fast Fourier transform</i>
<i>f-number</i>	<i>= (Focal length / diameter)</i>
<i>FR4</i>	<i>Fire retardant type 4 (glass epoxy laminate commonly used as PCB material)</i>
<i>Gb/s</i>	<i>Giga-bits per second</i>
<i>GRIN</i>	<i>Graded index (lens)</i>
<i>GUI</i>	<i>Graphical user interface</i>

HASL	<i>Hot air solder levelling</i>
HD-PUG	<i>High density packaging user group</i>
I/O	<i>Input/Output</i>
IPA	<i>Iso-Propyl Alcohol</i>
k_p	<i>Constant of proportionality (with respect to the droplet size control software)</i>
LAN	<i>Local area network</i>
l_d	<i>Length of electric field (in metres)</i>
m	<i>Mass</i>
MDSP	<i>Magneto dynamic solder pump</i>
MDT	<i>Materials Design Technology</i>
MIT	<i>Massachusetts Institute of Technology</i>
MPM	<i>{abbreviation not known} name of the company making continuous mode equipment</i>
NA	<i>Numerical Aperture</i>
nl	<i>nanolitre (volume)</i>
NPL	<i>National Physics Laboratory</i>
n_r	<i>Refractive index</i>
NSPAN	<i>Nortel Subsystems and Performance Networks</i>
NTT	<i>Nippon Telegraph and Telephone</i>
p.s.i.	<i>Pounds per square inch (pressure)</i>
PCB	<i>Printed circuit board (see also PWB)</i>
pl	<i>picolitre (volume)</i>
ppm	<i>Parts per million</i>
PWB	<i>Printed wiring board (see also PCB)</i>
PZT	<i>Lead zirconium titanate</i>
Q_d	<i>Charge on a droplet</i>
R&D	<i>Research and development</i>
R_{ds}	<i>Ratio of droplet to space</i>
RIE	<i>Reactive ion etching</i>
ROI	<i>Region of Interest</i>
SDH	<i>Synchronous digital hierarchy</i>

SEM	<i>Scanning electron microscope</i>
SONET	<i>Synchronous optical NETwork</i>
t	<i>Time</i>
TCA	<i>Teaching Company Associate</i>
TCD	<i>Teaching Company Directorate</i>
TDM	<i>Time division multiplexing</i>
UBM	<i>Under bump metallisation</i>
UDS	<i>Uniform droplet spray</i>
UK	<i>United Kingdom</i>
UV	<i>Ultra-violet</i>
v	<i>Velocity</i>
V_{ch}	<i>Potential difference on charging plates</i>
V_d	<i>Potential difference between deflection plates</i>
V_j	<i>Jet velocity</i>
WEEE	<i>Waste Electrical and Electronic Equipment (EU draft directive)</i>
x	<i>Distance traveled at a velocity (v)</i>

List of Figures

- 1 *Equipment configuration for continuous mode materials jetting*
- 2 *Schematic for ‘drop-on-demand’ mode materials jetting*
- 3 *Photographs illustrating effect that substrate temperature has on tin/lead solder droplets during impact, 95°C (top left) to 126°C (bottom right) [after MPM]*
- 4 *Eutectic tin/lead solder bumps deposited onto metallised silicon [after MPM]*
- 5 *60µm diameter bumps of tin/lead solder deposited onto 100µm diameter pads, metal system number 2*
- 6 *Photograph showing deflection of a continuous stream of balls [7]*
- 7 *Comparison of different solder deposition with respect to achievable pitch*
- 8 *A – 300µm core diameter optical fibres with microjet printed lenslets (after Cox et al.)*
B - Array of 100µm diameter hemispherical plano-convex microlenses (after Cox et al.)
C - 25mm long (1-16) branch waveguide, made with 116µm x 35µm hemi-cylindrical ridge waveguides (after Cox et al.)
- 9 *A - 4 hemi-elliptical microlenses - 284µm x 146µm x 20µm (after Cox et al)*
B - Array of 300µm square, 50µm high printed microlenses (after Cox et al)
- 10 *Variation of surface contact angle with substrate temperature with the deposition of optical thermo-plastic (after Cox et al.)*
- 11 *Mathematical approximation of uniform droplet generation from capillary instability*
- 12 *Charging and deflecting of droplets*
- 13 *Drop-on-demand mode droplet deposition*
- 14 *Bipolar Drive Waveform used to drive the Microfab drop on demand system*

15	<i>Simulation Control Variables Setup</i>
16	<i>Simulation Material Variables Setup</i>
17	<i>Simulation Output: Indication of point of solidification</i>
18	<i>Solidified 50 micron diameter solder microdroplet. Left: Experiment (Microfab), Right: Simulated</i>
19	<i>Continuous Mode Droplet Deposition</i>
20	<i>Schematic of Spray Forming Head (After Chun)</i>
21	<i>Droplet Formation Apparatus (After Chun)</i>
22	<i>Microfab Drop on Demand Mode Solder Micro Jetting Head</i>
23	<i>Microfab Micro Optic Jetting Device</i>
24	<i>Formation of Droplet with respect to Time and Drop on Demand Waveform</i>
25	<i>Jetting Device and Substrate Motion System for Optics Jet Station (Microfab Technologies)</i>
26	<i>MIT droplet detection uses blob analysis to find the centre to centre spacing of the droplets</i>
27	<i>MJT control software: process flow chart</i>
28	<i>Image of droplet stream</i>
29	<i>(inverse) 3D representation of the relative greyscale of the droplets</i>
30	<i>Histogram representation of the number of 'on' pixels due to presence of a droplet in an image after thresholding</i>
31	<i>Histogram representation of ROI relative gray-scale intensities</i>
32	<i>"Pixel to Real" Distance Conversion Dialog</i>
33	<i>Variation of disturbance amplitude with frequency</i>
34	<i>Effect of altering pressure on water droplets issued through a 400μm orifice, using a constant perturbation frequency of 1500Hz; a) at low pressure; b) at high pressure</i>
35	<i>Digitised Image of the Stream showing software location of stream</i>
36	<i>Setting the target ball space ratio</i>
37	<i>Image Analysis Metrics Display</i>
38	<i>Illustration of the droplet diameter length and space values in a uniform stream</i>

- 39 *Droplet volume with respect to the ratio of droplet to space due to increasing jet velocity*
- 40 *Main Control Dialog*
- 41 *Open Loop Pressure Control*
- 42 *Proportional Control of Control Valve*
- 43 *Closed Loop Pressure Control (After MKS Instruments)*
- 44 *Conversion from DXF CAD file to 6200 path data*
- 45 *Using the MJT Control software to download path data to XY table hardware*
- 46 *Manual XY table control dialog*
- 47 *Method of focussing the laser beam using diverging lenses (after Watts)*
- 48 *Overview of proposed closed-loop feedback mechanism (after Watts)*
- 49 *Illustration of the MIT mounting method using Bird Precision sapphire orifice*
- 50 *Non - catastrophic failure of the cement holding the sapphire orifice*
- 51 *Result of catastrophic failure of the cement holding the sapphire orifice*
- 52 *Alternate methods for orifice mounting*
- 53 *Orifice pre-mounted in bolt screwed into crucible*
- 54 *Metal orifice plate - mounting concept*
- 55 *Tungsten plate with spark eroded recess for laser drilling of orifice*
- 56 *Laser drilled holes in Tungsten plate*
- 57 *New laser drilled orifice with temporary charging plate design after stream directional variation causes build up of solder*
- 58 *Build up of solder at various points at the gasket / plate interface*
- 59 *SnSb6Cu3 solder balls (x40 mag.)*
- 60 *Cross Section of SnSb6Cu3 solder ball – note the petal-like material structure*
- 61 *Excimer ablated hole and non uniform break-up of stream*
- 62 *UCI adjustable head design*
- 63 *Branch adjustment of focusing and deflection plates*

- 64 *Adjustable mounting of jetting head*
- 65 *Current Nortel equipment with adjustable head and rotating 'branches'*
- 66 *Nortel laboratory set-up*
- 67 *Example configuration for a transmitting laser module*
- 68 *Detail from 370x125 array of 60 micron droplets on 200 micron centres*
- 69 *Filtration method in preparing solders for jetting*
- 70 *Array of Multicore lead-free (SnCu) solder on metallised Si wafer*
- 71 *Detail of Multicore lead-free solder on metallised Si wafer*
- 72 *Detail of Multicore lead-free solder on metallised Si wafer*
- 73 *Nortel Networks 980nm laser pump module case. Position of solder pre-form placement indicated by grey region in the lower recess*
- 74 *Eutectic SnCu solder deposited onto 980nm pump package gold substrate*
- 75 *Beam propagation from the end of a single mode fibre*
- 76 *Polymer lenses printed directly onto multimode fibres, of diameter 140 μ m*
- 77 *MRX-110 Polymer lenses printed on 8-strand Nortel Networks single mode fibre ribbon*
- 78 *End view of single mode fibre having printed lens with 3 droplets*
- 79 *Modelled optical system for deposition into glass collar / fibre arrangement*
- 80 *Relationship between amount of deposited droplets and lens radius of curvature*
- 81 *Design iterations of glass collar. Red cone indicating the expansion of the beam from the fibre*
- 82 *a) Initial trials using a collar on the fibre led to air being trapped between the fibre and the polymer. b) A recessed collar (unfilled) to allow for divergence of the beam*
- 83 *Optimum design of glass collar, for ease of machining, beam divergence and droplet deposition*

- 84 *1:3 aspect ratio lens, MRX110 polymer deposited on glass collar*
- 85 *Schematic of 8 channel MEMS switch currently in development*
- 86 *3 (of 8) 1:8 aspect ratio lens printed on boron silicate optical flat*
- 87 *Sapphire sphere reference wave*
- 88 *Transmitted wave fronts using white light illumination across entire aperture of the lens*

List of Tables

1	<i>Tin/lead solder adhered to these metal systems ('Adh' – Adhesion layer)</i>
2	<i>Information on material thickness, orifice diameter</i>
3	<i>Lead-free alloys identified for potential use in electronic products</i>
4	<i>Measurement of centre-centre distance, diameter and roundness of lenses printed on glass slide</i>
5	<i>Focal length error, in microns above rear surface of optical flat, for 8x1 lens array</i>
6	<i>Radius of curvature measurements for each lens in array</i>

1 Introduction

Nortel Networks is a global, multi-national supplier of telecommunications equipment with a turnover of \$23 billion, employing approximately 80,000 people worldwide of which over 7,000 are actively working in the UK. The Harlow laboratories are the home of NSPAN (Nortel Sub-systems and Performance Networks), an integrated division of Carrier Packet Networks, which carries out research and development for the next generation telecommunications products. Key to the successful production of new equipment is the deployment of advanced materials and processes capable of mass production, highly accurate placements and novel physical properties. Materials jetting was identified in 1996-7 by the staff of Materials Design and Technology (MDT) as one of the potential key enabling technologies for future products.

This report covers the work carried out on Teaching Company Scheme (TCS) No. 2275 "Materials Jetting for Advanced Interconnect", between February 1998 and February 2000. The project was undertaken at the Nortel Networks laboratories in Harlow, Essex. Technical direction and supervision has been provided by Mr Paul Conway, Reader at Loughborough University and Professor Ken Snowdon and Mr Chris Tanner of Nortel Networks.

1.1 Background and Technology

Analogous to ink jet printing, the Materials Jetting Technology (MJT) can be used to accurately produce and deposit repeatable quantities of molten material. Some of the following areas were identified as technologies, which could benefit from this work - solder deposition for advanced interconnection and packaging; solder ball production for ball grid array (BGA) and chip scale package (CSP) products; Optical polymer deposition for optical interconnect and micro-lens arrays and UV curing adhesive deposition for optical component fixing.

The basic concept of high temperature materials jetting has been expanded from the work on ink-jet printers in the late 1980's [1, 2]. The major challenge in modifying the equipment for materials that are not liquid at room temperature is accommodating the increased processing temperatures and controlling the material properties during flight to the deposition site. The initial work was predominately laboratory demonstrators dealing with low melting temperature indium based solder alloys, which focused on the separation of the material into a uniform droplet stream [3,4]. More recently, efforts have concentrated on the behaviour of the stream [5], modelling of droplet solidification [6] and controlling precise material deposition [7].

The technique for producing minute quantities of molten material can be separated into two distinct technologies; continuous-mode materials jetting (CMMJ); and drop-on-demand mode materials jetting (DODJ).

1.2 Continuous-mode materials jetting

This technology, figure 1, utilises the natural break up of a stream forced through an orifice as described mathematically by Lord Rayleigh in 1878 [8]. The stream break-up is made uniform by mechanically inducing a vibration in the material reservoir (near the natural drop forming frequency of the jet), causing pressure oscillations to propagate through the fluid [9]. The mechanical vibrations are produced using piezoelectric crystals, producing a continuous stream of droplets at rates of between 5,000 and 20,000 Hz, demonstrated by Chun at the Massachusetts Institute of Technology (MIT). Rick Godin, of the Speedline MPM Corporation, has quoted that continuous mode droplet formation can occur at rates of up to 44,000 Hz, also using a piezoelectric transducer to excite the liquid [10]. CMMJ nominally produces ball sizes that are approximately twice the orifice diameter, which can be altered slightly with driving pressure and vibration frequency. A closed loop feedback system has been set up at MIT, utilising this property, and is aimed at controlling sphere size for BGA components. Tolerances within +/- 3% of a target droplet diameter (for 850µm tin/lead spheres) have been demonstrated by varying the driving frequency [11].

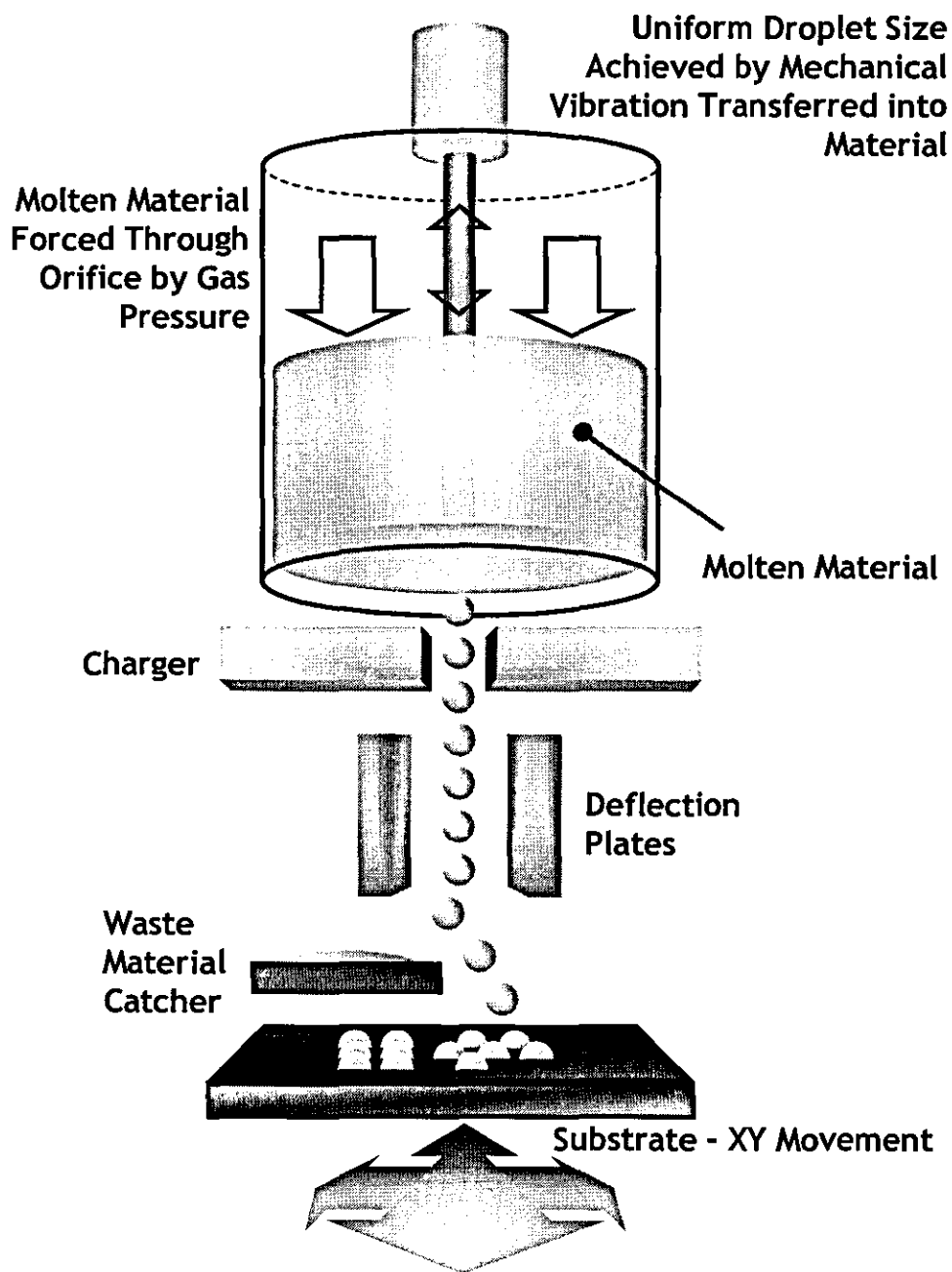


Figure 1 – Equipment configuration for continuous mode materials jetting

Charging plates surround the region where the stream breaks up, to induce a charge on the surface of each droplet. The main reason for charging the droplets is to prevent the stream from merging, however it has also been found that a constant spatial distance is upheld during flight.

Without intervention, all the droplets would impinge on the target. In most applications, the amount of droplets required to reach the desired location is quite low. Therefore, most of the stream must be prevented from reaching the target. This can be achieved by charging individual droplets and either:

- Removing them from the stream using a catching device; or
- Deflecting towards a substrate, using an electrostatic deflection field, and collecting the remaining droplets.

The incorporation of charging and deflection in continuous mode systems means that the distance needed for the material to reach its desired characteristics can be tens of centimetres, which provides a challenge in controlling the droplets during their flight. Figure 1 illustrates the principle of droplet deposition behind the continuous mode system adopted by the MPM Corporation [12]. MPM combined electrostatic droplet deflection in the Y-axis and substrate motion in the X-axis to deposit patterns of solder. A number of these jetting platforms were sold and distributed through Speedline Technologies worldwide, but in 1999 MPM stopped funding the materials jetting programme and ceased production of the jetting machines.

1.3 Drop-on-demand mode materials jetting

Drop-on-demand mode materials jetting, as the name suggests, produces individual droplets of material on demand, as presented in figure 2. Each droplet is produced by the displacement of a transducer coupled to the crucible, inducing a volumetric change in the liquid. The volumetric change causes pressure/velocity transients to occur in the fluid, causing a droplet to be issued from the crucible orifice [13]. Hansell first noted this technique for generating droplets in 1950 [46]. The energy required to

individually dispense particles on demand is larger than is required to break up a continuous stream, because the entire fluid column is disturbed.

The drop on demand jetting (DODJ) technology can produce ball diameters from 125 μm down to 25 μm [3]. This is due to the fact that this configuration produces material where the orifice diameter is roughly equal to the diameter of the ejected material. The rate at which balls are produced tends to be lower than CMMJ, however rates of up to 9,000 drops per second have been demonstrated [14].

In contrast to continuous mode technology the flight path of the droplet, using DODJ, from orifice to substrate, is to the order of millimetres. Although this allows for smaller dimensions in the overall system design, it inhibits the use of feedback control – once a pulse is sent to the droplet generator there is no way of validating the amount of material expelled from the orifice making its way towards the substrate. In very high precision applications, such as producing optical components and wafer bumping, controlling the amount of material deposited can become critical.

1.4 Technological issues

Materials Jetting is still very much a maturing technology and as such several issues must be addressed before it is widely accepted in the industry.

Both variations on the technique require the presence of a controlled atmosphere surrounding the jet orifice. In the case of solder alloys, too much oxygen will prevent droplets from forming, as the surface tension forces are increased by the oxide growth and inhibit the vibrations breaking the jet.

There are also limits with the piezoelectric materials used to create the mechanical vibrations. Priest [4] noted that at temperatures above 200°C, the common material, lead zirconium titanate (PZT), undergoes a phase change and loses its piezoelectricity. This is known as the Curie temperature of a piezoelectric material. The DODJ technology is particularly susceptible to high temperatures, because the PZT transducers are located near to the heating elements. The continuous mode technology

Material Held in Crucible by
small positive / negative
pressure depending on
viscosity of liquid

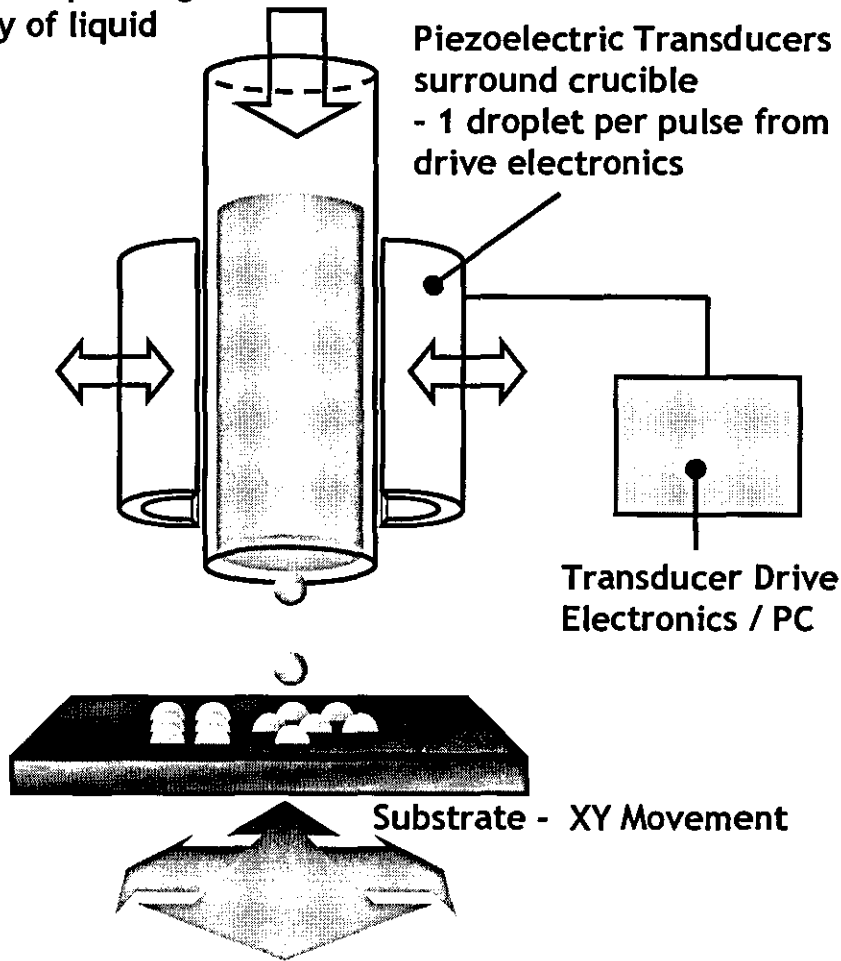


Figure 2 - Schematic for 'drop-on-demand' mode materials jetting

is less affected, because the piezoelectric crystals are mounted remotely from the molten materials, with a metal rod used to transfer the vibrations to the crucible [9].

Priest [4] also demonstrated that a non-oxidising environment is essential for droplet formation. This was illustrated with molten tin, which only formed droplets in nitrogen. Along with the oxidation of the metal surface, Priest also described how contamination in molten metals could lead to inconsistencies in the jet. Particulate matter (such as oxides or inter-metallic phases resulting from interactions with the crucible material) can sometimes be large enough to block the orifice and can cause variations in the stream direction and quality.

The 'Droplet Dynamics and Manufacturing Laboratory' at the University of California, Irvine, have concentrated on flight characteristics, droplet deflection and freeform fabrication. The research was aimed at depositing minute droplets (about 200µm in diameter) layer upon layer to fabricate a 3D component, as a novel method of rapid prototyping [7]. The initial research studied the solder ball shape when impacting a copper substrate at varying temperatures. Figure 3 shows a series of photographs where tin/lead spheres were deposited onto substrates at different temperatures. It can be seen that higher substrate temperatures increase the area of contact of the solder ball when solidifying.

The CMMJ technology allows individual spheres to be deposited at precise locations at high speed, but no specific information is available discussing the re-use and recycling of any waste material. In order to utilise the potential rates of deposition, a suitable recycling method must be devised.

1.5 Applications in electronics manufacturing

The majority of solder jetting work which has been published, has been directly involved with applying low melting point solder bumps to metallised wafers [13,15], figure 4, using drop on demand mode jetting. This process has now been established

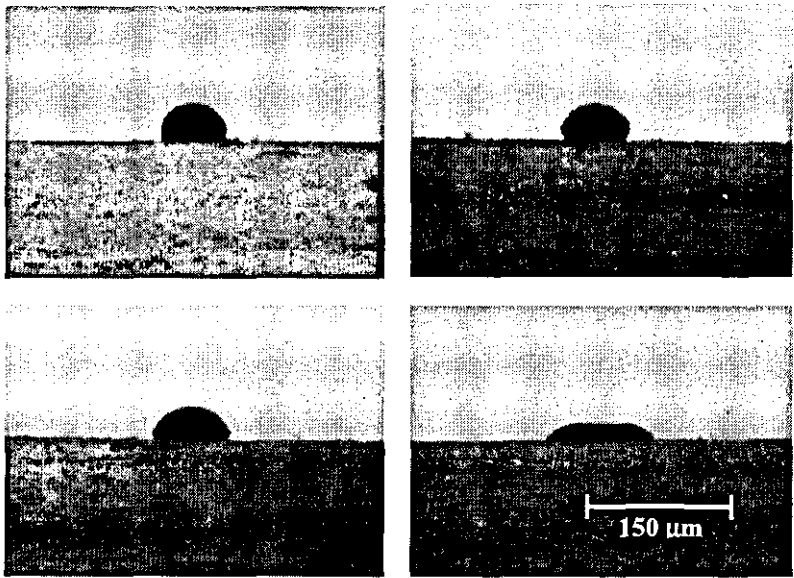


Figure 3 - Photographs illustrating effect that substrate temperature has on tin/lead solder droplets during impact, 95°C (top left) to 126°C (bottom right) [after MPM]

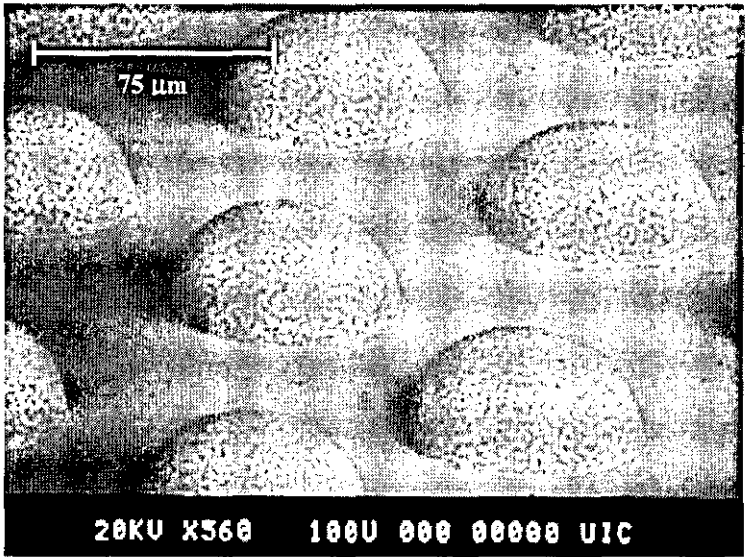


Figure 4 - Eutectic tin/lead solder bumps deposited onto metallised silicon [after MPM]

utilising the continuous mode technology by the MPM Corporation (now discontinued but a similar machine is available through Microfab), who have developed manufacturing workstations to directly bump silicon wafers using tin/lead solder. Since the system is non-contact it is capable of a large number of deposition patterns, via computer aided design (CAD) information, without altering equipment/tooling set-up.

Various solder ball diameters have been produced, ranging from 25 μm [13] with DODJ to almost 800 μm [16] using CMMJ. Although, to date, the smallest dimensions are created using the DODJ technique, droplets approaching 40 μm diameters can be produced by the continuous method. There is no limitation on larger sizes, however the technology is aimed at miniaturisation and Nortel has found that low viscosity materials (like solders) suffer from the molten material leaking out, at orifice sizes above 440 μm , inhibiting consistent jetting.

Also, when reducing material volume there is an increased need for more precise placement, which increases the cost of the positioning equipment portion of the hardware.

The continuous mode MPM workstation is capable of producing 50 μm to 300 μm diameter droplets, at rates of 44,000 (for 100 μm diameter) droplets each second and MPM claim that the 'time to jet a 5 part array of 68 ball BGA with 20 mil spheres is 10.6 seconds' [12]. Although this statement is vague, it could be assumed that they are jetting 10x 50 μm balls onto each pad (to achieve the 20 mil (500 μm) dimension), in other words 680 balls in 10.6 seconds. If this is true, at a rate of 44,000 balls each second, then it also implies that they are utilising 680 out of a possible 466,400 balls - equivalent to a yield of less than 0.2%. Although this calculation is only approximate, it does highlight the need for recycling unused material.

An investigation into the adhesion and solderability of eutectic tin/lead solder jetted onto metallised silicon has been conducted by Hayes [13]. The process parameters investigated included: substrate temperature; droplet size; droplet velocity; droplet temperature; number of drops per site; surface treatment to enhance solder-ability; environmental conditions; and distance to the substrate.

The results that showed acceptable adhesion to the metal layers, known as Under Bump Metallisation (UBM), are summarised in table 1. In each case an aluminium layer was bonded directly onto the silicon oxide and an adhesion layer, of unspecified material, was used to promote bonding to the following layer. This work has successfully demonstrated jetting solder balls directly onto metal surfaces. Figure 5 shows an array of droplets using the metal system number 2, where 60µm diameter tin/lead balls were successfully deposited onto 100µm gold flash pads.

	Metal system
1	Al-Adh.-Cu-Ni-Au
2	Al-Adh.-Cu-Au
3	Al-Adh.-Cu-Pd
4	Al-Adh.-Ni-Au
5	Al-Adh.-Cu-Ag

Table 1 - Tin/lead solder adhered to these metal systems ('Adh' – Adhesion layer)

Successful trials utilising charging and deflection of individual spheres led to the reality of 3D component fabrication. Figure 6 is a photograph of a number of solder balls deflected out of stream. Orme et al have also done simulations and modelling of the formation of 3D patterns using charged particles. Rapid solidification reduces the grain size and leads to a good structural component. It is also important that subsequent droplets arrive before the initial one has solidified, so that a satisfactory bond is formed.

There are many aspects of the electronics manufacturing industry, which could benefit from the flexibility of the solder jetting technology, these include:

- Uniformly sized ball production and solder sphere placement for Ball Grid Array (BGA) assemblies – a type of electronic package where a matrix of conducting spheres are used to attach it to a circuit board;

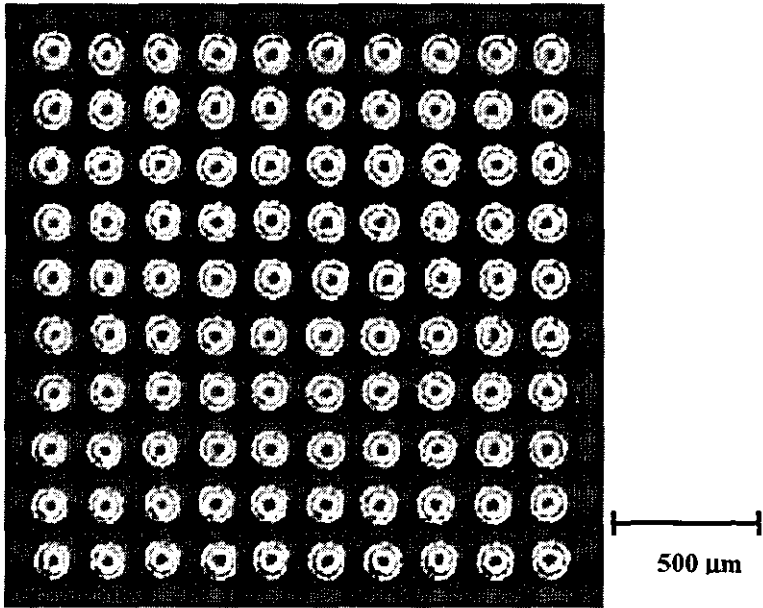


Figure 5 - 60μm diameter bumps of tin/lead solder deposited onto 100μm diameter pads, metal system number 2

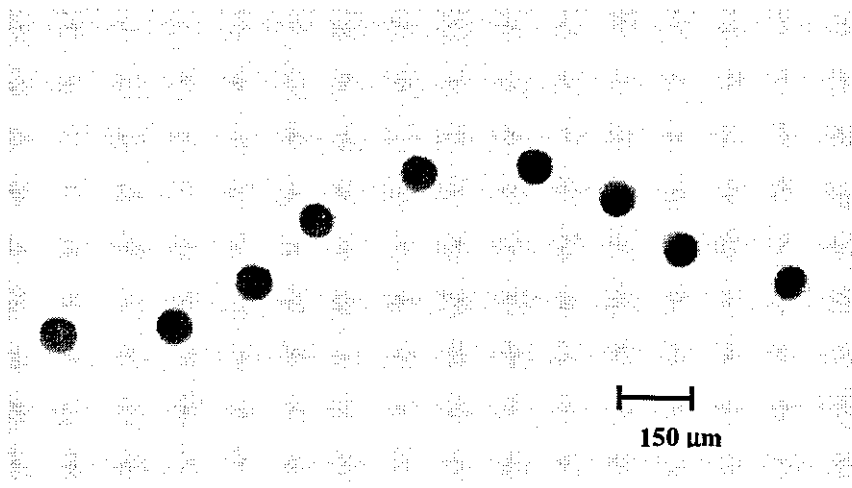


Figure 6 - Photograph showing deflection of a continuous stream of balls [7]

- Via filling for conducting between multiple layers in printed circuit boards;
- Pre-form replacement - enabling solder to be deposited directly into a package from the bulk material without the need for costly pre-processing;
- Adhesive/epoxy/silicon gel dispensing;
- Metal cladding/rapid prototyping; and
- Precision metal interconnects (such as fine tracks or 3D substrate connections).

All these applications use technologies that are now several years old. For example, screen-printing is a proven method of depositing metal, in the form of a solder paste, onto a substrate material. Then a component (e.g. capacitor) is added in position on the paste and re-flowing to create a solder joint. The main disadvantages are:

- New screens are required for each new design and,
- Repeatability can become a major issue at finer pitches (at below 300 μ m using the latest printing equipment), due to the apertures clogging.

Solder jetting removes these concerns, offers the possibility of stepping pad heights and depositing onto 3D substrates and also eliminates the need for solder fluxes. However, it is its increased precision over methods such as screen-printing and dispensing that will enable the drive to smaller components, figure 7.

1.6 Optoelectronic applications

Over the last decade, communications suppliers have experienced an exponential demand for data transmission bandwidth triggered by increased usage of all kinds. While the phenomenal growth of the Internet has been a major contributor to today's traffic levels, demand has been steadily increasing for many other services as well such as local area network (LAN) bridging, video transport, and even voice. The last of these is the result of more access lines, more cell phones, increases in 'working

from home' and various other factors leading to increased usage. Thus, what seemed like a nearly inexhaustible 2.5 Gb/s per optical fibre capacity a few years ago might now appear to be more like a bottleneck and electrically based time division multiplexing (TDM) systems are being eclipsed.

As service providers plan and implement solutions to rapidly expand network capacity, the cost containment and network flexibility of optical dense wave division multiplexing (DWDM) systems are critically important issues, given today's very competitive telecommunications arena. Maximum value must be obtained from currently installed fibre infrastructure to avoid or defer the large capital outlays and long lead times associated with new fibre deployment.

Optoelectronic production is still a very specialised process with high added value because of the amount of human labour involved. For example, coupling lenses are produced separately and manually placed in line with the semiconductors, however with materials jetting it could become possible to automate this process into one step. Lenses could be jetted directly on the semiconductor or fibre. The time and labour to place separate lenses within the package will not be necessary and manufacturing costs can be reduced enabling enhanced competitiveness in the market.

Plano-convex micro-lens and hemi-cylindrical waveguides have been deposited on glass, silicon and fibre ends by the jetting of optical polymeric and adhesive materials [17]. This technology, primarily carried out by researchers at Microfab Technologies and the University of Texas, has found the technique applicable in precisely placed refractive lenslet arrays, multi-mode waveguides and micro-lenses for optical fibres, figures 8A-C.

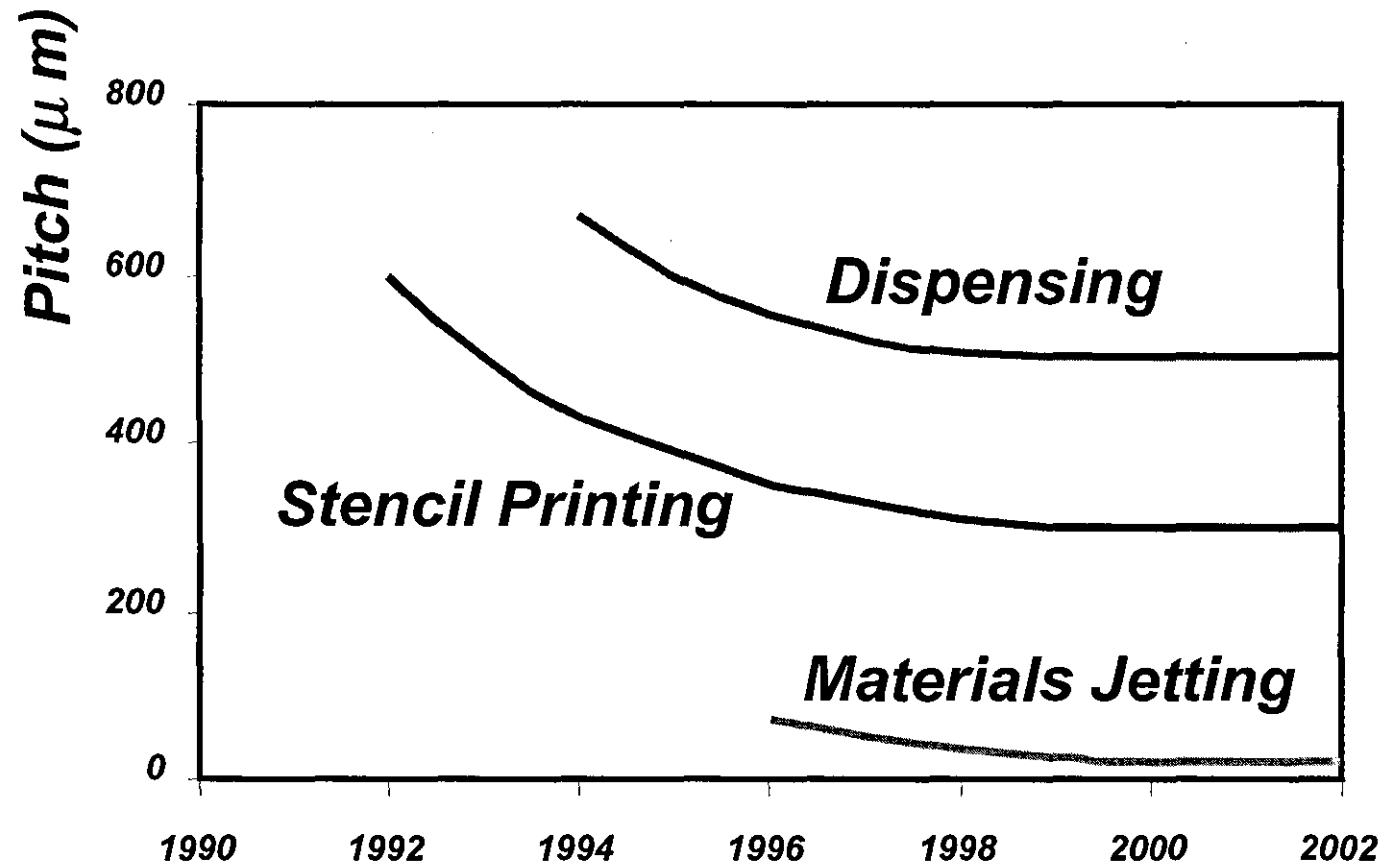


Figure 7 - Comparison of different solder deposition with respect to achievable pitch

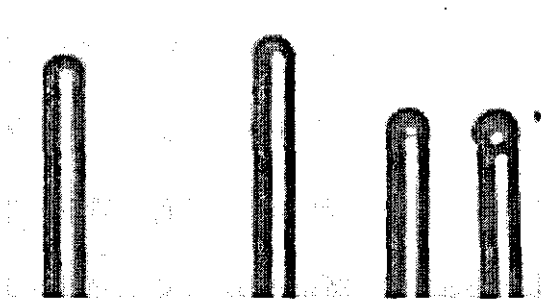


Figure 8A – 300 μ m core diameter optical fibres with microjet printed lenslets (after Cox et al.) [17]

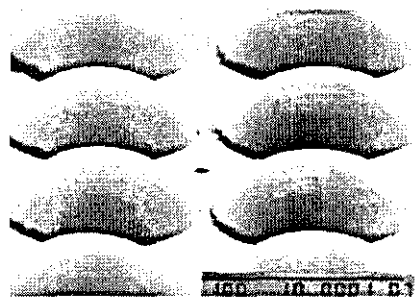


Figure 8B– Array of 100 μ m diameter hemispherical plano-convex microlenses (after Cox et al.) [17]

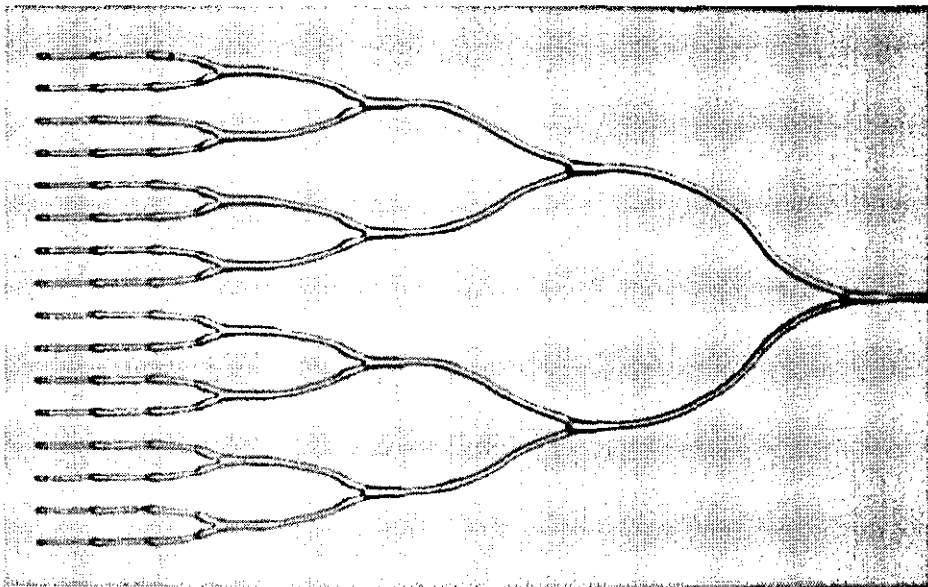


Fig 8C– 25mm long (1-16) branch waveguide, made with 116 μ m x 35 μ m hemi-cylindrical ridge waveguides (after Cox et al.) [17]

High ($n_r=1.704$) and Low ($n_r=1.53$) refractive index (n_r) materials, such as index tuned thermoplastics, hydrocarbon resins (melt temp 100-200°C) and UV curing optical adhesives can be jetted to form these components with less than 2% standard deviation from their nominal dimensions. So far, these optical components have only been deposited using DODJ. CMMJ, by its nature, would be well suited to the deposition of waveguides, due to its ability to produce fine lines [10].

By combining a number of droplets within close proximity (centre to centre spacing of 30-75µm) hemi-elliptical lenses, with separate focal lenses along their major and minor axis, can be fabricated on substrates, figure 9A. Similarly, by increasing the number of droplets along the major axis and therefore, increasing the radius of curvature ($\rightarrow\infty$), a hemi-cylindrical lens is formed which can be used for the collimation of edge-emitting diode lasers. For more advanced applications, like CCD pixel sensitivity enhancement, it is also possible to create square, gold bar-like, lenses [18], figure 9B. These lenses have exhibited 'speeds' (ratio of focal length / numerical aperture) of up to $f/0.76$.

Cox et al have also deposited almost spherical lenses with contact angles greater than 90°, figure 10, which is difficult using conventional lithographic processes. This can be achieved by altering the jetted materials ability to wet to the substrate, either by modifying the surface properties with chemical coatings or by varying the substrate temperature. Spherical lenses, such as these, can be used for beam collimation out of optical fibres or waveguides.

In addition to the technique being used to accurately deposit actual optical materials and components, jetting can be used to precisely control the amount of solder, or adhesive, applied to join and fix fibres into, for example, 'V-grooves' on silicon substrates. Currently, an amount of UV curing resin is placed on a glass slide, in the open, for the duration of a shift. Materials jetting would allow for the tiny quantities to be dispensed on demand and removing the handling of the resin by the operators. The procedure for fibre alignment in optoelectronic packages is still very much a hand crafted skill, due to the fact that the required precise automation is not available in the

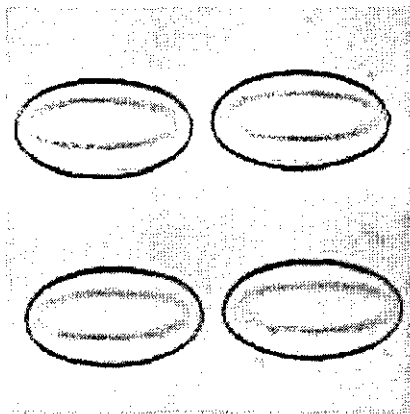


Figure 9A – 4 hemi-elliptical microlenses –
284 μ m x 146 μ m x 20 μ m (after Cox et al) [18]

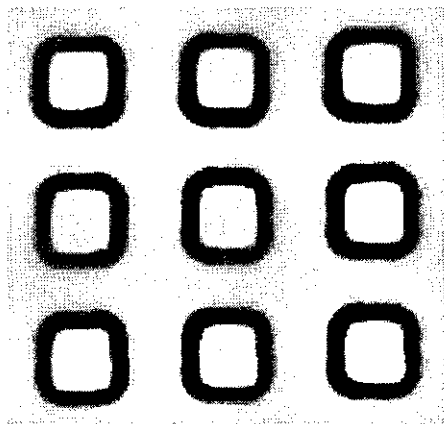


Figure 9B – Array of 300 μ m square, 50 μ m
high printed microlenses (after Cox et al) [18]

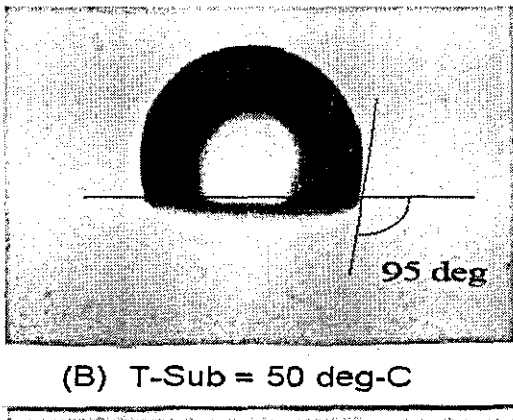
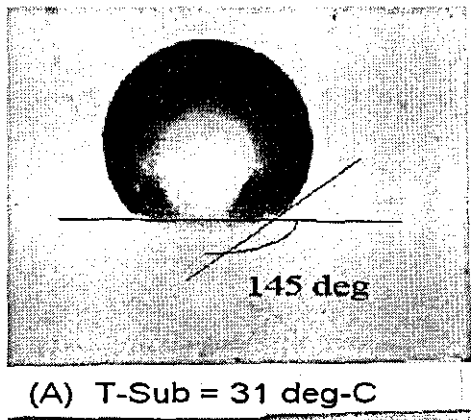


Figure 10 – Variation of surface contact angle with substrate temperature with the deposition of
75 μ m diameter droplet of optical thermo-plastic (after Cox et al.) [18]

volumes and growth rates needed. Materials jetting could provide automation in one, or several, stages of production.

In a similar vein, modern polymeric materials could be used to couple fibres and lasers together by introducing an intermediate fixing, wave guiding and/or modulating stage. Several non-linear and liquid crystal materials have been printed showing potential in this area.

Recently, Nippon Telegraph and Telephone (NTT) Corporation has reported a technology with which micro lenses having a diameter of 1 mm or less are manufactured using ink-jet technology wherein the ink that is employed by the printer is made into a mist and sprayed onto paper. Under the NTT approach, a liquid resin is formed into a mist and sprayed onto a plate producing small lenses that are hardened one by one using ultra-violet (UV) light. It is possible to produce 10,000 lenses every second with a high degree of accuracy. It will become possible to be able to spray the resin and install lenses directly on such things as semiconductors, thus producing high-speed optoelectronic communications devices at low cost. Since the resin is hardened in the hemispherical form that it has assumed on the substrate, it possesses a light gathering ability and it can be employed as a lens. Other work in this area includes the deposition of light emitting polymers for flat panel displays using the ink-jet technology, by Seiko Epson.

Lenses having a diameter of from around 20 microns to over 1 mm can be produced with a diameter error rate that is within 1%. Varying the amount or viscosity of the sprayed resin may change the size and shape of the lenses.

The *f-number*, which indicates the performance of a lens, is from about 1.8 to 15 depending on the size of the lens and attests to the fact that the performance is at the same level as that of high-grade lenses. In addition, it is forecast that it will become possible in the future to produce lenses that are 1 micron or less. It is not clear from this report what the yield of this technique is and whether single lenses can be produced at specific sites.

To date most of the work in this area has been concerned with multimode optical components having less demand on the optical performance that is satisfactory for

short haul office-to-office communications and back-plane interconnect. For the technique to be applicable to long-range communications devices higher quality lenses, which are capable of single mode performance, must be produced.

2 Physics and Hardware

2.1 Droplet Formation

The phenomenon of drop formation from a stream of liquid issuing from an orifice was noted as early as 1833 by Savart [19] and described mathematically by John William Strutt (Lord Rayleigh) [8] during 1878-1892. Rayleigh first reported a detailed analysis of the dynamics involved in an infinitely long column of fluid, and showed that the free surface of a column of fluid will undergo periodic oscillations, as a result of hydrodynamic instability. As the column propagates through space, surface tension then acts to minimise the surface area of the column. These oscillations cause necking along the column, which lead to break-up and droplet formation. However, for metallic elements and alloys, oxide formation on the surface of the molten material is shown [20] to have a drastic effect on the droplet formation process. The characteristic time τ gives an approximate time for necking to occur, and is related to the orifice size and the fluid properties by the equation

$$\tau = \sqrt{\frac{\rho \varnothing_o^3}{8\sigma}} \quad (2.1)$$

where ρ is the fluid density, \varnothing_o is the orifice diameter, and σ is the surface tension [21]. Since this time is governed, in general terms, by the internal mechanisms of fluids the droplets formed are of inconsistent size. To form a stream of uniform droplets an external oscillating source must be applied to the liquid.

If a perturbation is created on a liquid cylinder, or jet, with a wavelength greater than the circumference of that cylinder, the stream rapidly decomposes into a sequence of droplets whose diameters are

determined by the wavelength of the disturbance. This phenomenon can, therefore, be used to create a stream of uniform sized droplets, which are uniformly spaced relatively to one another. [22]

The amplitude of the instability, a_i , is given by the relation and shown graphically in figure 11

$$a_i = a_0 e^{\frac{1}{\tau}} \cos\left(\frac{2\pi z}{\lambda}\right) \quad (2.2)$$

where a_0 is the initial disturbance in the radius of the column, τ is the characteristic time, z is the propagation distance before necking occurs and λ is the wavelength of the disturbance [21]. The applied mechanical vibration initiates a surface tension driven instability on the surface of the capillary stream as it propagates through the orifice. This disturbance a ‘necking’ effect when a_i reaches a maximum value found using the material values in equation 2.1 and inserting this characteristic time into equation 2.2, forming droplets with an average separation of λ , figure 11. Using this theory it is possible to control the size of the droplets by altering the wavelength of the applied vibration where the droplet volume is given by the area underneath the graph between $z = 0$ and $z = \text{‘necking’ point}$.

Equation 2.2 places limits on the sizes of droplets achievable from a given stream. The lower bound being set by wavelengths shorter than the jet/orifice diameter and conversely, at wavelengths longer than twice the orifice diameter, harmonics of the driving frequency will make the break-up unstable. Therefore, it is not possible to make droplets arbitrarily small by making the wavelength smaller and smaller. It is found [21] that if the fundamental drive frequency is too low, several different droplet sizes can be produced simultaneously from one capillary – each droplet attributed to a different harmonic of the drive frequency. Therefore the droplet size should only be varied between the empirical limits $7a_0 < \lambda < 14a_0$ [20].

2.1.1 Droplet size

To achieve uniform droplet generation from capillary stream break-up, molten fluid is issued through an orifice of known diameter \varnothing_O by a pressure, Δp , with a controlled disturbance of frequency, f , applied to the material flow, figure 11.

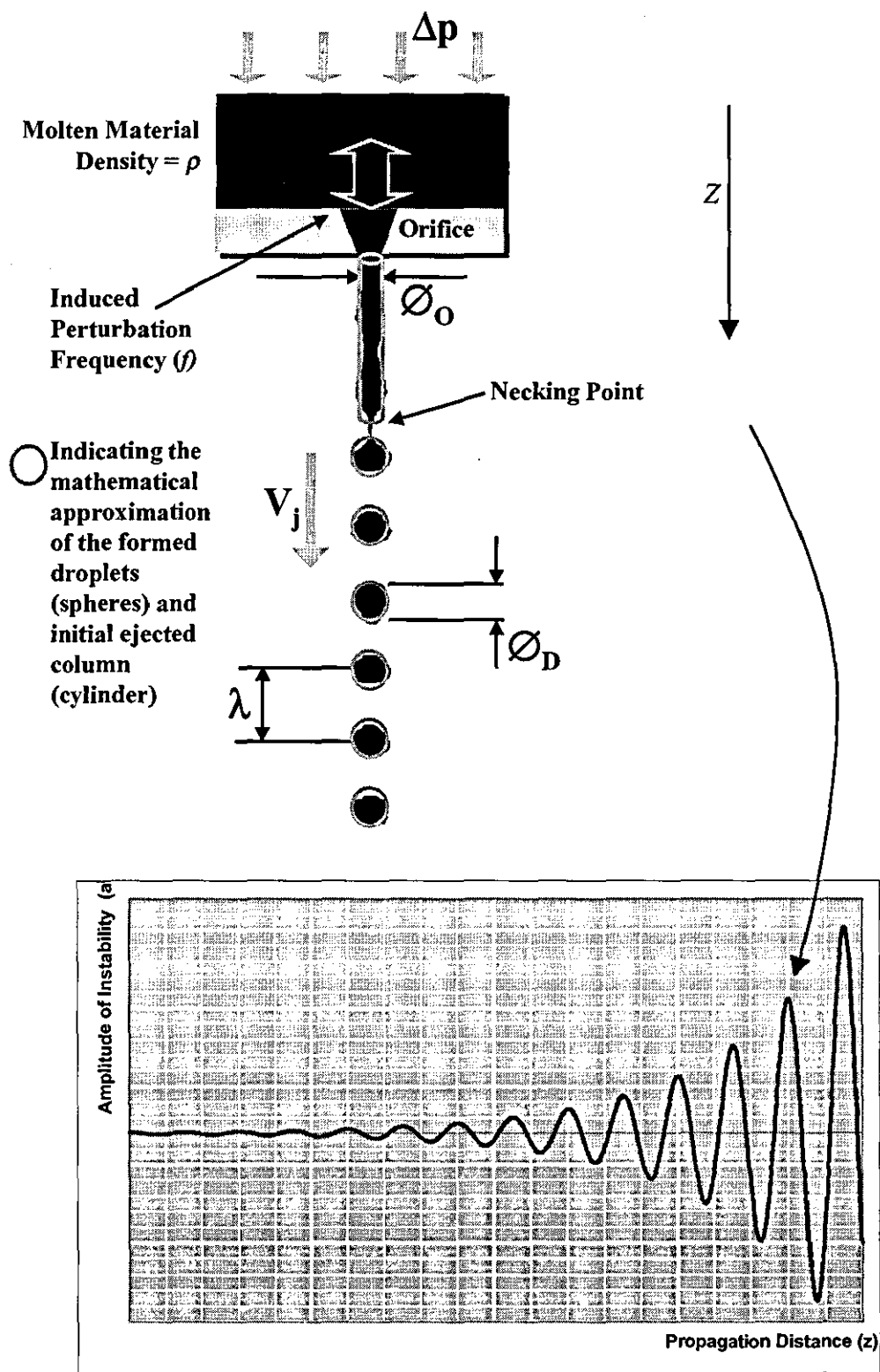


Figure 11 - Mathematical approximation of uniform droplet generation from capillary instability

Droplet size is calculated by considering the volume of the jet at the point at which it breaks into individual droplets. Considering an incompressible liquid, of density ρ , being forced through the orifice into a vacuum by a pressure, Δp , the velocity, V_j , of the resultant jet is given by:

$$V_j = C_{noz} \sqrt{\frac{2\Delta p}{\rho}} \quad (2.3)$$

where, C_{noz} is the 'discharge coefficient', which is an empirically determined value relating to frictional effects between the materials viscosity and surface tension properties [23].

By applying a sinusoidal perturbation to the jet, it is broken every $1/f$ seconds. The stream is broken into cylinders of length, $\lambda = V_j/f$, of diameter equivalent to the orifice diameter \varnothing_o . Therefore, the volume of each cylinder would become:

$$Vol_{cylinder} = \frac{\pi \varnothing_o^2 \lambda}{4} C_{noz} \quad (2.4)$$

As the cylinders fall they form spheres, due to surface tension, with a droplet diameter \varnothing_D and volume:

$$Vol_{droplet} = \frac{\pi \varnothing_D^3}{6} \quad (2.5)$$

Since (2.4) must equal (2.5), then:

$$\varnothing_D = C_{noz} \sqrt[3]{\frac{3\varnothing_o^2 \lambda}{2}} \quad (2.6)$$

Once the droplet diameter has been measured, it is necessary to relate the size of the liquid droplet to the size of the solidified droplet. This can be done using either a volume change on freezing value for the alloy, which, for example, in eutectic tin/lead solder is 2.4% [24], or by performing a conservation of mass calculation between the droplet and the ball. Alvarez derived an equation to approximately calculate the effect of solidification [11], relating the density of the liquid state to the density of the solid state, given by:

$$\delta_{sol} = \sqrt[3]{\frac{\rho_l}{\rho_s}} \quad (2.7)$$

Taking into account the solidification factor in (2.7), the volume of a droplet required to produce a specific volume of solidified material is better represented by:

$$\varnothing_D = \delta_{sol} C_{noz} \sqrt[3]{\frac{3\varnothing_o^2 \lambda}{2}} \quad (2.8)$$

2.1.2 Charging and deflection

Since the droplet generation has been demonstrated at speeds of up to 44,000 drops per second [14] it is likely that not every droplet produced will be utilised if they are being used in the deposition of the material at discrete locations. The limitations being set by the volumes required at each deposition site, speed of substrate movement and validation of the stream. Therefore, it is necessary to affect some droplets in flight to remove the excess. Considering the material in the jet to be conducting it is possible to induce an electrical charge on the material at the necking, or severing, point, figure 11. This enables the stream to be directed towards a site on the substrate, by means of 'deflection plates' in conjunction with substrate movement.

The charging effect is highly dependant on the position of the droplet stream with respect to the charging plates [25]. Small changes in horizontal position produce a large variation in droplet charge. Due to electrostatic repulsion between bodies with

like charges, the droplets are also kept from merging with one another in flight but this also causes the stream to ‘cone’, meaning that the droplets scatter as they travel toward the target. This scattering reduces the directional accuracy of the stream, important in applications where the droplets need to land at specific sites on a substrate. The level of spreading is proportional to the amount of charge placed on the droplet but then this also limits the amount of deflection that can take place.

Following from the definition of electric field intensity, a particle of charge, Q_d , travelling through a uniform electric field, E , experiences a force:

$$F = Q_d E \quad (2.9)$$

From Newton's second law ($F = ma$), the particle acquires an acceleration, $a = Q_d E/m$, where m is the mass of the particle. So, after a time t the displacement, δ , of the particle in the direction of the field, where $x (= vt)$ is the distance travelled at a velocity, v , perpendicular to the field, is given by:

$$\delta = \frac{1}{2} a t^2 = \frac{1}{2} \left(\frac{Q_d E}{m} \right) \left(\frac{x}{v} \right)^2 = \left(\frac{Q_d E}{2 m v^2} \right) x^2 \quad (2.10)$$

Considering a liquid being forced through a nozzle, with a sinusoidal perturbation, a stream of uniformly sized droplets are formed with a separation (λ)

$$\lambda = \frac{2 \varnothing_D^3}{3 \varnothing_O^2 C_{noz}^3} \quad (2.11)$$

Now considering the resultant droplets travelling towards a substrate with velocity, V_j , through a circular charging and parallel deflecting mechanism as shown in figure 12.

As the droplets pass through the circular electrode, of diameter d_c , voltage V_{ch} , they acquire a charge [25], of:

$$Q_d = \frac{2\pi\epsilon_0\lambda V_{ch}}{\ln\left(\frac{d_c}{\phi_o}\right)} \quad (2.12)$$

Where ϵ_0 = permittivity of free space ($F\ m^{-1}$).

Note that the electric field strength that is created by the deflection plates, acting on the droplet stream over length, l_d on figure 11, is $E=V_d/d$. Where V_d is the potential difference across the deflection plates, and d is the separation distance of the deflection plates.

By substituting the value of λ from (2.11) into (2.12), then substituting this new equation for Q_d into (2.10), and including the electric field strength created by the deflection plates E , the horizontal displacement of a droplet is given by δ , which simplifies to:

$$\delta = \left(\frac{2\pi\epsilon_0\lambda V_{ch}}{\ln\left(\frac{d_c}{\phi_o}\right)} \right) \left(\frac{E}{2mV_j^2} \right) l_d^2 = \frac{4}{6} \left(\frac{\phi_o^3 \pi \epsilon_0 l_d^2}{mV_j^2 \phi_o^2 C_{noz}^3 \ln\left(\frac{d_c}{\phi_o}\right) d} \right) V_{ch} V_d \quad (2.13)$$

The mass of each droplet, of density, ρ , is given by:

$$m = \frac{\rho \pi \phi_o^3}{6} \quad (2.14)$$

If the effects of the charge from adjacent droplets, gravity and air resistance are assumed to be negligible, then the horizontal displacement, δ , affected on one droplet travelling through plates of length, l_d , is given by:

$$\delta = \frac{1}{C_{noz}^3} \left(\frac{4\varepsilon_0 l_d^2}{\rho d_j^2 V_j^2 \ln\left(\frac{d_c}{\varnothing_o}\right) d} \right) V_{ch} V_d \quad (2.15)$$

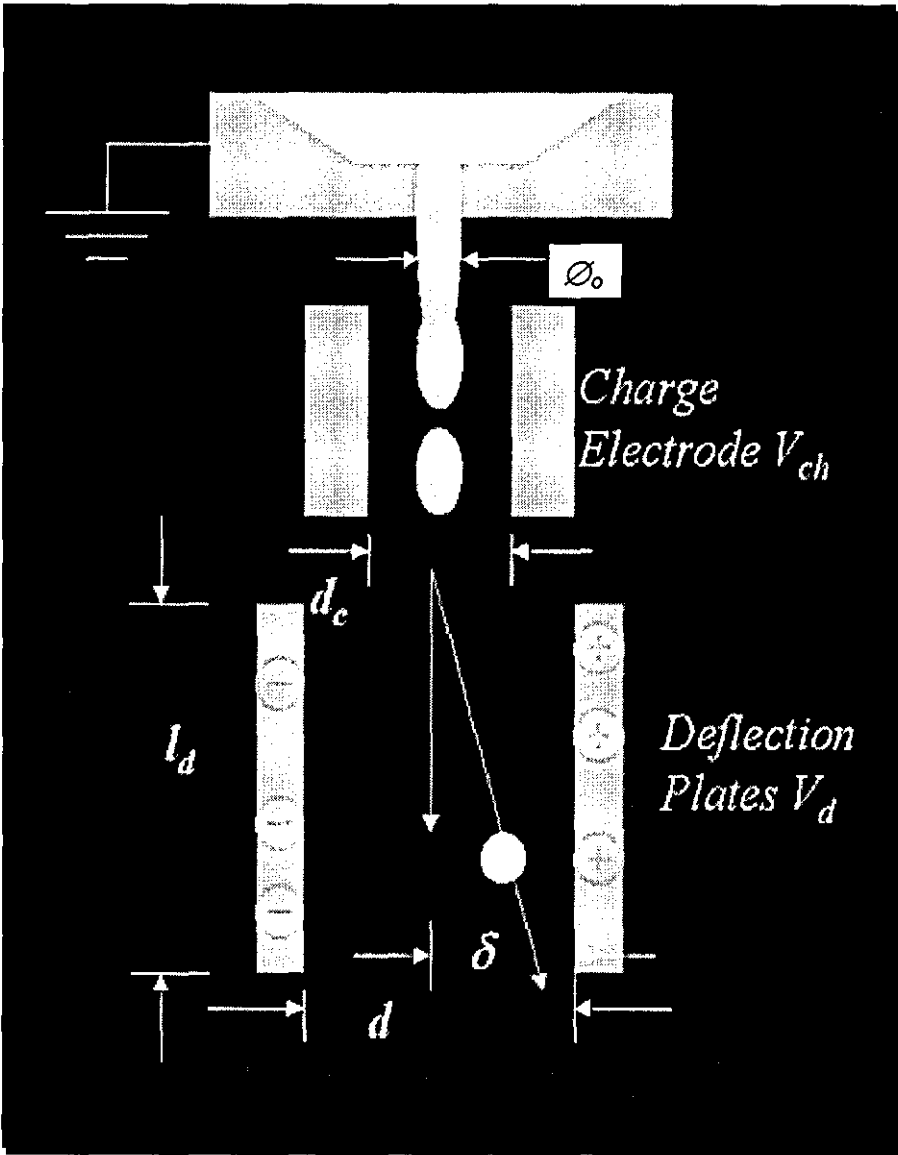


Figure 12 - Charging and deflecting of droplets

This is the amount of deflection for one isolated droplet without the effects of air turbulence, electrostatic repulsion from other droplets and gravity. These effects are simulated [16] using 4th Order Runge-Kutta numerical integration and yield the maximum horizontal distance between any two droplets at a given flight distance. Although this does not show the actual variation of each ball in conjunction with deflection the distribution can be used to work out the potential directional error in droplet flight path.

2.2 On demand droplet formation

So far this report has concentrated on the physics of droplet formation in continuous mode materials jetting. However, as previously stated, materials jetting is split into two distinct areas. ‘Drop On Demand’ mode releases a droplet with every pulse of the transducer attached to the molten material crucible, figure 13. Negating the need for charging and deflection, it is more suited to the deposition of dielectric materials and incorporation in optoelectronic device production but the processing temperatures are lower. Operations with higher temperatures, over 300°C, are presently being investigated [26].

The production of droplets by inducing a pressure pulse within the liquid was observed by Hansell [46] in the 1950’s. A molten material is held in a glass capillary surrounded by a piezoelectric actuator, an electrical pulse causes the transducer to contract, inducing a pressure wave in both the glass and therefore the molten material. The change in volume creates pressure transients, in turn forcing a drop out of an orifice at the end of the capillary.

Alternatively techniques use acoustic waves or a thin film resistive element wrapped around the capillary. When a high current is passed through it the molten material in contact with the walls vaporises and forms a bubble within the liquid, which in turn, forces out a droplet [27]. This report shall concentrate on the piezoelectric method.

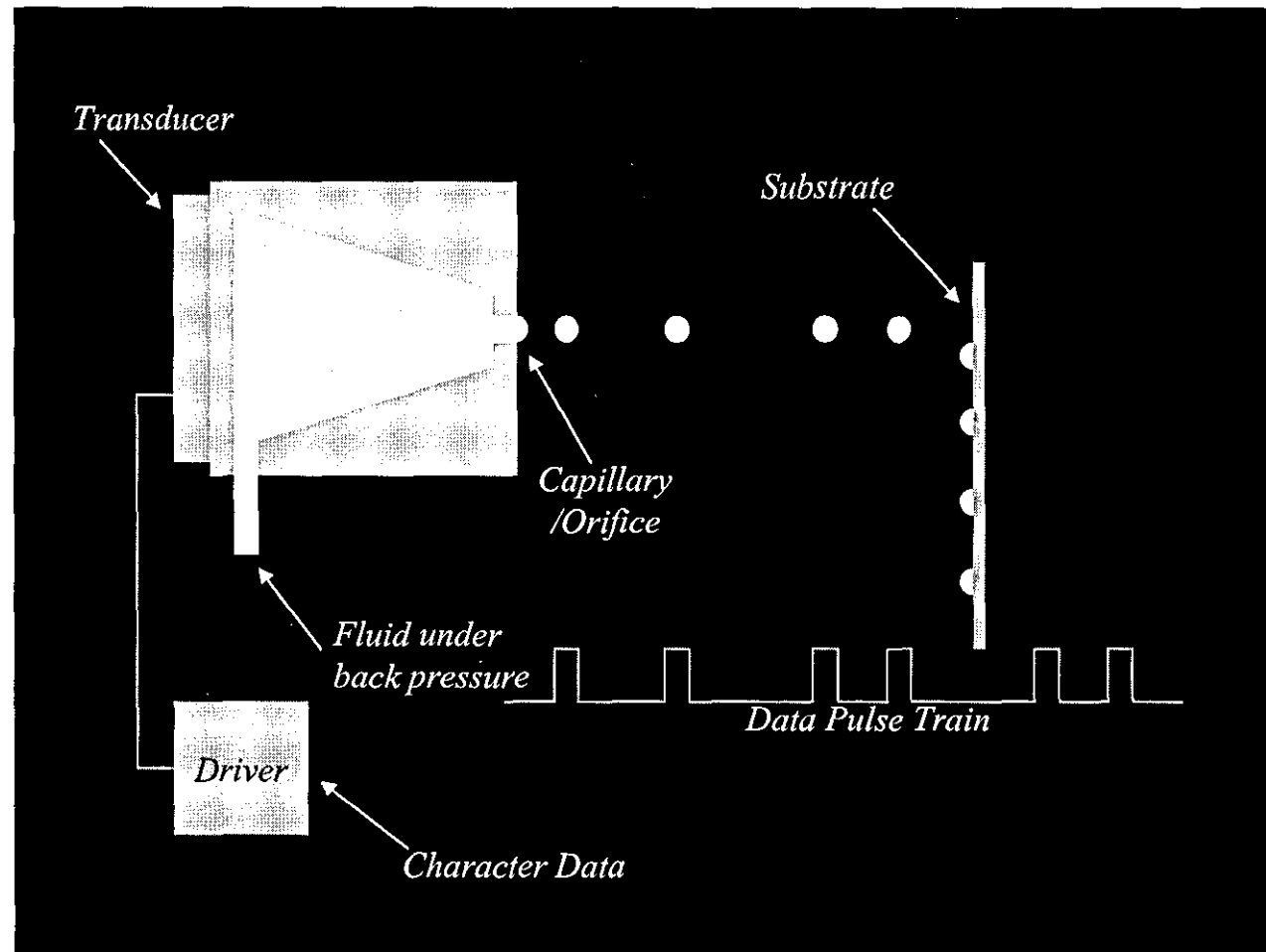


Figure 13 – Drop-on-demand mode droplet deposition

2.2.1 Drive waveform

Considering the positive part of the waveform illustrated in figure 14 the transducer is driven so that an expansion is initially created in the material forcing it out of the capillary. The width of the pulse defines the amount of material, which is released before the piezoelectric material forces the fluid back into the glass capillary, breaking off a droplet.

There is a finite amount of material that can be ejected with each pulse because all devices have a fluid acoustic resonance which means there is an optimum pulse width, which is defined as the highest drop velocity for a given pulse amplitude [28, 29]. The second part of the waveform can be used to cancel some of the residual acoustic oscillations that remain in the device after drop ejection. For the case when the piezoelectric transducer is coaxial with the acoustic cavity, the optimum bipolar waveform has equal positive and negative amplitudes with the second delay time twice that of the initial one [26].

2.2.2 Fluid properties

The generally accepted material property requirements for a Newtonian fluid to be used in demand-mode inkjet devices are a viscosity of 0.5–40 cps and a surface tension value of 0.20–0.70 N/m [26]. These properties are nominal and fluids outside these ranges can be jetted albeit with increased difficulty. Instabilities in the droplet formation are seen as satellite droplets that form at the same time, as the main part of the material is released from the orifice. Higher viscosities act to dampen the acoustic waves that create the drop and the satellites, but require a higher drive voltage.

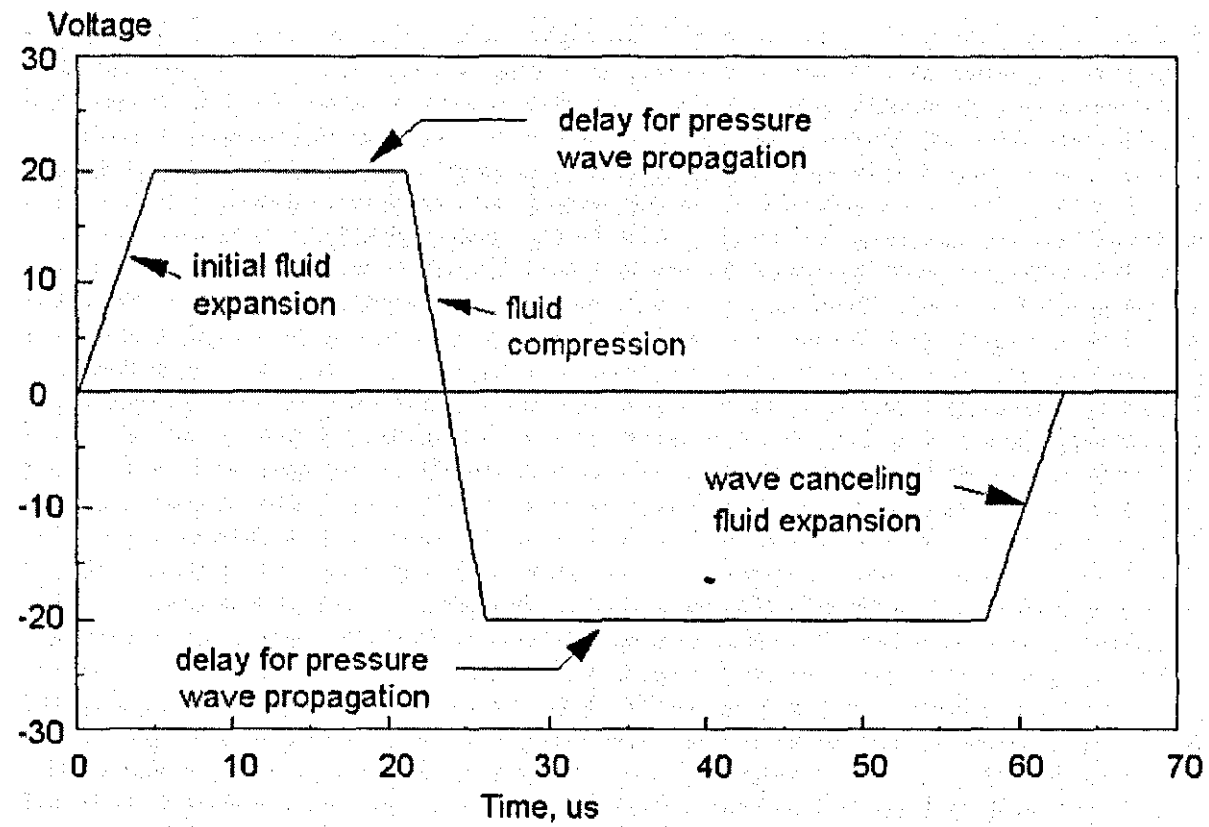


Figure 14 - Bipolar Drive Waveform used to drive the Microfab drop on demand system

Fluids that are particulate based can also be jetted so long as the particles are $\leq 5\%$ of the orifice diameter since anything larger will lead to instabilities in the droplet generation [26].

2.3 Modelling

Theoretical simulation of the process will reduce the time needed for material recycling, optimisation and set-up of the production and deposition of droplets. The physics behind solder jet break-up has been studied by Essien [5] and confirms the theories of Rayleigh and Weber in conjunction with results gained with an experimental droplet generator. They also note the drastic effect of oxygen on jet break up. If oxygen is not removed from the atmosphere then no break-up can occur.

Using the demand mode system titled 'magneto dynamic solder pump (MDSP)', developed by Smith at IBM in 1995 [27] Essien identified the optimum time needed for volume displacement, in relation to orifice size, to take place for a well formed droplet to be created. For example, when the volume needed to force a droplet from a 200 μm orifice is disturbed in a time greater than 0.3ms then there is a possibility that no clean break-off of the droplet will occur and satellites may form. Essien also notes that the size of the droplet formed varies linearly with applied pulse amplitude.

The next step to be modelled in the deposition process is the actual flight path from the orifice to the substrate. A typical simulation for the flight path of droplets, studied in length at MIT, will have several parameter inputs, such as initial droplet velocity, diameter, charge and thermal state [25]. Acting on these values using a fourth order Runge-Kutta integration enables several profiles to be produced, such as:

- Velocity v. flight distance;
- Spread width (of the droplet path) v. flight distance;
- Thermal state v. flight distance;

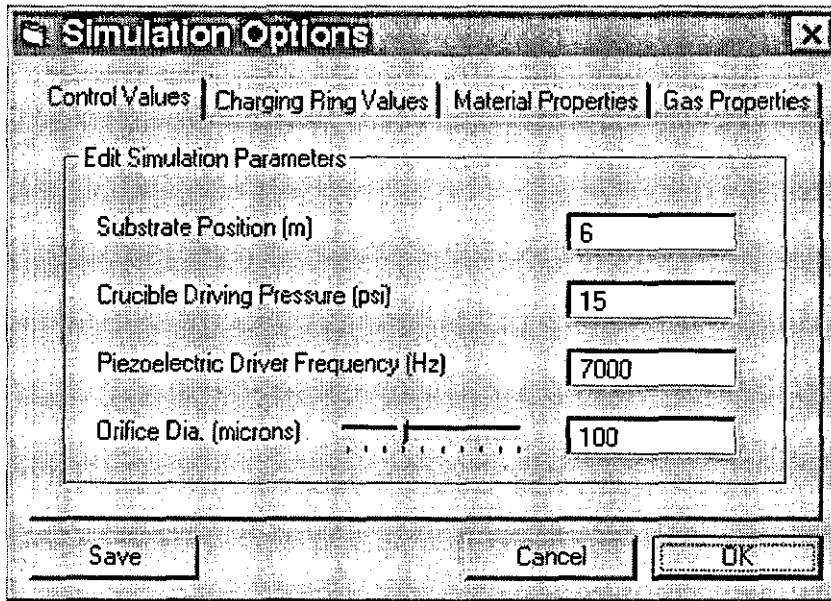
- Mass flux distribution;

To deposit the droplets by the continuous jetting method, the stream must be deflected away from and towards the chosen deposition sites on the substrate. These results enable the optimised control of the droplets.

The droplet flight path simulation code developed by MIT, originally in Matlab, has been adapted in to an easily configurable version, written for a Windows based computer in Visual Basic. A full graphical user interface allows the user to adjust the parameters for the run so that the simulation can be aligned with the current equipment set-up, figure 15. The algorithms developed at MIT [25] are used as the basis for the software and the additional code built around this engine presents on screen a set of variables, such as the orifice diameter and ambient gas, which are changed depending on the initial conditions of jetting. The materials and the gas properties used in the simulation are now linked to a database, which is easily maintained and added to, containing values such as the melt density, specific heat and temperatures.

The current program allows eutectic binary alloys to be simulated, figure 16. All material combinations are valid as long as they have a defined eutectic point on their phase diagram. If more complicated phases and ternary alloys are to be simulated the database must contain detailed information from their phase diagram. The development time needed for this is beyond the scope of this hardware research programme.

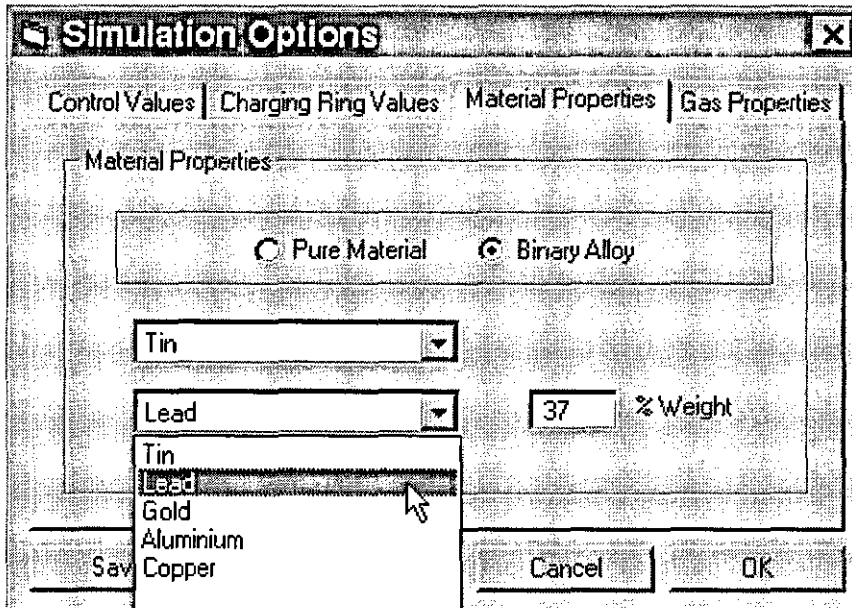
On running the simulation, the required information is displayed in graphical form indicating how the liquid fraction, or temperature, of the material changes with time and/or distance, figure 17. This is particularly important for deposition, where these properties are critical to the final microstructure of the material.



The image shows a 'Simulation Options' dialog box with the 'Control Values' tab selected. The dialog has four tabs: 'Control Values', 'Charging Ring Values', 'Material Properties', and 'Gas Properties'. The 'Control Values' tab contains a section titled 'Edit Simulation Parameters' with four input fields: 'Substrate Position (m)' with a value of 6, 'Crucible Driving Pressure (psi)' with a value of 15, 'Piezoelectric Driver Frequency (Hz)' with a value of 7000, and 'Orifice Dia. (microns)' with a value of 100. At the bottom of the dialog are three buttons: 'Save', 'Cancel', and 'OK'.

Parameter	Value
Substrate Position (m)	6
Crucible Driving Pressure (psi)	15
Piezoelectric Driver Frequency (Hz)	7000
Orifice Dia. (microns)	100

Figure 15 - Simulation Control Variables Setup



The image shows the 'Simulation Options' dialog box with the 'Material Properties' tab selected. The dialog has four tabs: 'Control Values', 'Charging Ring Values', 'Material Properties', and 'Gas Properties'. The 'Material Properties' tab contains two radio buttons: 'Pure Material' and 'Binary Alloy', with 'Binary Alloy' selected. Below the radio buttons are two dropdown menus. The first dropdown menu is set to 'Tin'. The second dropdown menu is set to 'Lead', and a list of materials is visible: 'Tin', 'Lead', 'Gold', 'Aluminium', and 'Copper'. To the right of the dropdown menus is a text field for '% Weight' with a value of 37. At the bottom of the dialog are three buttons: 'Save', 'Cancel', and 'OK'.

Material	% Weight
Tin	37
Lead	
Gold	
Aluminium	
Copper	

Figure 16 - Simulation Material Variables Setup

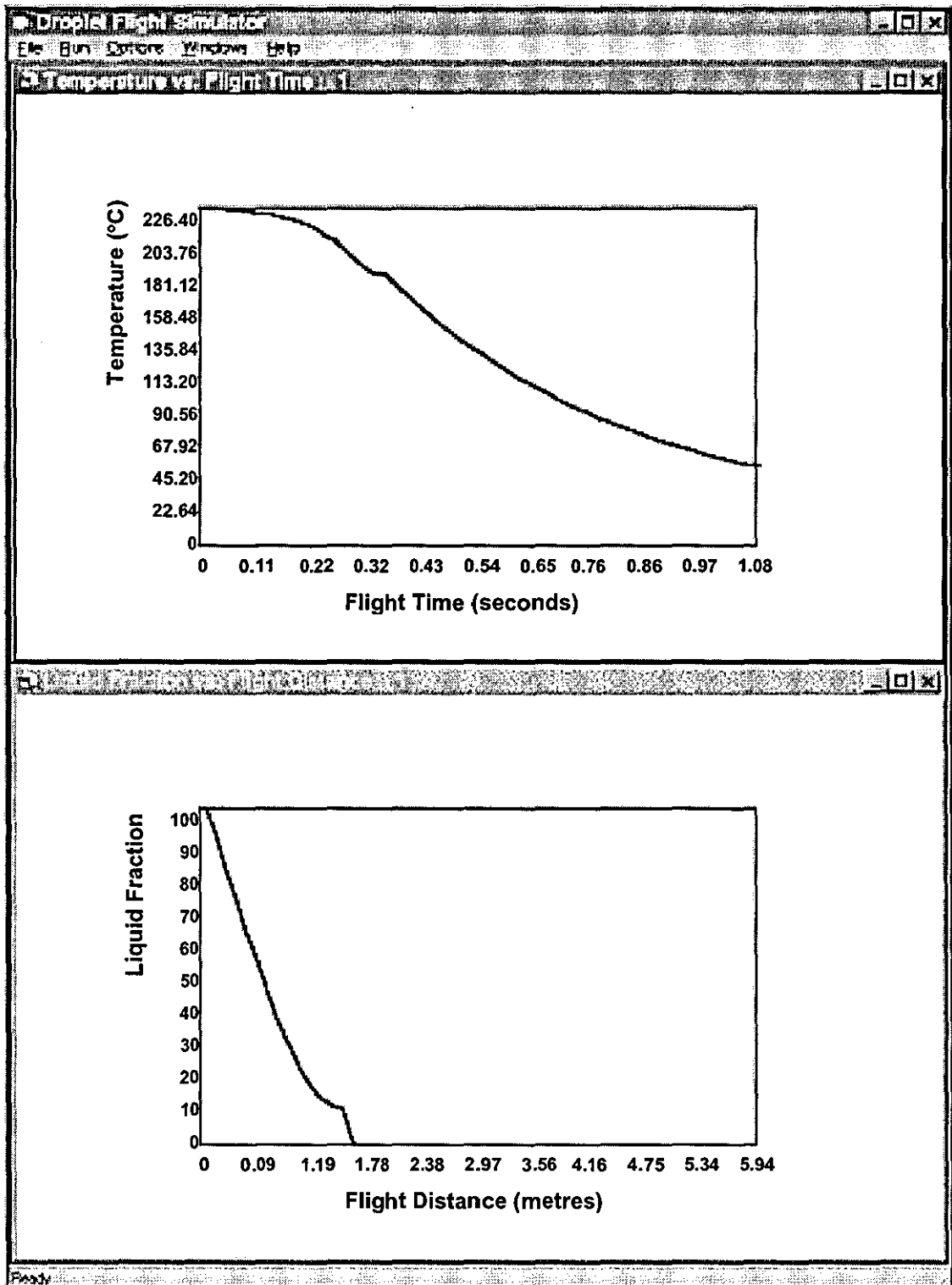


Figure 17 - Simulation Output: Indication of point of solidification

Since the aim of this work is to enable the process to impinge on a component to fix it, both mechanically and electrically with a required amount of material, it is important to consider the behaviour of molten droplets as they solidify on a solid surface. As a molten droplet hits the target it is known to spread, bounce and splash. Understanding the bouncing phenomenon is especially important in electronic packaging where the shape of an individual solder droplet is critical for the quality of connection.

To obtain the desired deposition and get a nicely shaped droplet with a high degree of spreading but a low degree of splashing, oscillation and bouncing, it is necessary to keep the ratio of oscillation time to solidification time low with respect to contact angle. This is achieved, in real terms, by ensuring the wetting potential of the droplet to the surface is maximised and the flight distance and impact speed are optimised [30].

Theoretical, and experimental, investigations into the fundamental heat transfer, fluid dynamics, and solidification phenomena occurring during deposition of picolitre sized molten solder droplets have been performed [6, 31]. Aimed at drop-on-demand jetting, the flight path of the modelled droplet is to the order of about 1mm, which impinge on a substrate at 1ms^{-1} . Substrate temperature, recoil (due to surface tension) and viscous effects of eutectic tin-lead are taken into account as the spherical droplet impacting on a multilayer substrate is modelled, solidifying to its final shape. Adding to previous work on transport phenomena in non-traditional manufacturing Waldvogel [6] investigates

- *Deposition of picolitre size liquid-metal droplets one on another (pile-up)*
- *Three-dimensional heat, fluid flow and solidification phenomena; and*
- *Effect of substrate composition on final shape.*

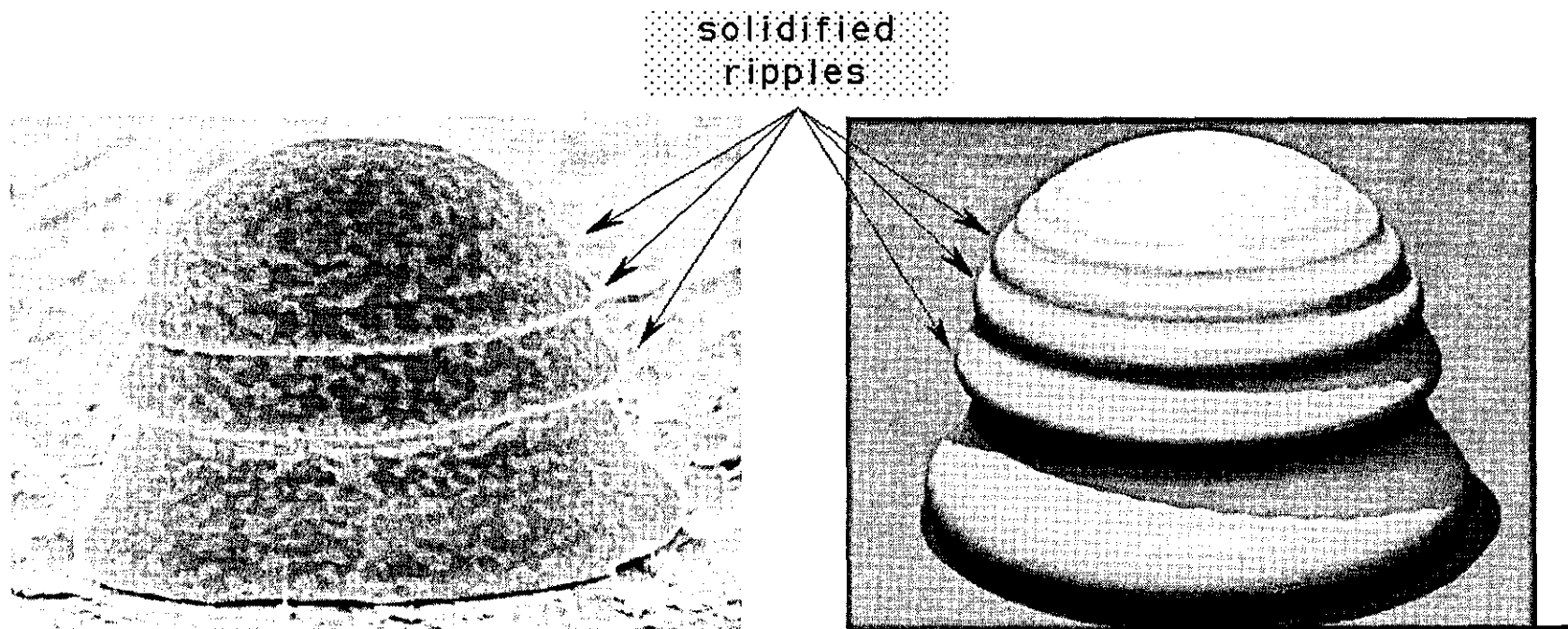


Figure 18 - Solidified 50 micron diameter solder microdroplet. Left: Experiment (Microfab), Right: Simulated

Several simplifying assumptions have been made in the above model, figure 18. Values such as the wetting characteristics of the substrate, surface oxidation, liquid/solid interfaces within the droplet and the heat transfers from the free surfaces of the deposited droplet are all approximated. The quantitative comparison of the experimental and theoretical data reveals only a small difference between both sets of results due to un-simulated phenomena showing the potential of mathematically optimisation of the process before experimental trials. The investigations so far have only illustrated the importance of an understanding of the droplet solidification process. The effect of an increase in substrate temperature was shown to delay the onset of freezing with respect to the droplet oscillations, which leads to an increase in the qualitative predictability only.

2.4 Case studies

2.4.1 MIT Droplet-based Manufacturing Group

The droplet based manufacturing (DBM) group, part of the Laboratory for Manufacturing and Productivity, Dept. of Mechanical Engineering, Massachusetts Institute of Technology, was established in 1992 to exploit the 'Uniform Droplet Spray' (UDS) process. Patented and developed at the DBM group at MIT, UDS exploits the capillary instability phenomenon of liquid jets for producing uniform liquid metal droplets, which allows for a greater control of the thermal state and mass flux of the droplets.

Many possible applications of the UDS process exist, in particular rapid prototyping, spray forming, spray coating, and the production of uniform metal powder production as well as the droplet generation head for continuous mode materials jetting. A licence, and initial equipment, for UDS was purchased as the basis for the project at Nortel Networks. Using a combination of uniform droplet production, charging and

deflection and data driven substrate movement, as outlined in figure 19, the aim is to be able to deposit droplets as small as $40\mu\text{m}$ on a substrate or package.

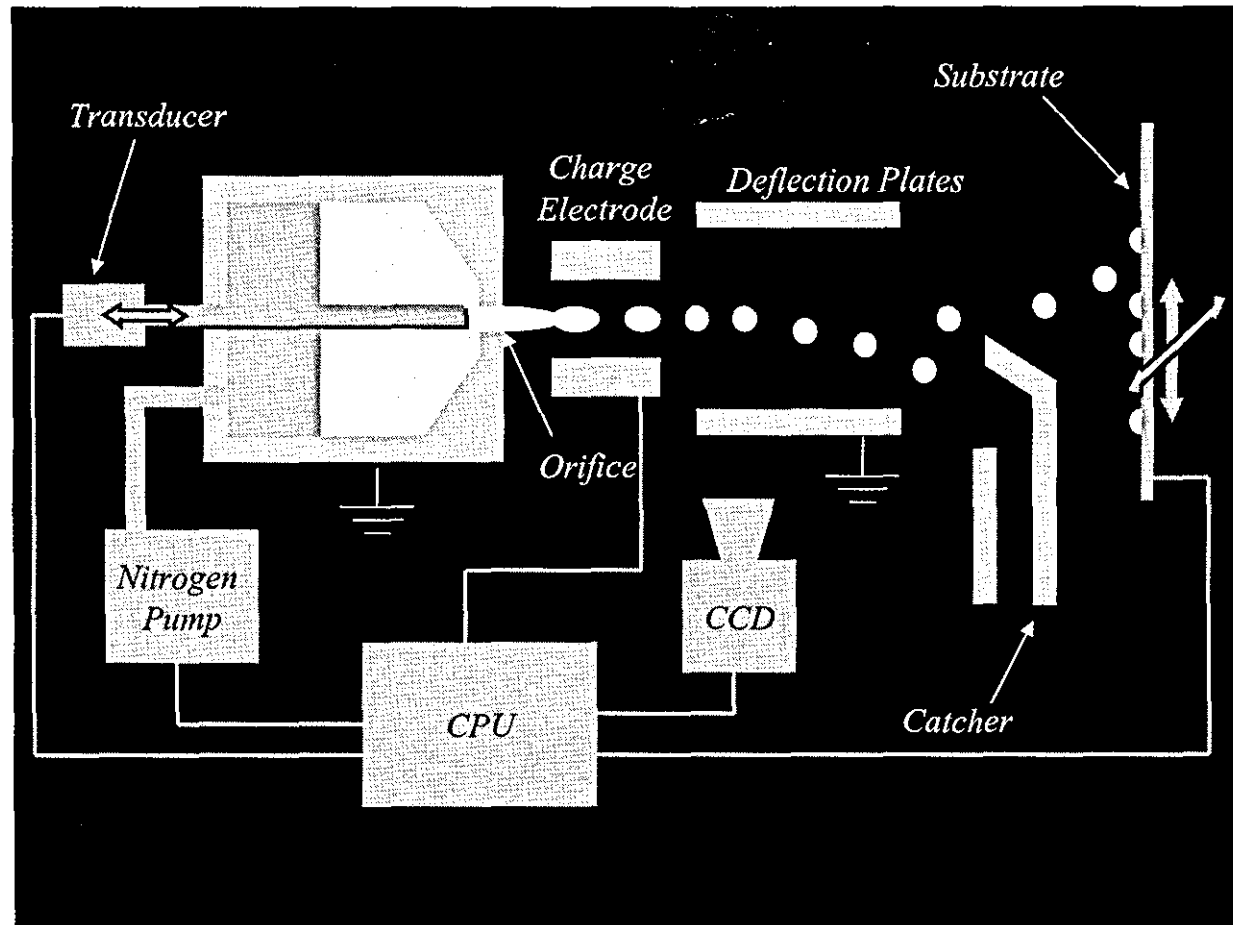


Figure 19 - Continuous Mode Droplet Deposition

The fluid contained in a crucible is forced through an orifice, with dimensions approximately half that of the required droplet diameter, whilst a constant electromechanical vibration is applied. As the liquid issues from the orifice, the pressure oscillations, created in the liquid by an electromechanical device, force the stream to break-up at regular intervals, figure 20. This creates a jet of uniformly sized droplets whose size can be varied by increasing or decreasing the driving frequency applied to the transducer. As the basis of the equipment for this project, a uniform droplet generation head was purchased from the Massachusetts Institute of Technology (MIT). The equipment invented by Prof Jung-Hoon Chun and Christian H Passow is

"A method for producing charged uniformly sized metal droplets in which a quantity of metal is placed in a container and liquefied, the container having a plurality of orifices to permit passage of the liquefied metal there-through. The liquefied metal is vibrated in the container. The vibrating liquefied metal is forced through the orifices, the vibration causing the liquefied metal to form uniformly sized metal droplets. A charge is placed on the liquefied metal either when it is in the container or after the liquefied metal exits the container, the charging thereof causing the droplets to maintain their uniform size. The uniformly sized droplets can be used to coat a substrate with the liquefied metal." [9]

MIT have 3 sets of apparatus, which are all used for jetting solder alloys. The majority of the work has been conducted with pure tin and eutectic tin/lead alloys, and solder powders ranging from 50-800 μ m diameters have been accurately produced. MIT are aware that polymers and glasses are potential materials for the UDS process but they have not carried out any practical work in these areas, as yet. Recently they have reported using a plasma to charge the droplet stream. Since 1998, the research group at MIT, consisting of 7 members, has concentrated on several key areas of the technique including;

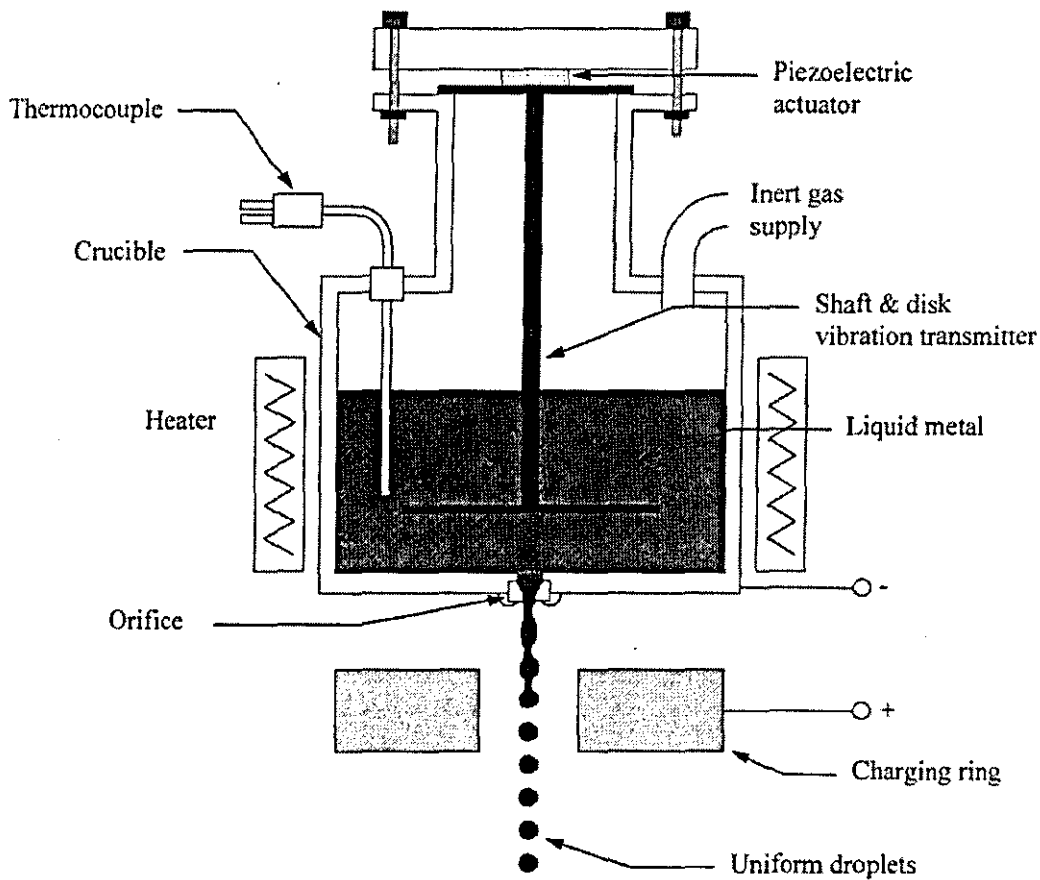


Figure 20 – Schematic of Spray Forming Head (After Chun) [9]

Feedback of droplet size - this has successfully been demonstrated is capable of controlling volumetric dimensions to within $\pm 3\%$. This work is being targeted towards the production of larger spheres for Ball Grid Array (BGA) applications. This research is of particular interest to optoelectronic manufacture where the volumes deposited into the electronics package are critical. Chapter 4 details the refining of the hardware, vision systems and algorithms used to achieve closed loop feedback for smaller ball sizes (down to $50\mu\text{m}$).

High melting temperature alloys and metals - MIT have successfully created powders, with droplet diameters $\approx 250\mu\text{m}$, of pure Aluminium (melt temperature 660°C) and pure Copper (1200°C). This process is still very much in development and cannot yet be achieved on demand, showing how difficult it is to achieve.

Droplet deflection and spreading on impact - Predictive and experimental trials are used to study the deflection and deposition of solders. Being able to predict these two values will improve the deposition of materials into a package or onto a substrate.

2.4.2 Experimental procedure

As outlined in figure 21 the head is enclosed in an inert (N_2) atmosphere and the liquefied metal is also forced through the orifice using nitrogen. Prior to production of the droplets the chamber is evacuated and flushed with N_2 , before being filled with N_2 to a positive pressure of about 10 p.s.i. The pressure difference, between the driving pressure (in the crucible) and chamber pressure, needed for stable break-up through an orifice of, say, $100\mu\text{m}$ is approximately 15 p.s.i., i.e. the crucible needs to be pressurised to 30 p.s.i.

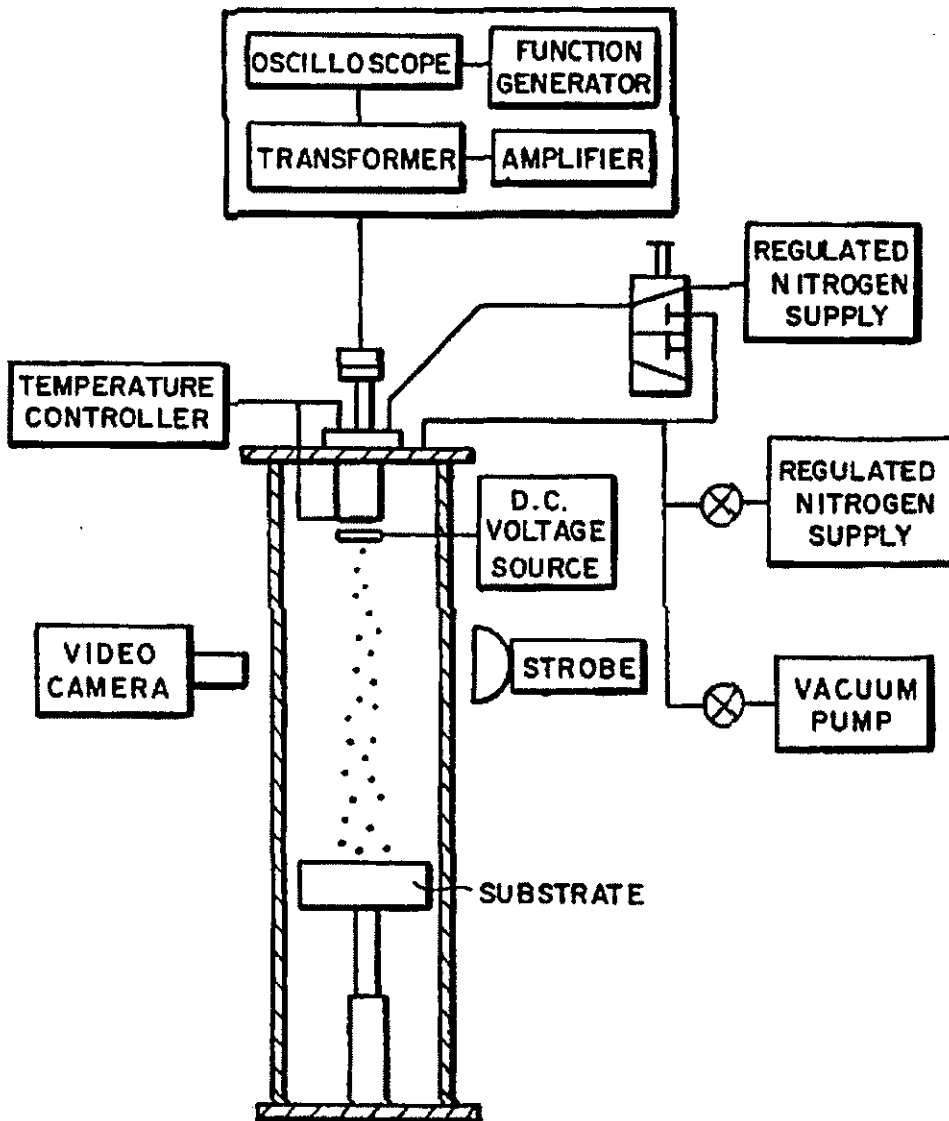


Figure 21 - Droplet Formation Apparatus (After Chun) [9]

2.4.3 Microfab Technologies Inc

Microfab Technologies Inc. are the leading commercial exponents of this technology and have over fourteen years experience in developing ink-jet/micro jet printing processes to reduce costs and increase flexibility in a variety of manufacturing applications. They have micro jet printed a wide range of materials, including liquid metal solders, fluxes, adhesives, epoxies, thermoplastics and UV-curing materials.

Their technology has demonstrated the ability to place 25-125 μ m diameter solder bumps onto metallized wafers [30]. It has also been used to create vertical inter-connect, apply adhesives for component bonding, form micro-optical components and deposit polymers doped with fluorescing materials [17]. More suited to the deposition of dielectric materials, demand mode printing is a versatile and more mature technology than continuous mode droplet generation; it lends itself well to adoption in hybrid packaging technologies, where many materials are used in the same product, especially those required by optoelectronic devices.

Fluid viscosities in the range 0.2-40 cps and surface tensions of 0.2-0.7 N/m can be handled and drop volumes as low as 20 pl and as high as 1 nl can be dispensed. The maximum diameter of a droplet that can be issued from an orifice of a certain diameter is three times that of said orifice [26]. Experimentally, operations with higher viscosities and at over 300°C are being developed.

The Microfab equipment is capable of producing and depositing droplets with an accuracy approaching several microns. The print platform is equipped with a downward looking vision system, allowing for fiducial location and inspection of the jetted materials. The accuracy is limited when new materials are tested since the droplet spreading characteristics at the point of impact with the substrate are not known quantitatively. Optional coatings to influence the wetting behavior can be applied and software utilizing XY-stage linearity and temperature correction algorithms are incorporated into the hardware control to improve placement accuracy.

The high-temperature solder jet drop-on-demand print head and device are suited for dispensing droplets of polymers and liquid metals (e.g., solders). The print head

includes ductwork to provide an inert atmosphere at the device tip, e.g., dry nitrogen for jetting solder. The glass tube is fitted with a piezoelectric actuator and mounted into a metal housing with integrated flush surface fitting that provides mechanical protection and support. The print device housing is insulated by an air gap from the piezo element and is attached to the print head, figure 22. The basic internal construction, figure 23, of the print head is a glass tube of 0.7 mm inner diameter with the tip drawn to an orifice of 30-60 μm in diameter.

In high temperature drop-on-demand printing the most important variable is the driving waveform applied to the piezoelectric actuator, the profile of which is outlined in figure 24. This controls the ejection of each droplet due to the glass capillary being affected by each cycle of the waveform. A simple “On-Off” pulse that moves the piezoelectric transducer and then returns it to the rest state can drive a piezoelectric demand mode ink-jet device, i.e. the positive part of the drive waveform only, but the optimum pulse width is more distinct if the piezoelectric transducer is driven so that a negative pressure is created in the fluid initially, and the return to rest state creates a pressure rise.

In their current set up, the controlling computer allows for 3 modes of operation - single shot trigger, continuous mode and burst mode, where a set number of drops are ejected per the equipment being triggered. The typical cycle time for each waveform is about 2ms, with rise and final rise times of about 5 μs and dwell times of 60 μs . Fall time is set to as small as possible a value, i.e. 0s, where the limitations of the waveform driver govern the actual time. The +VE Voltage and Echo Voltage are chosen to be plus and minus 58V. Figure 24 shows how the droplet is formed, and ejected, during one cycle of the waveform.

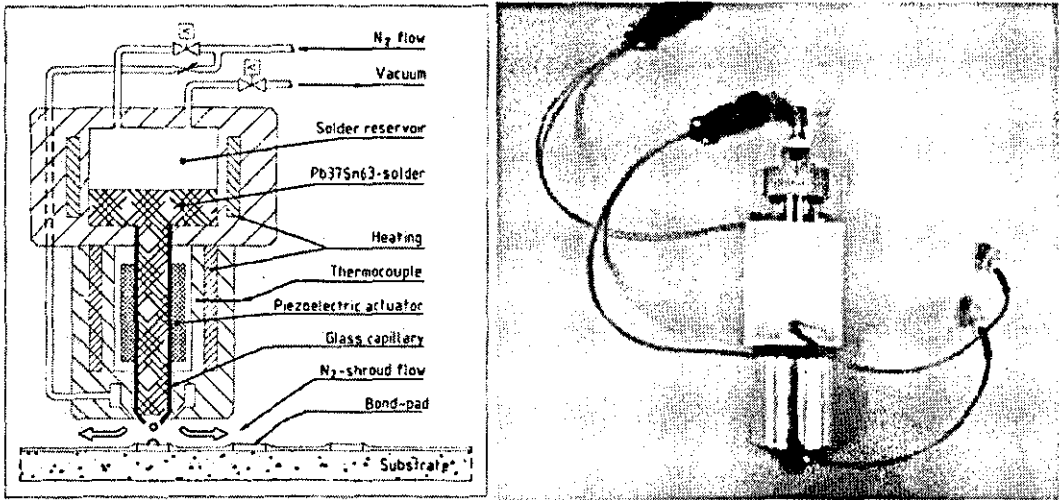


Figure 22 - Microfab Drop on Demand Mode Solder Micro Jetting Head

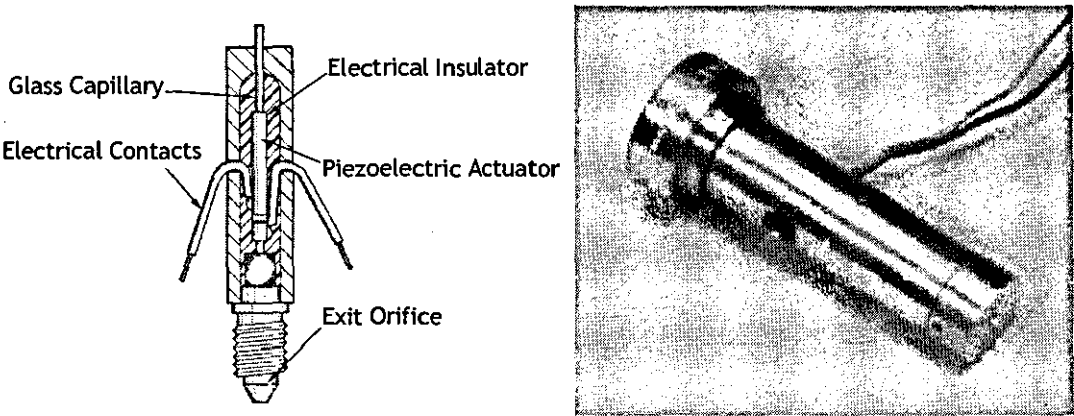


Figure 23 - Microfab Micro Optic Jetting Device

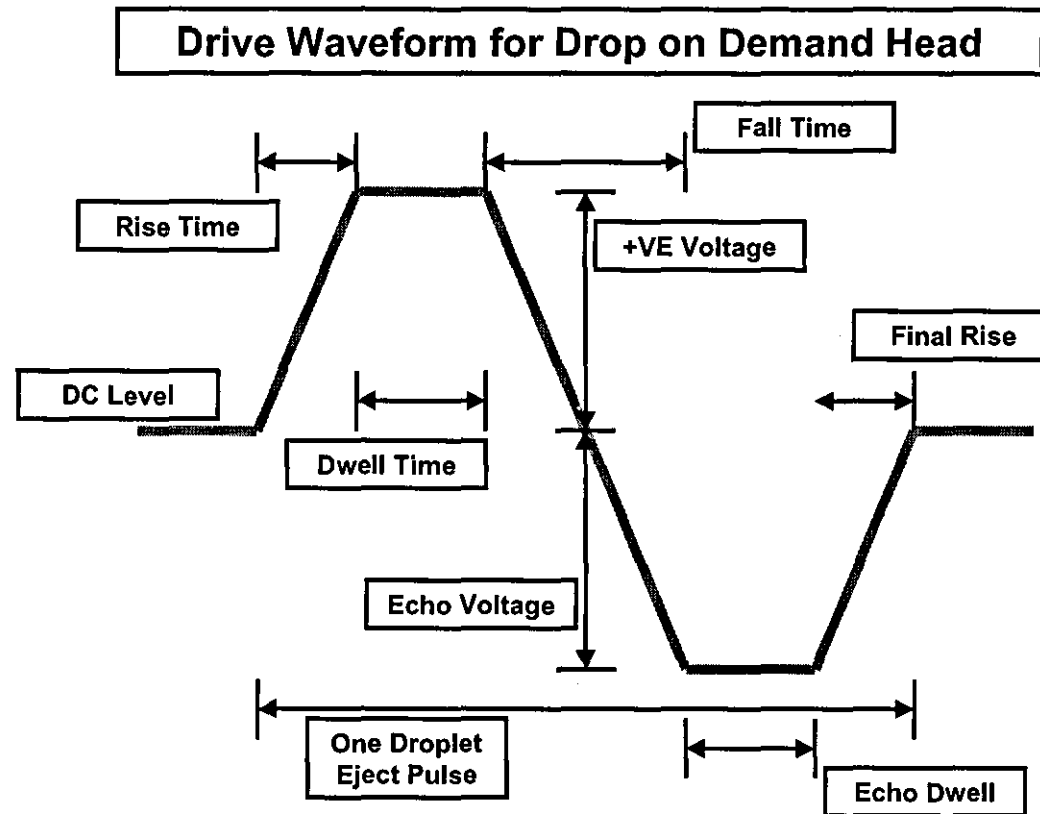


Figure 24 - Formation of Droplet with respect to Time and Drop on Demand Waveform

As the cycle starts the positive voltage expands the glass capillary retracting the liquid back up into the device. This is then ejected as the voltage decreases, forcing the liquid out, past the equilibrium position, producing a droplet. The DC Level is adjusted in conjunction with the gas backpressure to achieve the best equilibrium position of the liquid. In principle, a contraction of the piezoelectric actuator introduces several pressure waves in both directions that reach the orifice as a superposition of vibrations with several modes of system frequencies [26]. These harmonics lead to the formation of satellites in addition to the droplet formed by fundamental waveform. Optimising the echo voltage and dwell time serves to dampen these effects.

2.4.4 Gas Subsystem

In addition to the electrical drive of the system, the backpressure applied to the device also governs the quality and repeatability of the jet. For the MRX-110 Polymer the MKS Type 250 vacuum controller holds the back pressure (negative - vacuum) at 15 Torr to within ± 0.02 Torr. The small vacuum is needed to hold the polymer material within the jetting device - the size of back vacuum/pressure depends on the viscosity of the material - solder jetting requires a small positive pressure.

To dampen any pressure variations, and stop particles backing up to the vacuum, the 1/4 inch supply pipe leading to the device is fitted with a fine in-line filter.

When using this system the station is 'exercised' for up to 3/4 hour before deposition is attempted to ensure clean ejection of material. This is achieved by continually ejecting droplets at a rate of approximately 2 per second, whilst the equipment is warming up. For 100 μ m diameter droplets, only 3 micro-litres of material would be ejected over this time.

2.4.5 Motion System

Outlined in figure 25 is the 'Optics Jet' system, which allows for the deposition of polymers for micro-optic components. The current set-up allows for two heads side by

side enabling the concurrent deposition of different materials, for example - polymers with differing refractive indices. The deposition system is semi-automated. It uses a computer-based interface giving the operator control over the waveform driving the jetting device, the number of droplets, deposited array size and separation and movement speed.

The downward looking camera monitors the movement of the substrate whilst looking for the deposition site. The positioning system then moves in the x direction a set amount so that the position of the device head replaces the camera. Therefore, during the actual deposition, the substrate is not monitored and is reliant on the accuracy and repeatability of the positioning system.

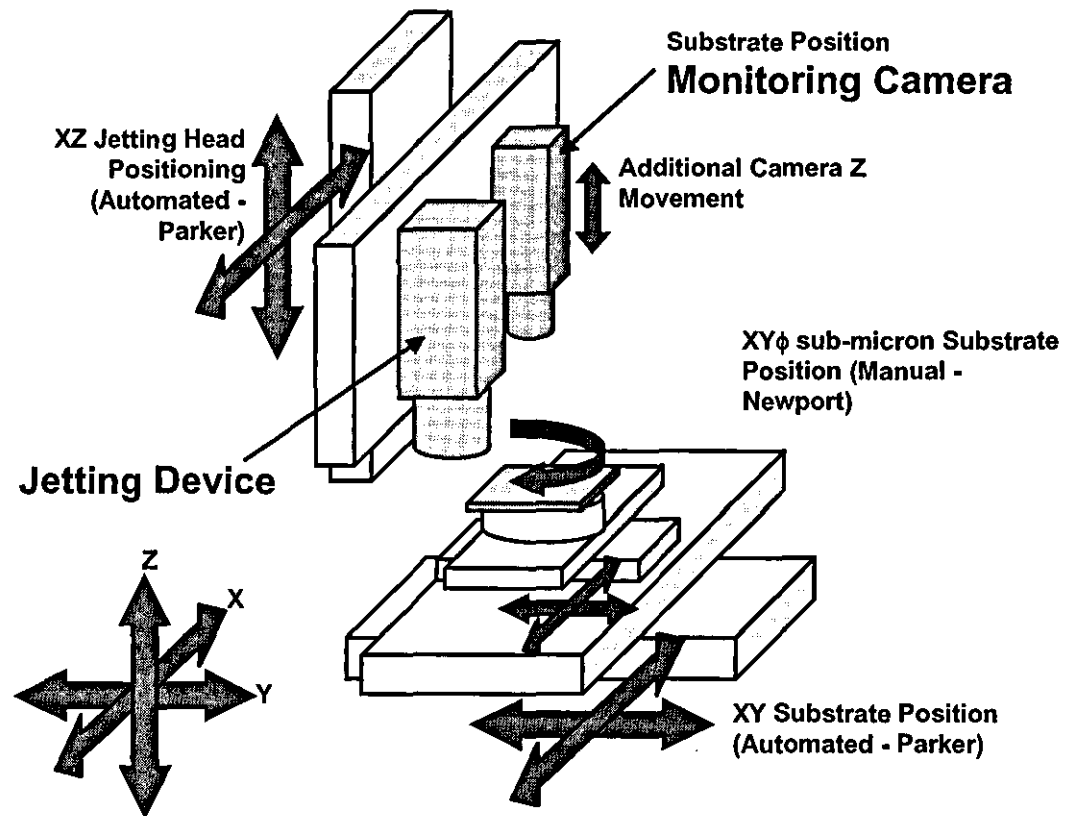


Figure 25 - Jetting Device and Substrate Motion System for Optics Jet Station (Microfab Technologies)

3 Process Development 1 - Software

The research carried out on the continuous mode equipment at Nortel Networks has been concerned with several hardware and software aspects, these development stages have been split into the following areas:

- Droplet detection, measurement and control
- Orifice redesign
- Stream control

This chapter will outline the software methods developed at MIT and Nortel Networks for controlling the droplet size and a potential hardware solution that increases the resolution and speed of measurement, essential for electronic and optoelectronic device production. It will also address the hardware repeatability issues of the orifice and stream control, essential if the process is going to become a reliable, high precision manufacturing tool.

The previous developments of the CMMJ equipment are summarised, and the modifications made to the process hardware are presented introducing two new approaches to improve on the previous methods to control the droplet diameters and stream direction repeatability.

3.1 MIT Software

As previously discussed in Section 2.4.1. (page 38), Alvarez (of MIT) has implemented a method of closed loop feedback for continuous mode machines [11]. An image of the droplet stream, frozen by stroboscopic illumination, is acquired using a charge coupled device (CCD) camera. The image is transferred to a computer via a 'frame grabber' add-on card, which captures a video image of the stream, which is

used to analyse the separation between the ejected droplets. Measurement is achieved using edge detection techniques, which identify abrupt changes in the grey scale¹ values of this image. The software scans the current image looking for dark regions representing droplets. If the cross-sectional area of one of these regions satisfies that of an estimated size, as determined by the operator, then a droplet is 'found'. Direct measurement of the diameters are not feasible with droplets above 500µm, because droplet shape oscillations will not have stabilised until the droplets have passed outside the field of the camera. To account for the shape variations, the centre points, measured in pixels for each droplet, are determined from the maximum and minimum, horizontal and vertical edge values, figure 26.

This is valid because the droplet's shape oscillations are axis-symmetric, so the centre points would still be in the same place. The algorithm then continues to look for two further droplets. The average spacing, or wavelength, between each droplet, λ , is calculated and the droplet diameter is found from

$$\phi_D = C_{noz} \sqrt[3]{\frac{3\phi_o^2 \lambda}{2}} \delta_{camera} \quad (3.1)$$

C_{noz} is an experimentally determined [16] coefficient relating to the frictional, viscosity and surface tension effects of the material being deposited. δ_{camera} ; converts the number of screen pixels to a distance in metres.

The difference between this measured ball diameter and the desired size is then compared. Altering the frequency of the applied electro-mechanical vibration will slightly change the induced break-up length, thereby increasing or decreasing the droplet size by computer control.

¹ Relating to the relative intensities of pixels within an image.

MIT have successfully demonstrated this feedback method for producing solder balls for BGA packages for large size droplets of around 650 microns, to within $\pm 3\%$ of the nominal diameter. Smaller droplet sizes could also be measured if more powerful camera optics are implemented. One limitation of this approach is that once the

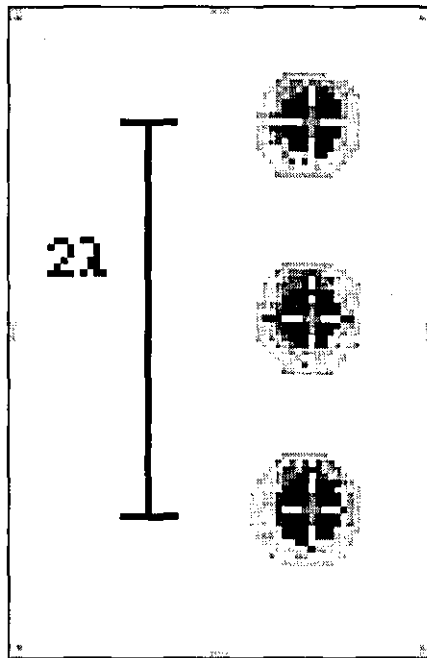


Figure 26 - MIT droplet detection uses blob analysis to find the centre to centre spacing of the droplets

camera calibration factor has been established, it is not possible to adjust the camera optics without re-calibrating the pixel size factor. Care must be taken not to affect the camera once it is set. As smaller droplet sizes are measured, there comes a risk that slight variations in the stream direction would cause the droplets to become 'out of focus', adjusting the camera optics to compensate would then alter the conversion factor. Also, since a CCD camera captures images at a rate of 25-30Hz and the smallest of droplets can be produced at much greater rates (i.e. > 20KHz) the resulting image is the superposition of many minutely differing views of the 'frozen' stream (up to a ~1000 depending on the speed of the strobe illumination).

The development of a new algorithm is presented in this chapter, which improves the robustness of the measurement method and aligns the technique so that it is fully scalable down to the smallest producible ball size (~40 μ m). This algorithm is incorporated into control software, which will be able to control all aspects of the continuous mode jetting technique, from the ball production, through charging and deflection, to substrate movement.

In addition, a potential hardware solution is presented which could further improve the resolution, accuracy and speed of droplet size analysis.

3.2 Software development

The software, written in Visual C++ 5.0, has the capability to control the separate constituent parts of the continuous mode materials jetting hardware as part of an automated system. Considering the process control diagram, figure 27, the software is split into two distinct threads. The ball size control algorithm, thread one, is synchronised with the secondary thread, which controls the deflection and substrate movement. Using a multitasking operating system, such as Windows NT, the application programming interface (API) allows for programs to be built which are able to run and synchronise the number of threads as outlined in figure 27.

Communication between the threads is critical, and as such the process is set up so that deposition will not take place until the droplet volume is validated.

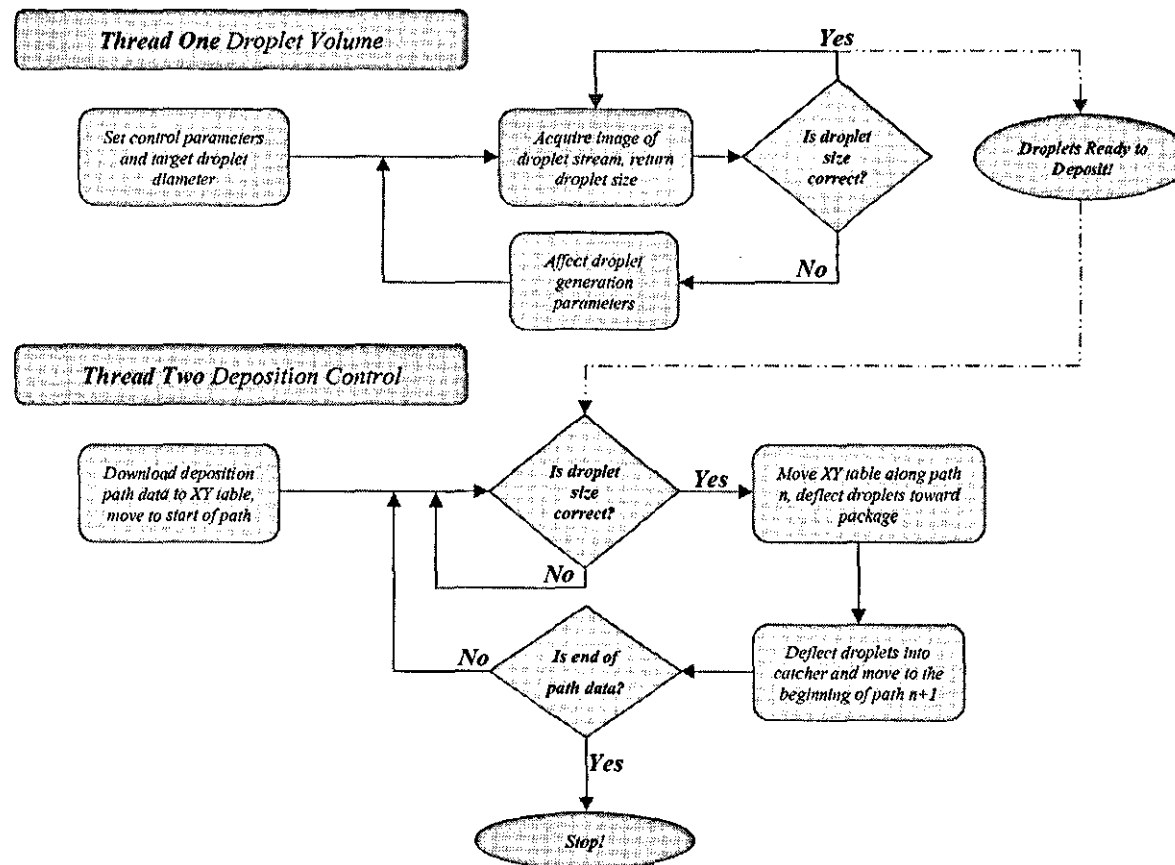


Figure 27 - MJT control software: process flow chart

3.3 Histogram Method of Droplet Size Measurement

A continuous mode droplet generation process for smaller dimensions will inevitably require a closed loop feedback system to work for droplet diameters approaching $40\mu\text{m}$ (i.e. 34 pl). Detecting the droplets by the edge detection techniques for smaller droplet sizes, as described in the previous section, will result in reduced accuracy due to the resolution of the optical system.

Expensive optical components are not needed if the relative intensities within the image are analysed, instead of attempting to detect each droplet. Using the same optical set-up as described in chapter 2 (figure 21), an image is captured, but this time is reduced in size by the operator to only include the droplet stream. The selected window is referred to as the region of interest (ROI), figure 28, and is a useful method of eliminating any unnecessary processing. The ROI is then scanned, row-by-row, building a histogram representation of the grey scale values within the image. Since the droplets are illuminated from behind, it is necessary to invert the values for the histogram.

The computer stores the image as a 2D array of grey-scale values, figure 29, this allows for mathematical, or more specifically 'image processing', algorithms to interpret the image data and produce a meaningful numerical analysis. In this case it is necessary to find the distance between the droplet centres so that a value can be fed into equation 2.6 to yield the droplet diameter. Previous methods [11] use gradient operators, which locate the leading and trailing edges of a droplet to determine its position. This approach works well for large changes in grey-scale and well-defined ball shapes. As the droplet size decreases the edges and ball shape become less distinguishable so a more robust method of finding the centre-to-centre spacing is presented.

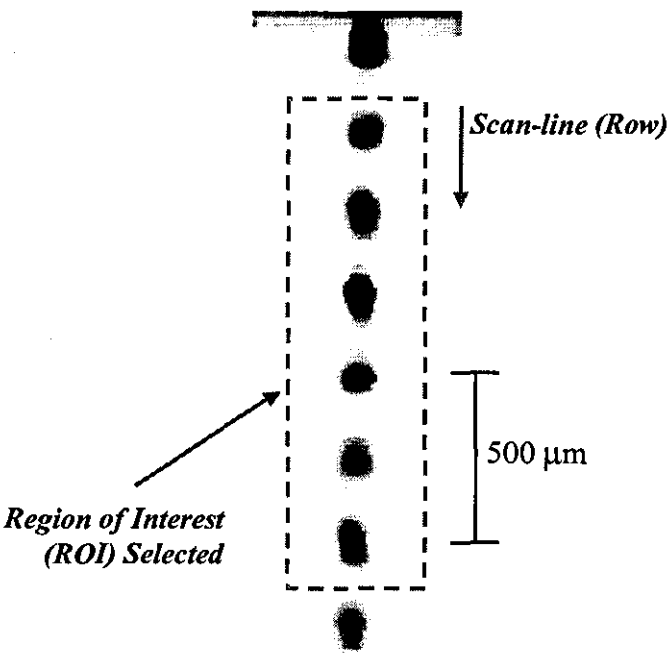


Figure 28 - Image of droplet stream

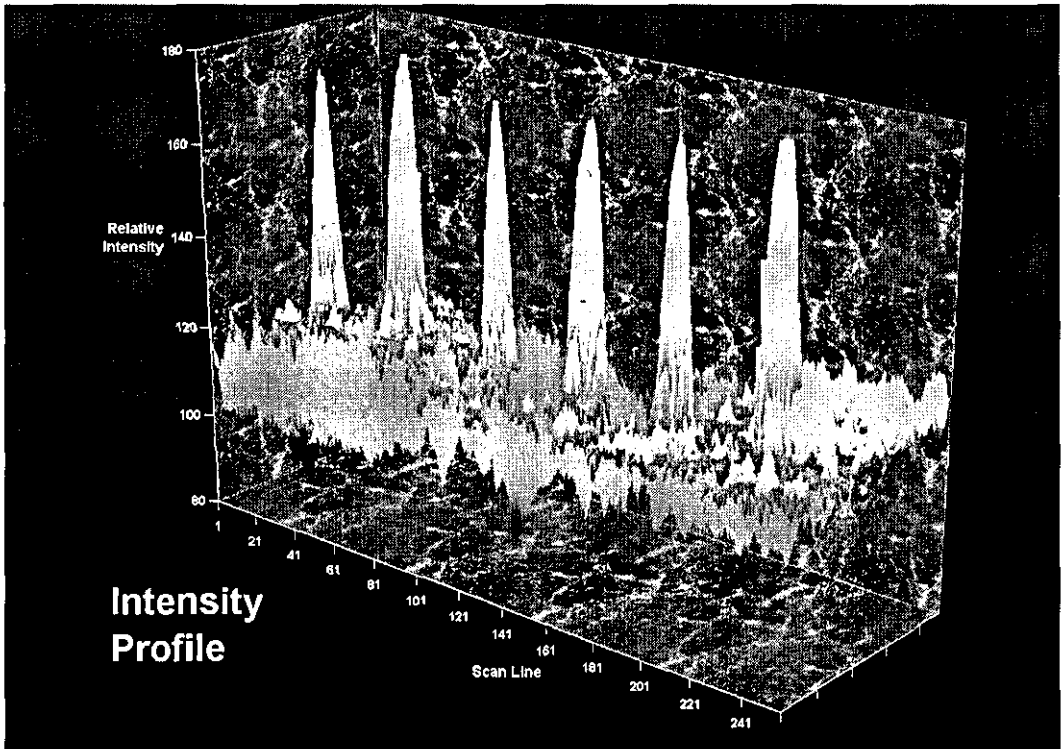


Figure 29 - (inverse) 3D representation of the relative greyscale of the droplets

Considering the grey-scale map as a 1D histogram, a Fourier transform is performed on the data, which gives the fundamental frequency of the data, or the number of peaks. If the number of scan-lines is then divided by this number, the peak-to-peak distance in pixels is found.

There are two ways to build the histogram. If a threshold operator is passed over the ROI, a binary image of the droplets is created. Then, as the image is scanned, the number of 'on' pixels is summed, figure 30. The advantage of this method is that the position of the droplets is well defined. However, one problem is that the intensity of background illumination, or noise, over the image may vary, which frequently occurs when using stroboscopic devices.

This problem has been overcome by incorporating an adaptive form of histogram. By summing the total intensity in each row (or scan-line) in the region of interest, the droplets are super-positioned upon the varying illumination intensity, figure 31.

Pronounced peaks are observed, which relate to the positions of the droplets within the image. To obtain a value for the stream wavelength, and hence the droplet diameter (equation 3.1), the peak-to-peak values must be filtered out of the histogram. The actual positions of each peak are of little relevance, and the average distance between the peaks only needs to be established. The frequency of the fundamental pseudo-waveform illustrated in figure 31 can be found by performing a discrete Fourier transform (DFT) on the data series. The discrete Fourier transform maps a function from a finite number, N , of sampled points to N complex numbers.

In this application, computational speed is a critical factor. To achieve the most efficient processing time, a specific case of DFT known as the Fast Fourier Transform (FFT) can be utilised, which reduces the number of operations from N^2 to $N \log_2 N$. The clearest derivation for this algorithm is given by Danielson and Lanczos [32], who show that a DFT of length N can be written as the sum of two discrete Fourier transforms, each of length $N/2$.

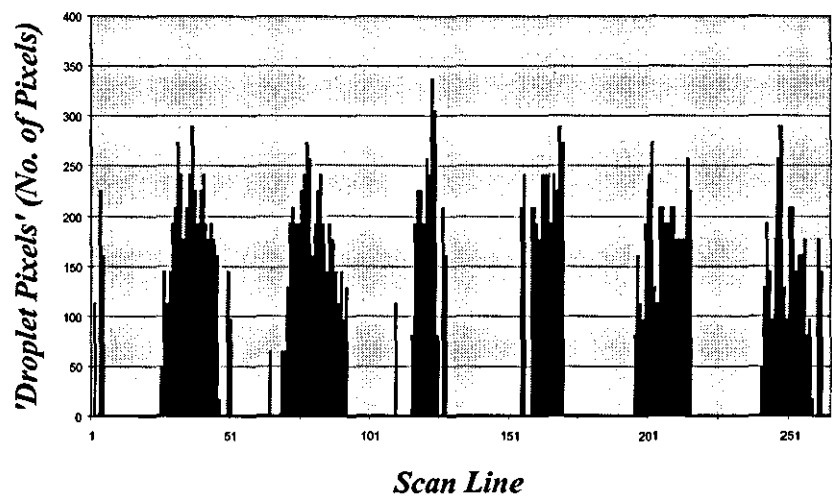


Figure 30 - Histogram representation of the number of 'on' pixels due to presence of a droplet in an image after thresholding

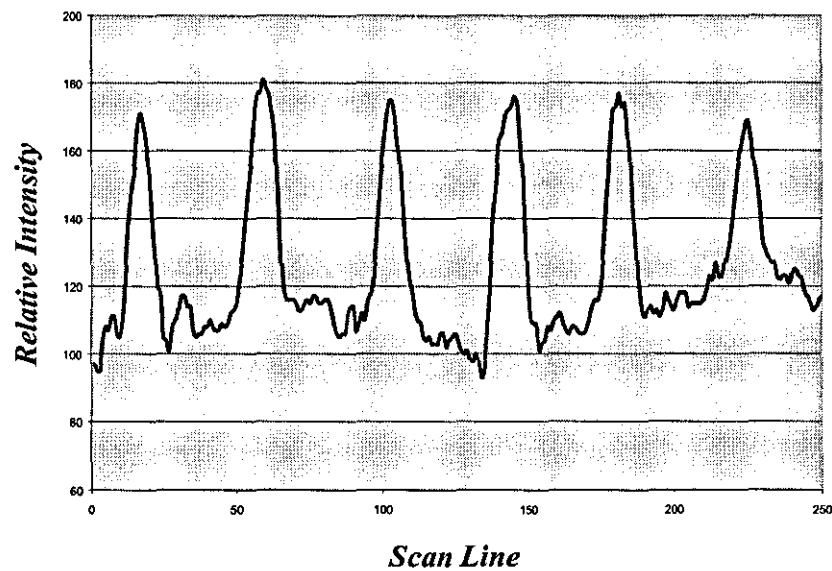


Figure 31 – Histogram representation of ROI relative gray-scale intensities

The maximum value in the resultant data series indicates the fundamental frequency of the sampled data. Dividing the total number of scan-lines by this value gives the corresponding wavelength. This is then used in equation 3.1 to yield the droplet diameter, affecting the hardware based on the difference between measured and target droplet size.

Previously reported techniques [11] incorporate a proportional control algorithm, which affects the frequency proportional to the magnitude of the control error. The processing time using the new algorithm is greatly reduced, and each individual cycle takes 150ms compared to a previously reported value of 700ms. One possible advantage of this method is that the measurement accuracy increases as the droplet sizes decrease. This is due to the fact that as the droplet diameters are reduced, more are present in a set distance and therefore examined by the algorithm, as opposed to fixing the number of balls to be assessed to make the measurement. Unfortunately the process is still limited by the response time of the CCD camera and the need to perform any size-pixel calibrations.

The value in pixels is converted into a real value by including a conversion factor, δ_{camera} , which can be calibrated by setting the camera at the desired focus and magnification and then measuring a known value. This is achieved, using the MIT equipment, by placing a calibration slide, with 3 fixed droplets a known distance apart, in place of the droplet stream before the run. A calibration program is then run which measures the distance between the droplets and because λ is known in this instance, the conversion factor can be calculated.

In an attempt to simplify this process an alternative method has been developed. As outlined in figure 32, the charging plates can be imaged and, because they will be in the same focal plane as the droplet stream, so the conversion factor will be valid as long as the camera is not adjusted. This removes the need to position an additional piece of equipment, the glass slide, and can be performed at anytime during the run.

The measurement lines are moved by the user to coincide with the known distance (i.e. their height). Entering this actual distance in millimetres gives the required real to pixels conversion factor, given by

$$\delta_{camera} = \frac{mm}{pixels} \quad (4.2)$$

Depending on the quality and power of the camera and its lens and the resolution of the computer screen this value has the potential to add large errors into the ball measurement algorithm. It is also very sensitive to changes in the magnification of the camera meaning that it is still not possible to adjust the camera in-situ once this value has been set.

3.3.1 Droplet-to-space ratio measurement method

Using the above DFT method some resolution is lost as the droplet diameter increases due to the discrete nature of the algorithm. In addition, the variation in perturbation amplitude, due to resonance and harmonic effects in the transducer, figure 33, leads to variations in the stability of the break-up as the frequency changes.

An alternative method has been derived, which also removes the need for any optical calibration, therefore eliminating a value for δ_{camera} . The feedback control variable can be determined from the linear relationship between the droplet volume and jet velocity. The jet velocity can be altered, by adjusting the pressure inside the crucible, which can be used to control the droplet size.

The effect of altering pressure is illustrated in figure 34, as the crucible pressure is increased, the droplet volume also increases.

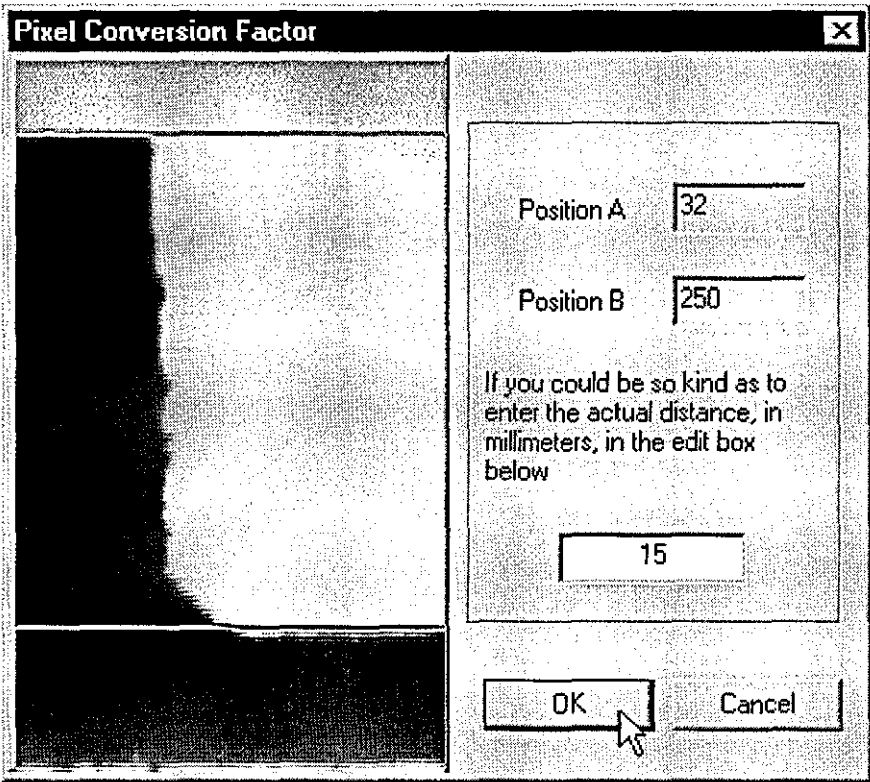


Figure 32 – “Pixel to Real” Distance Conversion Dialog

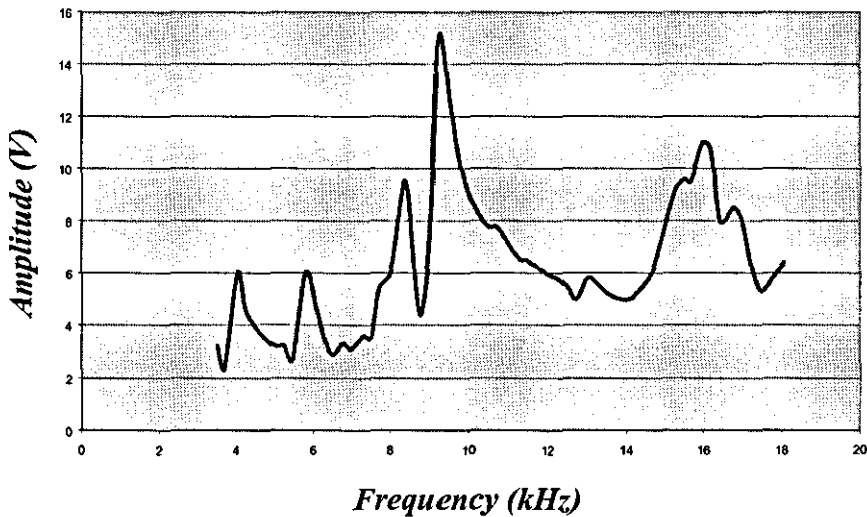


Figure 33 - Variation of disturbance amplitude with frequency

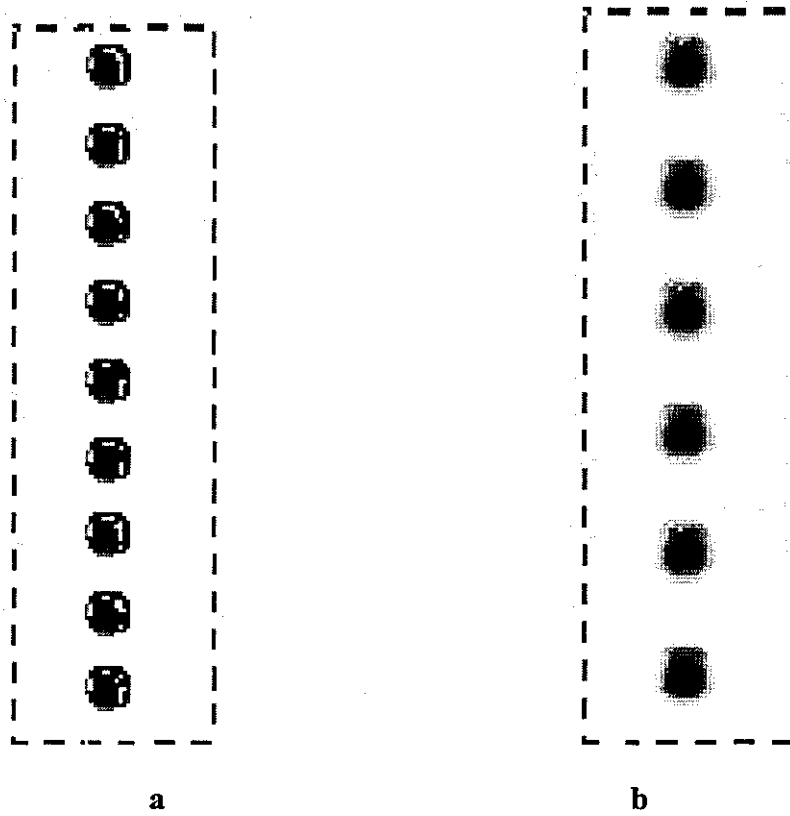


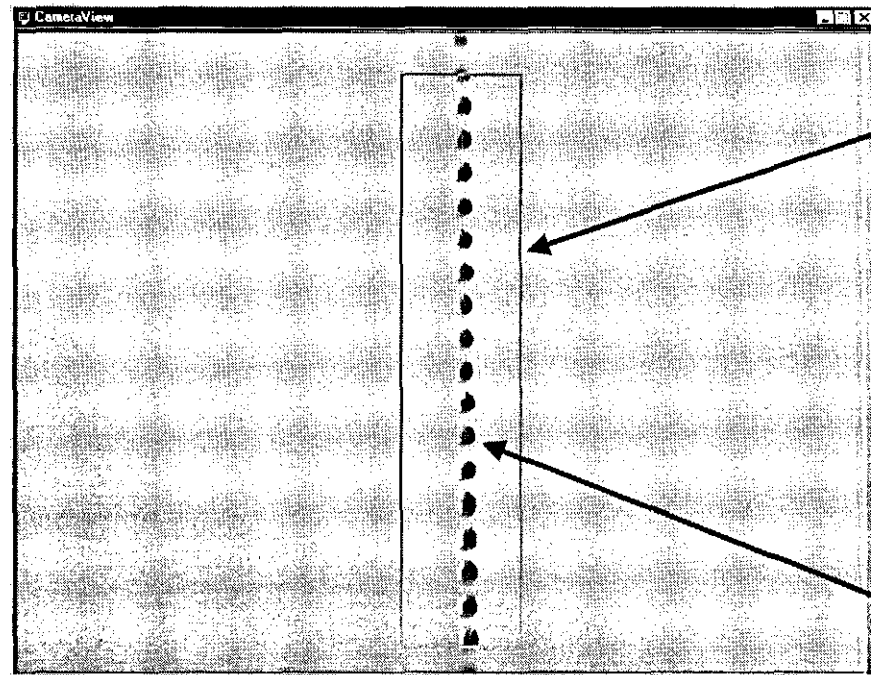
Figure 34 - Effect of altering pressure on water droplets issued through a 400µm orifice, using a constant perturbation frequency of 1500Hz; a) at low pressure (~5psi); b) at high pressure (~15psi)

3.3.2 Droplet volume control thread

Using an image of the droplet stream, captured using stroboscopic illumination (Chadwick-Helmuth model 109) and a CCIR camera linked to a muTech M-Vision 1000 Video Digitiser PCI board, the video digitiser board enables images to be 'grabbed' from the camera to the computers memory. The image is then segmented in order to highlight the area of the image that contains the droplet stream. The segmentation also serves to reduce the processing time needed to analyse the stream as the image processing operators do not need to iterate over the whole image. Using a graphical user interface (GUI) it is possible for the image to be segmented manually by the operator. The live video of the stream is displayed on the screen with a rectangle highlighting the region of interest superimposed on top, figure 35.

Using the ball space method as the fundamental control variable means that the need for camera calibration is eliminated since this ratio will remain constant no matter what magnification is chosen. This has the consequence that the user can alter the camera focus mid run without the fear of losing calibration. Using a modified version of equation 2.6 the software simply requires the user to enter the current orifice diameter and required ball size, figure 36. Once the program is set to feedback mode it constantly tries to alter the hardware in an attempt to align the measured ratio with the target. Using an average of the previous 30 readings the pressure is adjusted proportionally to the amount of error between the measured ratio and the target. The software code for this is outlined in Appendix 1, Listing A, Lines 110-128. Using the simple form of the incremental proportional control algorithm;

$$C = k_p e \quad (4.3)$$



By selecting a "region of interest" within the captured frame unnecessary processing can be eliminated. The user can alter this area at any time correcting for any errors in camera or stream alignment. By selecting a region close to the stream will reduce the potential of noise affecting the calculated ratio.

Edge detection operators can be optimised by the user. By altering the sensitivity of the sobel operators the detected edges give the position of each material sphere.

Ball Space Ratio is calculated from the number of scan-lines containing a leading edge (green) AND a trailing edge (blue) within the region of interest.

Figure 35 - Digitised Image of the Stream showing software location of stream

where the control action, C , is the change in the amount of voltage applied to the valve due to the error, e , in the ball space ratio. The constant of proportionality, k_p , is a user defined variable which relates to the change in valve position per control action. Software Code - Listing A, Lines 130-156. These values are controlled from the main program dialog window (see later, figure 40), which allows full control of the proportional control to the valve. The text box labelled Voltage Change (mV) is used to alter the constant of proportionality – if this is set to zero no action occurs. The 'Set Point (V)' relates to the nominal position of the valve at the start of a production run. Manual control of the valve is also possible using the Increase / Decrease buttons. Since the action of measuring the ball space error (Cycle Time), figure 37, takes less than 200ms it is necessary to inhibit a race condition occurring with the valve. A Time Delay is added where no control action is sent to the valve to allow for actuator movement.

In order to utilize the jet velocity as a feedback variable, a suitable set of algorithms must be established to monitor the droplet dimensions. Now consider two cylinders of material travelling at the same velocity. One being broken into discrete droplets at some frequency, f . By definition, over a distance they must contain the same volume of material. As the broken stream forms into droplets they separate by a uniform 'space', figure 38.

If all the droplets formed per unit time were placed side-by-side, and the length along the central axis, i.e. the sum of their diameters, was divided by the total space remaining, then in order to equal the length of the unbroken stream, it can then be written that the ratio

$$R_{ds} = \frac{\sum \text{Droplet.values}}{\sum \text{Space.values}} \quad (4.4)$$

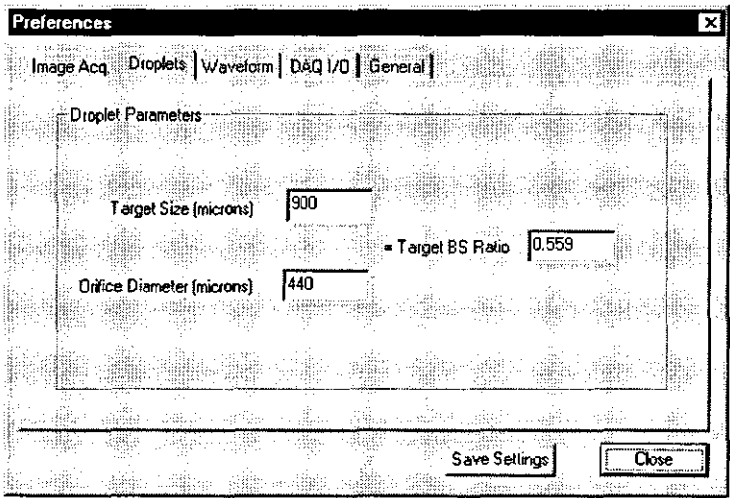


Figure 36 - Setting the target ball space ratio

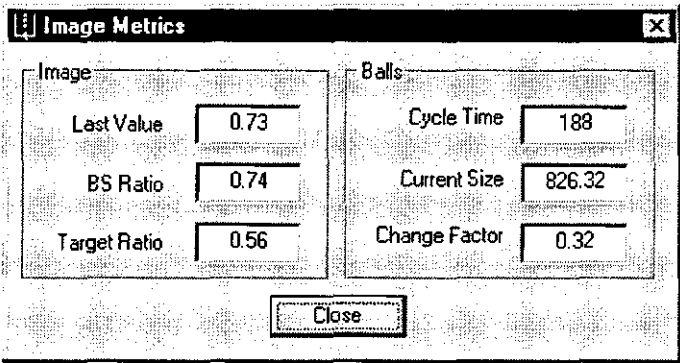


Figure 37 - Image Analysis Metrics Display

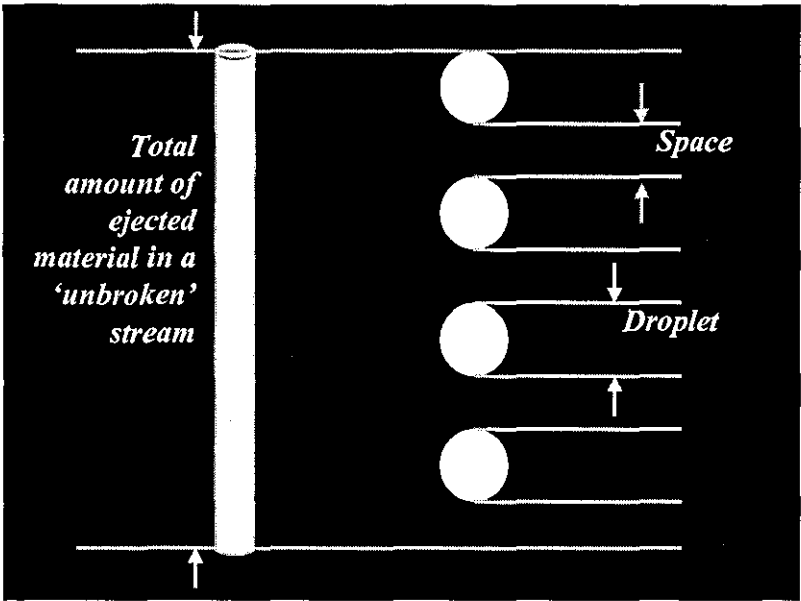


Figure 38 - Illustration of the droplet diameter length and space values in a uniform stream

If the stream is travelling at a velocity, V_j , R_{ds} is given by;

$$R_{ds} = \frac{\varnothing_D f}{V_j - \varnothing_D f} \quad (4.5)$$

The total volume of material ejected from the orifice over a unit time

$$V_t = V_j \pi \left(\frac{\varnothing_o}{2} \right)^2 \quad (4.6)$$

Combining (4.5) and (4.6)

$$V_t = \left(\frac{\varnothing_D f}{R_{ds}} + \varnothing_D f \right) \pi \left(\frac{\varnothing_o}{2} \right)^2 \quad (4.7)$$

The total volume of ejected material forming f number of balls if found from

$$V_t = \frac{4}{3} \pi \left(\frac{\varnothing_D}{2} \right)^3 f \quad (4.8)$$

Since (4.6) must equal (4.7)

$$\varnothing_D^2 = \frac{3\varnothing_o^2}{2} \left(\frac{1}{R_{ds}} + 1 \right) \quad (4.9)$$

The required diameter of material, \varnothing_D , including a solidification factor to take account of shrinkage during cooling or curing, is used to calculate an initial value for the target droplet / space ratio, R_{ds} . This is then used as a reference value for the feedback loop, and is found from

$$R_{ds} = \left(\frac{2S\varnothing_D^2}{3\varnothing_o^2} - 1 \right)^{-1} \quad (4.10)$$

where \varnothing_D = droplet diameter

\varnothing_o = orifice diameter

S = Shrinkage Factor (%)

The droplet to space ratio has been plotted against the droplet volume for a target diameter of 375 μ m, to demonstrate how slight adjustments to the ratio can influence the droplet volume, figure 39.

In this example, a droplet to space ratio of approximately 1.065 would be targeted to achieve a droplet diameter of 375 μ m. If the droplet to space ratio was controlled to within $\pm 5\%$, the diameter range would vary between 370-380 μ m, which equates to a diameter size control of 375 μ m $\pm 1\%$. This highlights how using the droplet to space ratio as a feedback parameter, offers the potential for very precise ball size control

The value for R_{ds} is stored, along with the orifice diameter, for use in the feedback algorithm. When the feedback system is initiated, the current value for R_{ds} is calculated by measuring the amount of dark pixels, representing the droplets, along the stream's central axis. This value is then compared with the target value affecting the pressure controller leading to the crucible.

The ratio value is of particular interest because it will function regardless of droplet size, wavelength or velocity; and only requires the orifice diameter to calculate the discrete volumes.

220 um orifice 11000Hz vibration freq

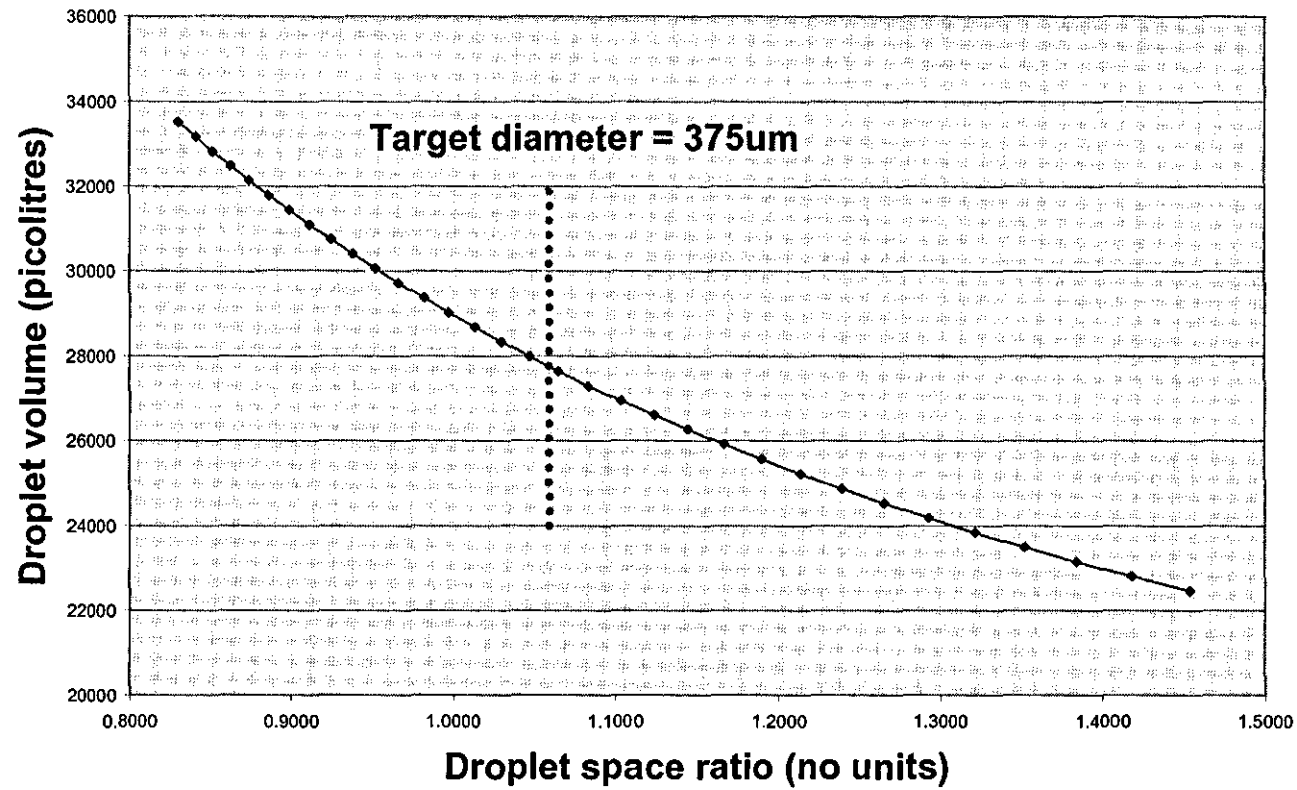


Figure 39 – Droplet volume with respect to the ratio of droplet to space due to increasing jet velocity

3.3.3 Gas flow sensitivity

As previously highlighted, it is considered that using pressure, as opposed to the transducer vibration frequency, will reduce resonance in the system. It was thought that because the control parameter is the separation between the droplets it would not be necessary to include feedback from the chamber regarding the actual pressure since the droplet space is inextricably linked to this value.

Using the pressure / flow control software based system outlined in figures 40 and 41, it is found that the cumulative effect of the unknown flow rates and response time of the control valve, the speed of control is too low to be effective. The control action from the computer opens and closes the valve on the exhaust flow. This is shown to change the droplet spacing non-linearly – since the opening and closing of the control valve does not directly relate to flow. This is highlighted in figure 42. The bright purple line represents a reference voltage from the valve indicating its open/closed position and the dark purple line indicates the action sent to the valve (control action is directly proportional to the error in ball space ratio). The graph of control action over time is indicative of proportional control over time but as can be seen the valve has a severe time lag. Since it has not been possible, to date, to quantify this instability with the current set-up, this is a topic for further investigation, using feed-forward control with the proposed gas control system shown in figure 43.

Satellite droplets can be observed when large changes in pressure occur during droplet creation. This is in accordance with equation 2.2 since the propagation distance of the stream before it is broken is being altered. To overcome this it is now necessary to alter the disturbance frequency to fix the amplitude of instability within the limits to create a stable stream.

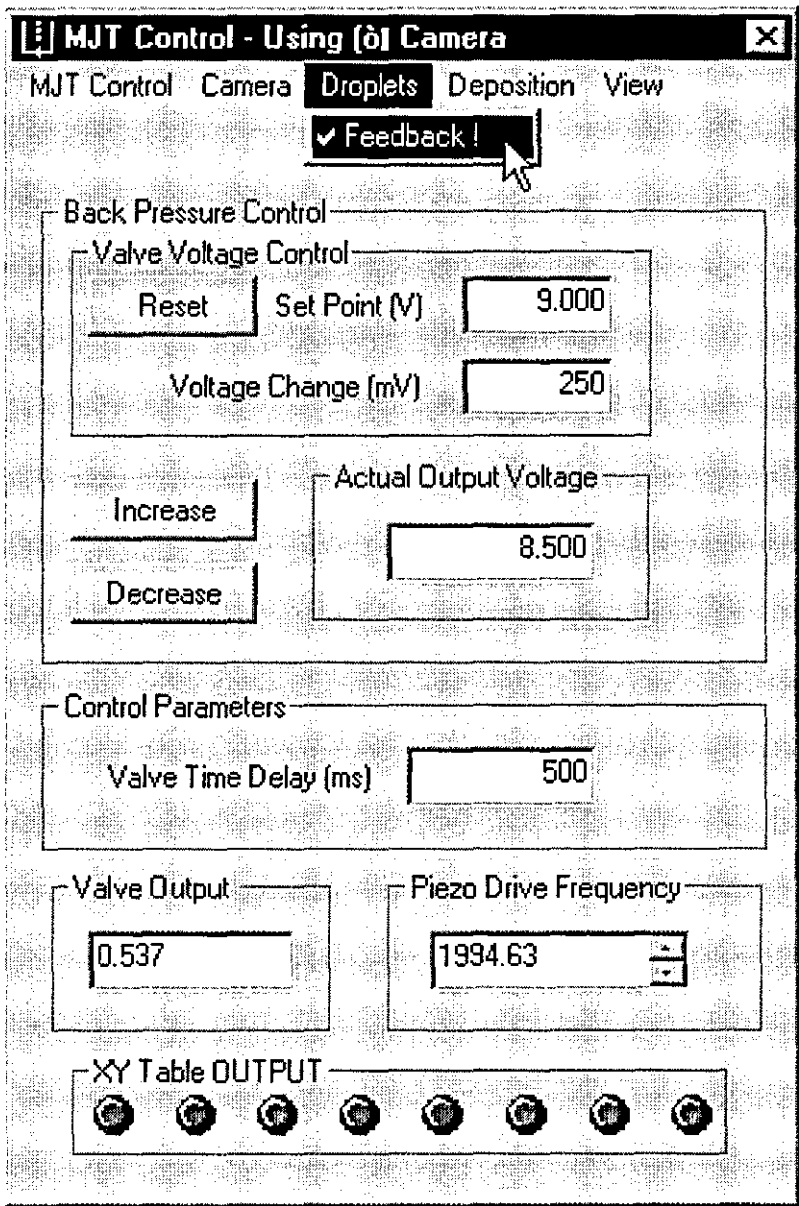


Figure 40 - Main Control Dialog

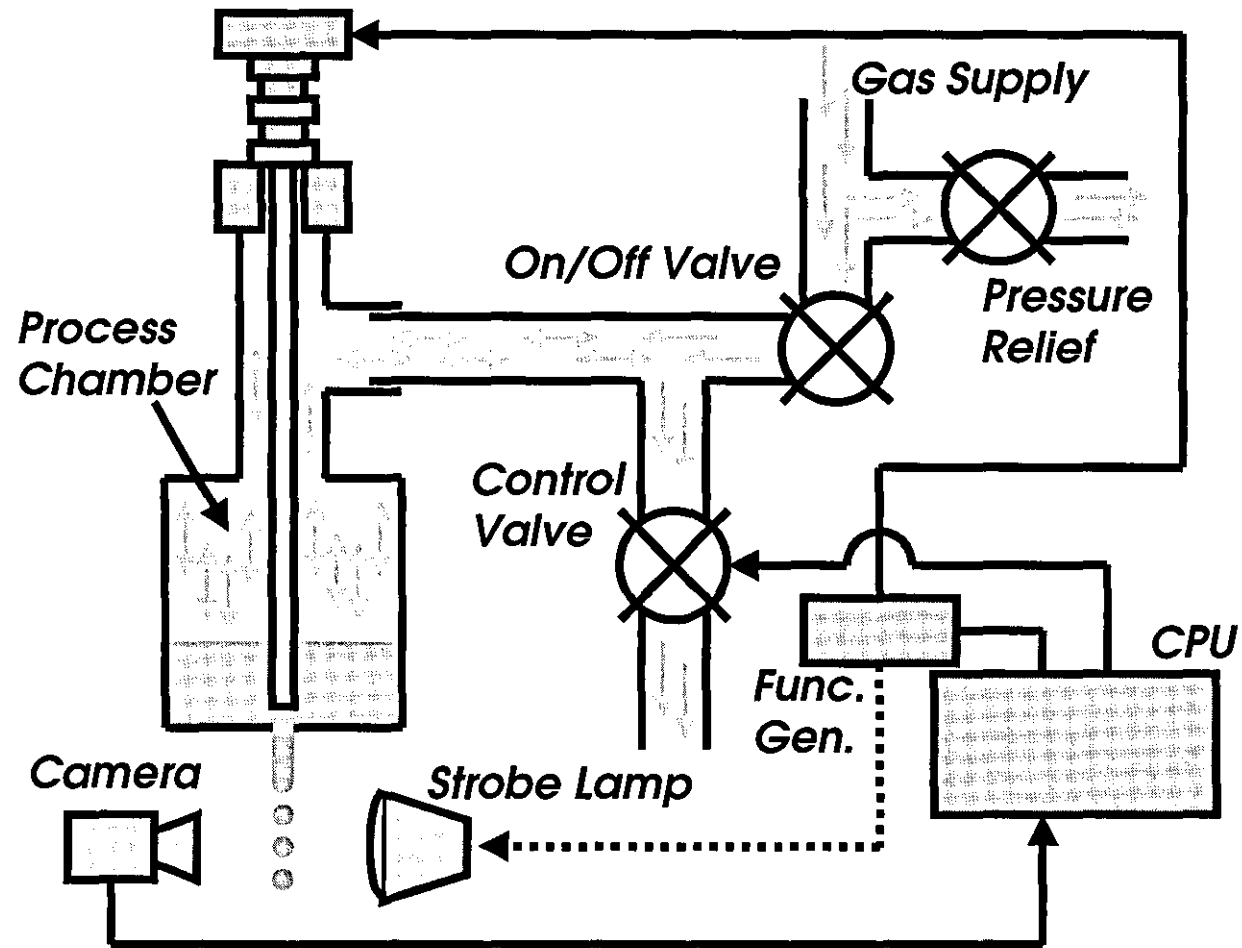


Figure 41 - Open Loop Pressure Control

Proportional Control
Created on 26/08/1999 at 11:04
Target Ratio : 0.74

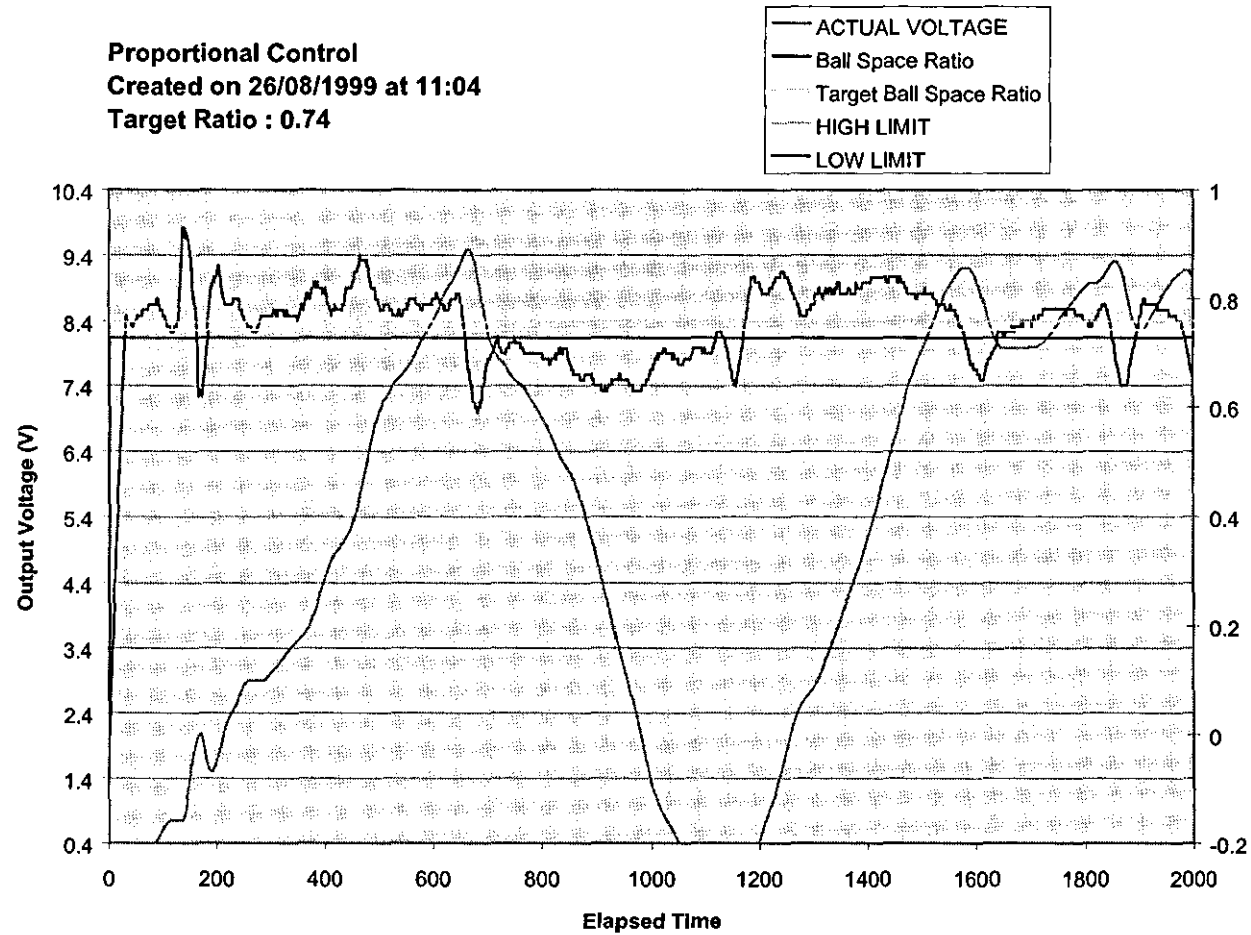


Figure 42 - Proportional Control of Control Valve

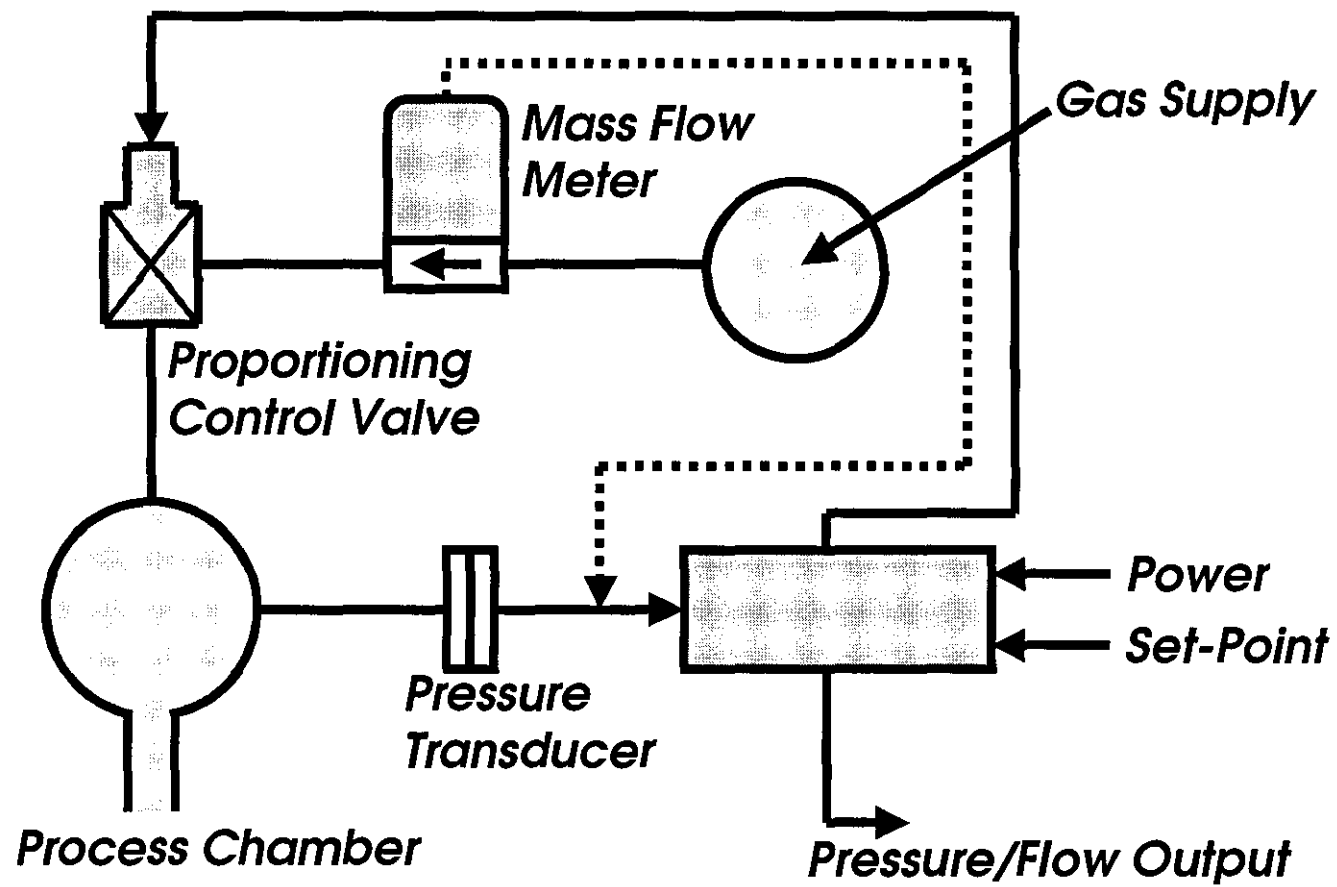


Figure 43 - Closed Loop Pressure Control (After MKS Instruments)

3.4 Substrate motion control

The ultimate aim of the technique is to deposit the jetted material upon a substrate. To do this, the ball production portion of the hardware control must be synchronised with the deflection of the stream and the movement of the substrate. Using a computer aided design (CAD) package, such as AutoCAD[®] LT, deposition paths are mapped out and, in conjunction with an additional software package, figure 44, can then be converted to a series of commands, which are downloaded to the XY table controller (Parker Hannifin Compumotor 6200 2 Axis Indexer).

The software supplied by Parker-Hannifin Corporation, entitled CompuCAM, which allows a drawing exchange format (DXF) image created in a CAD package to be converted to a text file containing a series of motion control instructions. This ASCII script file can be edited to include extra commands, which the motion controller hardware can use to synchronise with the jetting control software. Specifically, instructions need to be added to the script, which inhibit the substrate movement until the deposition thread indicates that the droplet size falls between the correct limits. Using a technique known as ‘handshaking’, an 8-bit digital signal is sent between the motion control hardware and the jetting control software via a data acquisition board (Data Translation DT302) installed in the computer.

If lines are added to the script file, to signify critical points in the path data, the motion controller will send a digital signal to the computer telling it to validate the droplet size. If the droplet size falls between acceptable limits then the computer will send a signal back to the XY table indicating that it is okay to continue tracing out the path, else the droplet control software will halt the XY table until the size measurement is satisfied. Once the script file has been created by CompuCAM and edited to include the extra commands it can then be imported to the droplet control software by selecting the option ‘->Deposition->Send Motion PRG...’ from the command menu , figure 45.

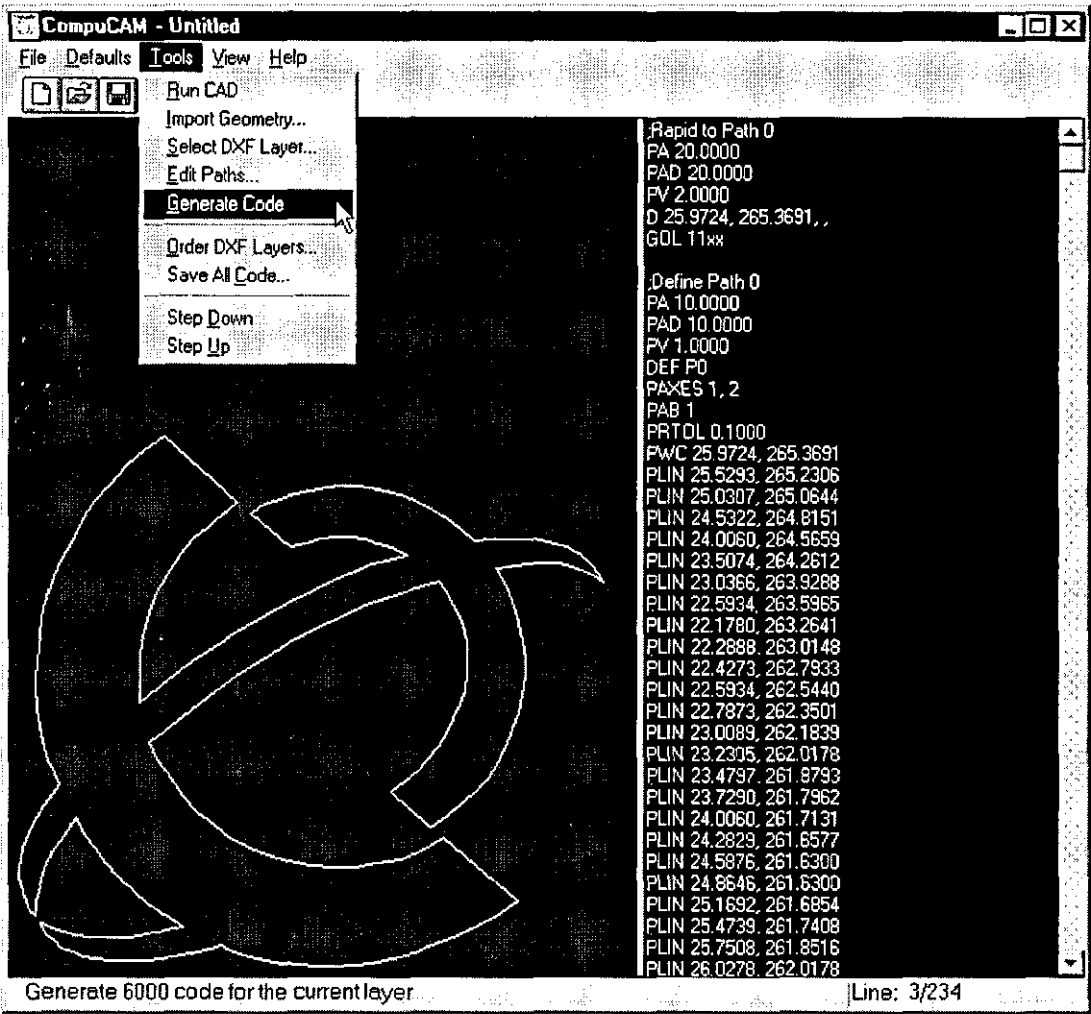


Figure 44 - Conversion from DXF CAD file to 6200 path data

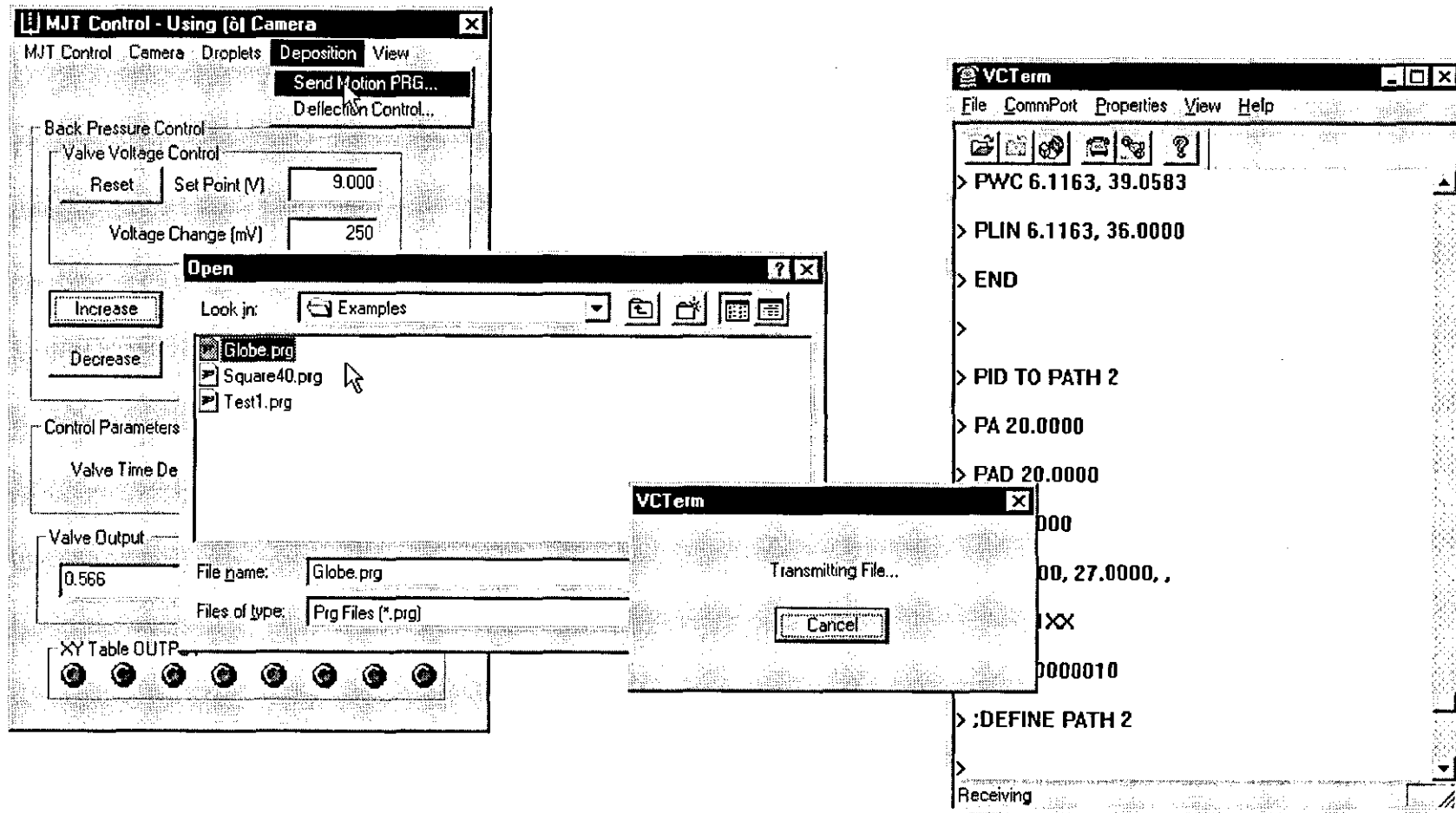


Figure 45 - Using the MJT Control software to download path data to XY table hardware

The user selects the desired path data that, in-turn opens a simple terminal emulator (enabling the CPU to communicate with external devices via the COM port), which downloads the data to the motion control hardware.

Built into the droplet size control algorithm is a command, which periodically checks the digital input from the data acquisition board, relating to the handshaking. Once the path data is resident in the XY table hardware memory it waits until a signal is sent from the size control thread indicating it is ready to start tracing the path and depositing material. If the total path is split into discrete sections, by handshaking commands inserted into the script file, it is possible to continually validate the droplet production throughout the run. This handshaking also enables deposition to be ‘switched off’ (i.e. the stream deflected) if the substrate needs to move to the beginning of a new section.

3.4.1 Manual Control

In some instances the apparatus may not be used for patterned deposition, e.g. for BGA sphere production. Therefore the user would need a more ad-hoc approach to the automation of the droplet production. By incorporating a manual control dialog, figure 46, the user can move each axis of the XY table separately and deflect the stream by a chosen amount. For example, the user can monitor the droplet production metrics displays whilst using the ‘Deflection & Collection Control’ dialog to move the collecting or waste vessels in and out of the stream.

3.5 Description of Ancillary Controllers

The control software is implemented under Windows NT Workstation 4.0 on a Digital Equipment Corporation (DEC) Pentium II 400MHz, fitted with the following Industry Standard Architecture (ISA) and Peripheral Component Interface (PCI) plug-in-cards to drive the piezoelectric stack, stepper motor controllers and capture images:

Deflection & Collection Control

Deflect

Voltage (mV)
1000

Position 1		Position 2		Position 3	
0	20	20	20	40	20

Home / Reset

Setup...

Save Params

Figure 46 - Manual XY table control dialog

- *µTech* MV1000 image grabber (PCI)
- *ETC* M321 frequency generator (ISA)
- *Data Translation* DT-302 Input-Output (I/O) (PCI)

A Hitachi VKM98-E CCD camera fitted with a RS Telescopic lens is used in conjunction with a Chadwick-Helmuth Slip-Sync-Strobex Model 109 stroboscope to freeze and capture images of the stream break-up.

ETC M321 frequency generator ISA card produces a sine wave between 0-40KHz, which is sent to the piezoelectric crystals and synchronises the pulse generator, to ensure that the images captured are synchronised to the droplet stream. The signal sent to the piezoelectric crystals is monitored on a Techtronix 7613 oscilloscope and is then passed through two-stages of amplification. The first stage is an InterM Personal Address Amplifier PA-1000B complete with a 333 ohm 100V speaker output, then the signal is amplified through a standard 160VA Toroidal transformer to produce an output (ac) signal of up to 300V.

3.6 Alternate droplet detection and measurement

An alternative method is proposed to measure the droplet to space ratio, which eliminates the need for image capture and software algorithms, enabling faster feedback that analyses every droplet as opposed to an extended sample. By positioning a laser-diode and photo-receiver at the centre of a focussed stream, the ratio of droplet to space can be monitored very accurately. One approach would be to use a series of optics to focus a collimated laser beam onto the centre of the droplet stream, then refocus the beam onto the photo-receiver to get the maximum amount of light onto the target, see Figure 47.

Optical method to focus collimated light source

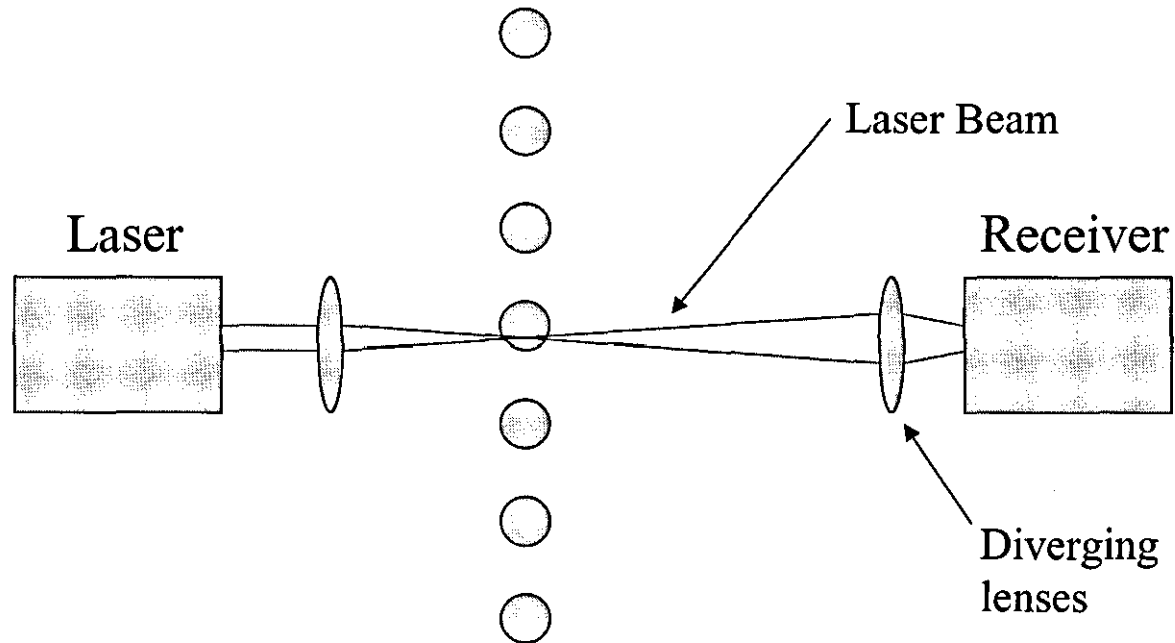


Figure 47 - Method of focussing the laser beam using diverging lenses (after Watts).

The output signal from the photo-receiver would be a real-time representation of droplet presence. Using appropriate signal conditioning (e.g. optical isolator and/or Schmitt trigger) the output signal of the photo-receiver could be made compatible with standard digital Transistor-Transistor Logic (TTL) circuits. An overview of the proposed measurement process is represented in figure 48. By generating a square wave using a stand-alone frequency generator, and splitting it into two paths, one half could be sent directly to a counter/timer and the other sent to an AND gate. The AND gate would also need to be connected to the output signal from the photo-diode.

Counter 1 represents the number of pulses received from the frequency generator when no droplets are present between the laser and receiver (i.e. a number of counts representing the total space measurement). Counter 2 represents the total number of pulses produced by the frequency generator during the time period. By subtracting the value of Counter 1 from Counter 2, it is then possible to obtain the value for the droplet presence (i.e. the number of counts for the droplet presence measurement).

This concept was tested using an integrated diode and photo-receiver detecting the movement of a needle (~5Hz) with a Data Translation DT-302 data acquisition input/output (I/O) board and a personal computer (PC), but a full demonstration model using a laser-source and the necessary optics still needs to be conducted. The potential advantages of this set-up over the conventional image capture and software analysis are:

- Response time could be reduced from 150ms to <100 μ s.
- Resolution of the measurement would increase.
- Every droplet would be evaluated during the sample period.



Figure 48 - Overview of proposed closed-loop feedback mechanism (after Watts)

4 Process Development 2 - Hardware

Development and Test

To use the continuous mode jetting (CMMJ) technology for material production and deposition, the orifice is the most critical element to achieve the necessary uniform material break-up. The high speeds at which the material exits the orifice inhibit active correction of the stream. No suitable detection method could be implemented in this system, without it becoming the main source of cost, to redirect bad material from the deposition site. Therefore, a repeatable and robust design of the exit orifice is necessary to guarantee the quality and direction of the stream to ensure no damage is caused to the substrate.

Any detritus or irregularities on the walls of the orifice will cause the stream to be deflected and, similarly, if wetting of the molten material happens inside the exit hole of the orifice, the jet consistency and direction will be affected.

The original orifice mounting method designed at MIT, was to cement a tiny sapphire gem, figure 49, to a counter sunk hole in the centre of the crucible flange using a high performance ceramic material, Autostic™. The gems, supplied by Bird Precision Orifices Ltd, are made with high-grade material and machined with precision holes, guaranteeing a circular aperture throughout the depth of the crystal, ensuring good stream break-up and minimised wetting. However, mounting the gems to the base plate of the crucible in this manner leads to the following difficulties:

It is impossible to predict the direction of the jet stream until the equipment is running, because it was difficult to guarantee the small crystals' co-planarity with the bottom of the crucible. The directional error in the stream was randomly inconsistent with each run being up to 5° off the perpendicular.

Only a **limited number of experimental trials** could be performed on the equipment each day, because of the lengthy drying time that was needed to fix new gems in place.

The orifices need to be replaced after each trial because the **adhesive cement suffered from fatigue stress**, cracks would appear eventually resulting in the crucible leaking. Figure 50 shows cracks in the cement allowing solder to seep through and figure 51 shows one example where the orifice was completely blown out due to the cement failing. Both instances allowing large drops of solder to leak onto the substrate, one being much more destructive than the other but both equally unacceptable.

Also, the **additional gasket material** needed to secure the crucible flange (not shown) to the crucible, also leaked on occasion, causing catastrophic failure, preventing the equipment from being used until dismantled and cleaned.

4.1 Orifice redesign

All of the above points indicate a non-repeatable process that could not be transferred to high reliability device manufacture. In an attempt to resolve these problems, two alternative methods for orifice mountings and design have been investigated, figure 52. Both methods remove the need for cement, and help to reduce the variation in the stream direction.

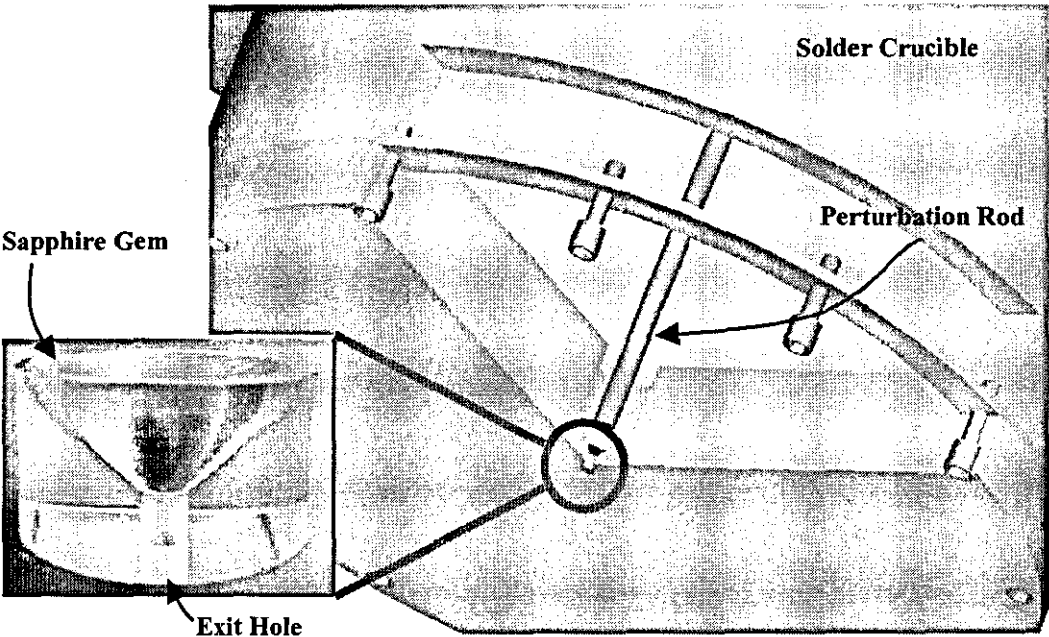


Figure 49 - Illustration of the MIT mounting method using Bird Precision sapphire orifice

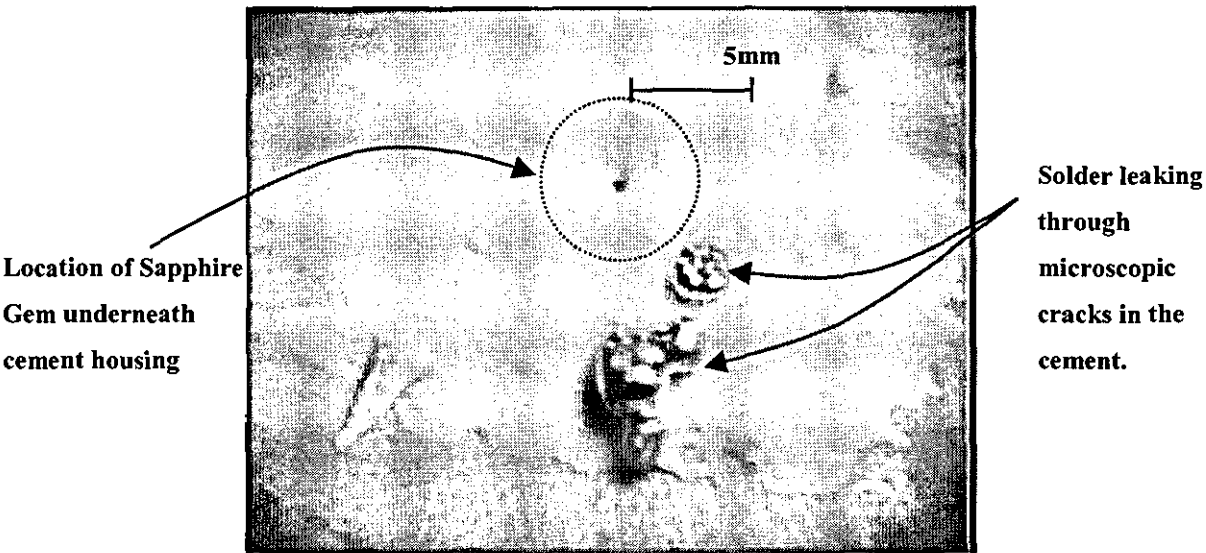


Figure 50 – Non - catastrophic failure of the cement holding the sapphire orifice

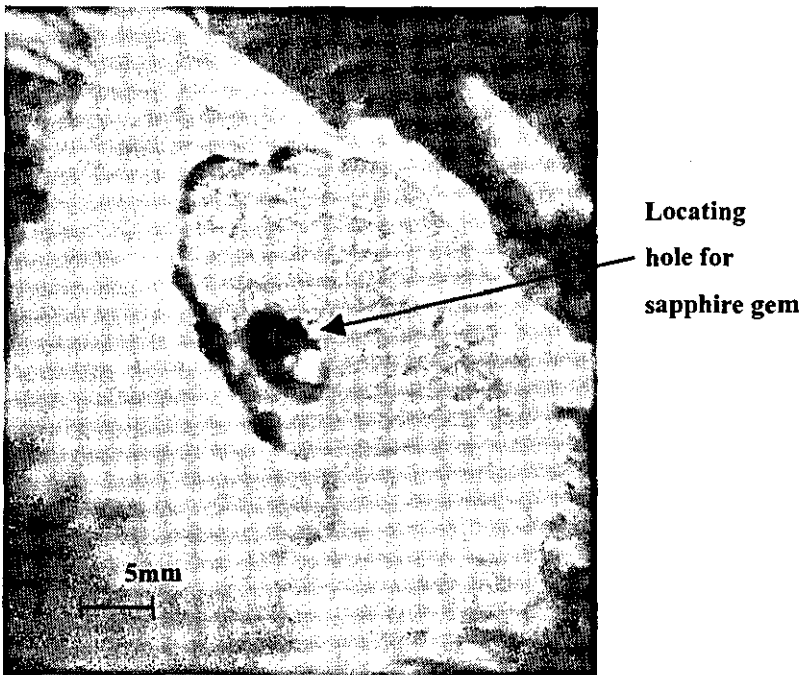


Figure 51 - Result of catastrophic failure of the cement holding the sapphire orifice

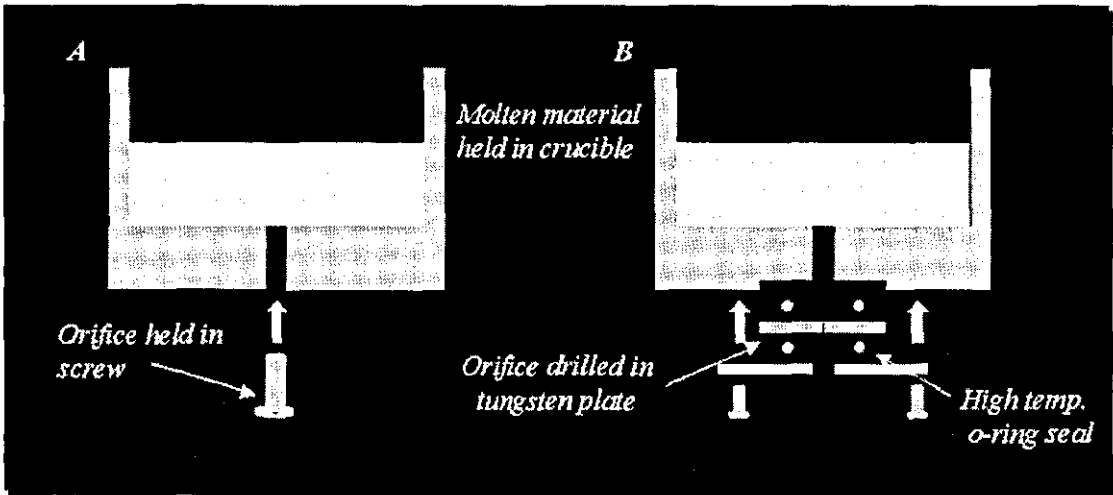


Figure 52 - Alternate methods for orifice mounting

4.1.1 Orifice pre-mounted in a component

The solution shown in figure 52A uses a pre-machined orifice gem with the same design and quality to that used by MIT. However, in this configuration, instead of having to fix the gem to the crucible using cement, it is supplied pre-mounted in a simple hex head brass bolt of specifiable dimensions. The parts, supplied by Cooper-Walker Microelectronics, based in Edinburgh, are fitted with an orifice having an aspect ratio of approximately 5:1 (wall length to aperture diameter) and are interference fitted inside the bolts. The bolt is screwed directly into the crucible, with a high temperature gasket material, offering the following advantages:

- The time taken to change an orifice was significantly reduced;
- Each orifice could now be used more than once; and
- The jet direction variation was reduced.

After experimental trials, the orifices, still had inconsistencies due to the following observed issues:

- Solder was capable of wicking down the thread of the bolt and leaking out of the crucible.
- Variation in the jet-stream direction was still observed in some samples, but was now limited to 2° off the perpendicular.

Brass had been chosen specifically to prevent the solder wicking down the thread, because it has a higher coefficient of thermal expansion than the stainless/steel crucible. It was anticipated that this would seal the gap in the threads when jetting materials above room temperature. To overcome this wicking problem, a washer and gasket material (Klingersil™ C4400) were introduced to prevent any leakage occurring. Figure 53 is a photograph of this set-up, showing the hexagonal-headed bolt fitted to the bottom of the crucible.

During the testing of the components, occasional random movement of the stream was observed. Although this movement did not occur very often, and the stream variation

was far less than 4° off the perpendicular, there was considerable potential for the material to coat the charging and deflection plates during trials. MIT have also reported this stream variation using the original orifice cementing method. Shin [33] references this phenomenon in a feasibility study of the droplet generation equipment and has theoretically calculated what is referred to as ‘jumpiness’, averaging 0.005° over 10 runs. The jumpiness is thought to be a result of the orifice vibrating within its mounting, and is most pronounced using higher material through-put rates.

One potential concern with mounting the gem using an interference fitting is the possibility of blowing the orifice out of the component. This has occurred once at 350°C with a crucible gauge pressure of 25 p.s.i. and is most likely to occur as the crucible temperatures and pressures are increased.

4.1.2 Laser-machined holes

An alternative to mounting single crystal materials with pre-machined holes is to create a precision hole directly in the jetting crucible (using suitable materials). In practice, it is not feasible to create a number of different crucibles to accommodate different orifice diameters for the experimental laboratory equipment, so a variation using a larger orifice plate and metal flange was designed to fit different orifices to the same crucible, figure 52B.

Figure 54 shows in detail how the present crucible design can be adapted to accommodate a 25mm square metal plate with laser-drilled orifice. A recess slightly wider than the aperture leading to the orifice is created to house a high temperature gasket material. The plate is held firm against this using a recessed flange, secured using bolts, with a drilled material flow aperture and additional gasket material. This flange has two secondary functions – it acts as a housing for the charging plates and because of the larger footprint of the plate it can be used to adjust the angle of the orifice, hence stream direction, by differentially tightening the securing bolts. Potentially this action could be automated using closed loop feedback control of the material flow and powered threads for the bolts.

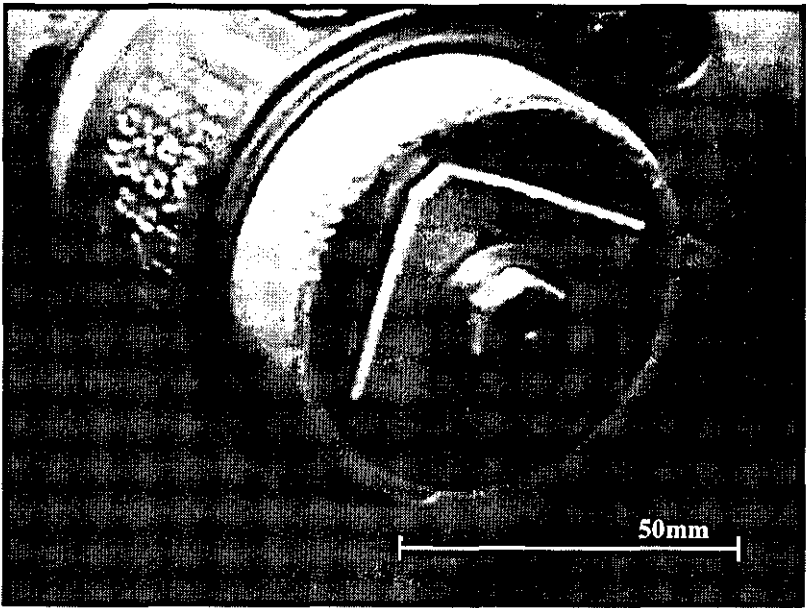


Figure 53 - Orifice pre-mounted in bolt screwed into crucible

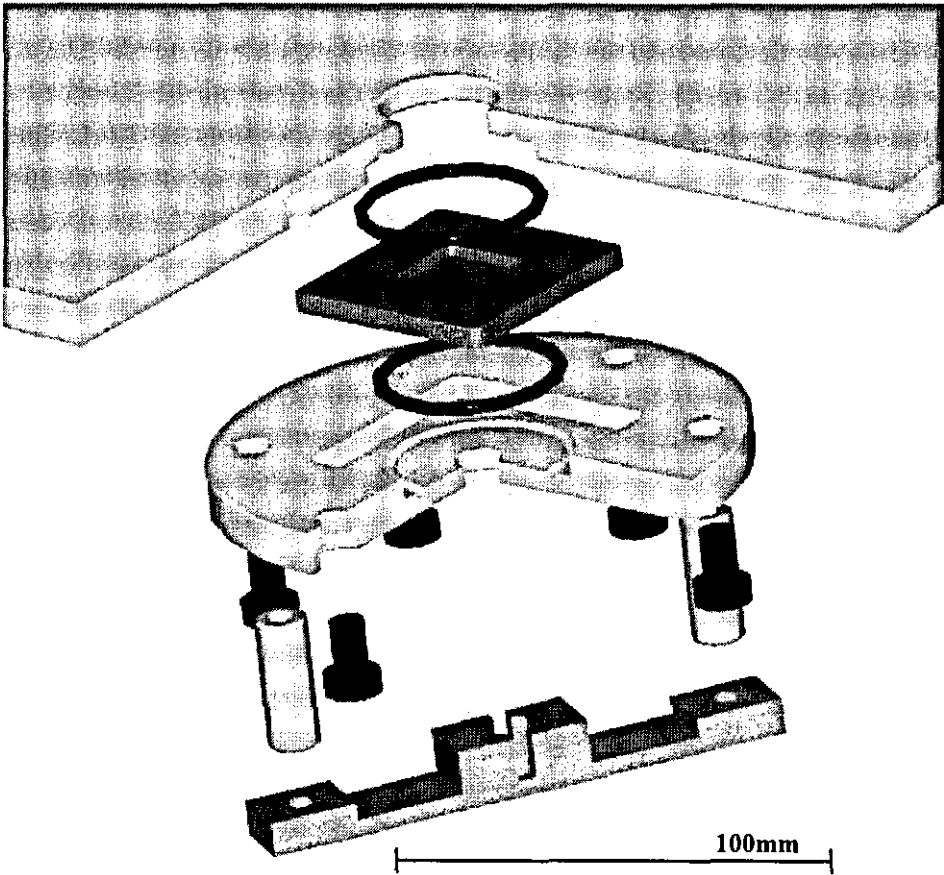


Figure 54 - Metal orifice plate - mounting concept

Laser drilling of the orifice means that the thickness of the material, used for the plate, limits the choice of orifice diameter and taper. Because of the focussing of the laser beam angled walls are formed on holes with a large aspect ratio. For this application straight walled holes are required, to ensure that the stream does not atomise, so a minimal taper is required, as outlined in table 2.

Material thickness	Orifice diameter	Taper
1000 µm	40-1000 µm	5-100 µm
500 µm	30-1000 µm	5-50 µm
200 µm	5-1000 µm	10-30 µm

Table 2 - Information on material thickness, orifice diameter

A fine grain metal is preferable to a single crystal or ceramic material, because higher machining precision (>5µm diameter holes) can be achieved using a (copper-vapour) laser. Tungsten plates of dimensions 25mm by 25mm, and 1000 µm thickness were chosen. These were then spark eroded in the centres to reduce the wall thickness to approximately 200 µm, figure 55, so that the taper is minimised.

Tungsten was selected as a suitable orifice material because it does not alloy with the standard materials used in electronics soldering, it has the highest tensile strength of any metal above 1600°C [34]. Tungsten is therefore a suitable material for the levels of pressure (<100p.s.i.) required to jet material through orifices below 50µm diameter. Pure tungsten is also available in a very fine grain structure, therefore allowing for precision machining using lasers.

AEA Technology [35] and Exitech [36] are specialists in laser micro machining producing holes in metals for fuel injection systems and ink-jet nozzle plates. These examples, figure 56, were produced by AEA Technology, Abingdon, using a copper vapour laser but similar results can be achieved using excimer illumination (Exitech).

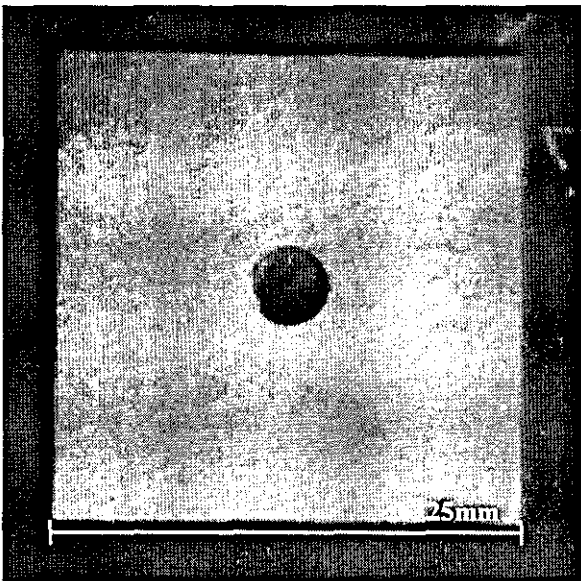


Figure 55 – Tungsten plate with spark eroded recess for laser drilling of orifice

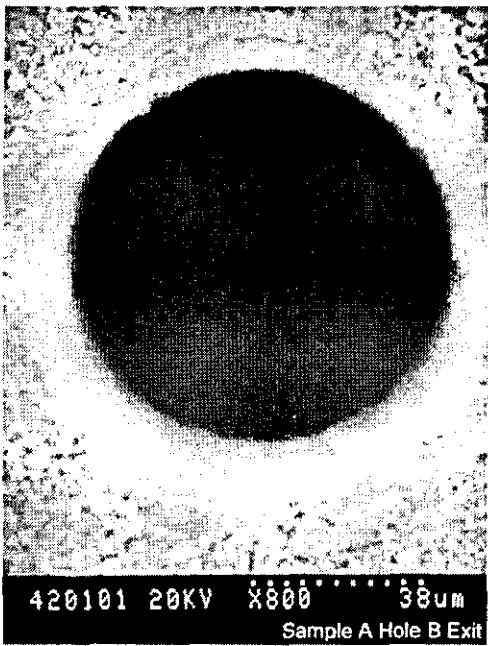
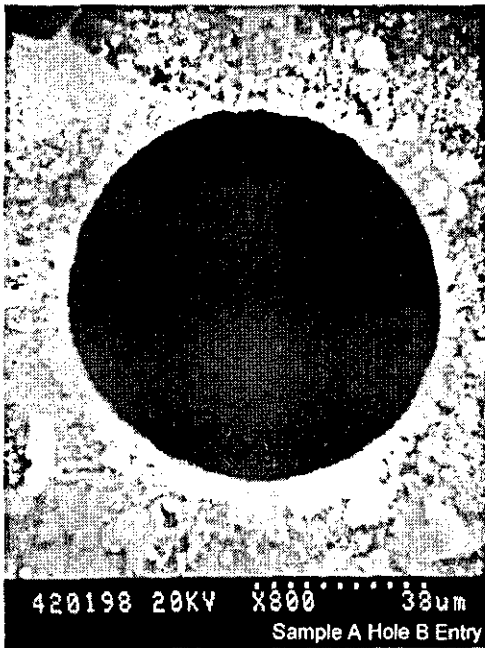


Figure 56 - Laser drilled holes in Tungsten plate

Trials were conducted to confirm that uniform break-up could be achieved and to establish the repeatability of the laser drilling process. The results were promising, showing that uniform droplet break-up was possible and that two adjacent holes machined independently would produce two parallel jets.

Further discussions with AEA Technology regarding the possibility of taking a hex-head bolt and profiling a similar orifice was also believed to be achievable at a cost of about £150 per sample. Although this has not been tested yet, it is thought to be an ideal method of manufacturing orifices that can be quickly attached to the equipment. The previous trials using the Cooper-Walker mountings had successfully proven the method of rapidly changing different orifice sizes. If the orifices were manufactured in this manner in the future, then much higher temperature materials (above 1000°C) could also be jetted using a graphite crucible, without any risk of the gems being blown out. It is also thought that the stream variation would be minimised.

The Cooper-Walker orifices were most suitable for the laboratory equipment because they only cost £3 and can be delivered within a two-week timeframe. This allows for a wide range of orifices diameters to be tested on the equipment at a low cost.

A more in depth costing and performance study needs to be conducted to analyse the most cost effective method of orifice production since neither method is 100% reliable. Both mounting methods still have the potential to leak and produce stream variation, figures 57 and 58.

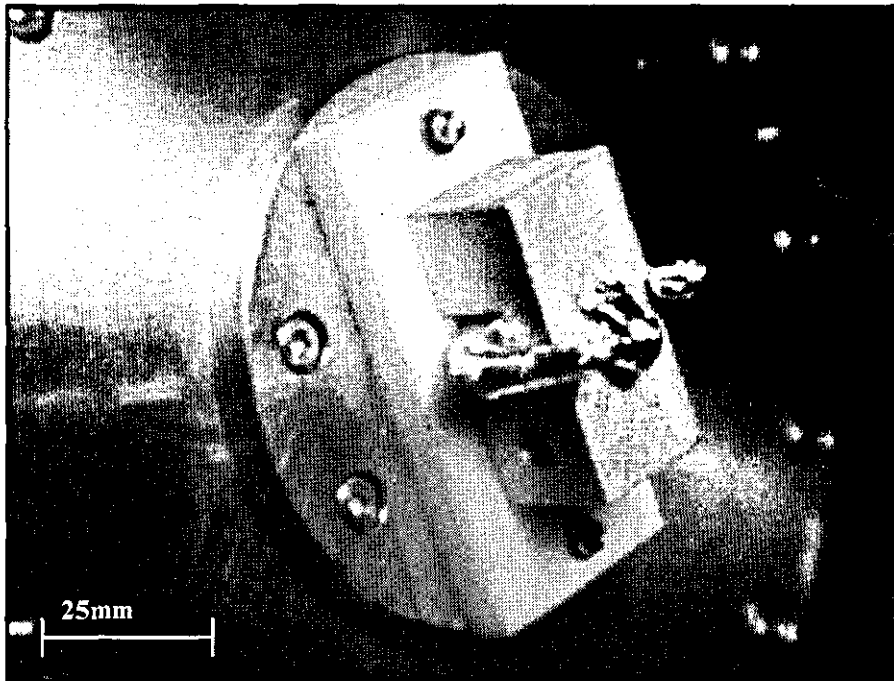


Figure 57 - New laser drilled orifice with temporary charging plate design after stream directional variation causes build up of solder on the charging plates

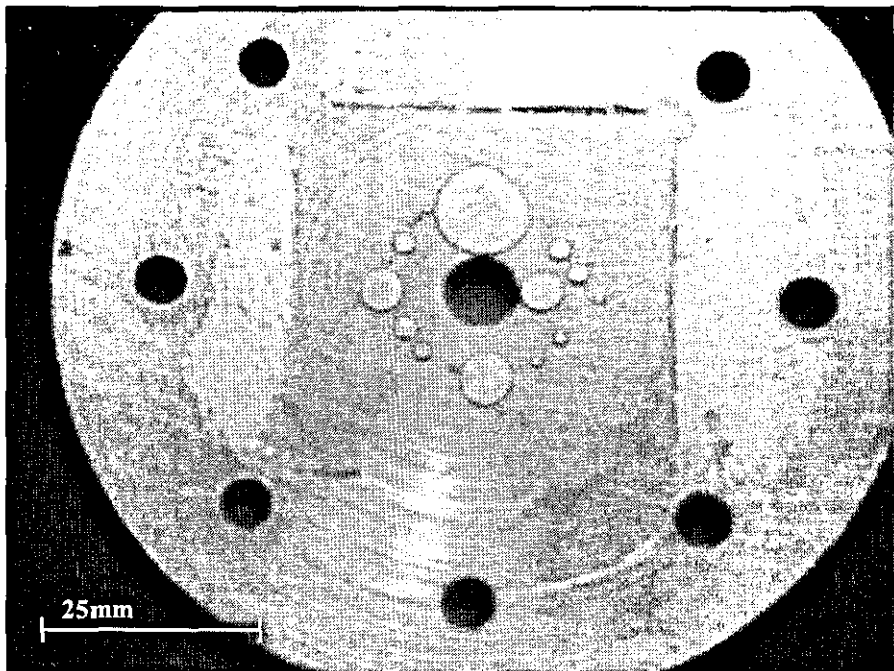


Figure 58 - Build up of solder at various points at the gasket / plate interface

4.2 Lead Free Solder Sphere Production

In January 2004, all companies will be forced to reduce the content of lead in electronics and optoelectronic products to less than 0.1% in order to comply with the Waste Electrical and Electronic Equipment (WEEE) draft directive, being prepared by the Environmental Division of the European Union (EU). The majority of solder spheres used in electronics packaging at the present time contain enough lead to become affected by the WEEE directive, so lead-free alternatives need to be identified. Using the Cooper Walker orifice designs, several diameters of balls for BGA applications have been created using an array of novel and lead free solder types, table 3 [37].

Lead-free Alloy	Composition
Tin/Copper	Sn99.3 Cu0.7
Tin/Silver	Sn96.5 Ag3.5
Tin/Copper/Silver	Sn95.8 Cu0.7 Ag3.5
Tin/Antimony/Copper A	Sn97.5 Sb0.5 Cu2
Tin/Antimony/Copper B	Sn91 Sb6 Cu3

Table 3 – Lead-free alloys identified for potential use in electronic products

Ideally the jetted spheres would be allowed to cool completely in an N₂ atmosphere but this means that larger ball sizes would need a flight distance of over 3 metres. In order to overcome this space issue a cylindrical vessel filled with ethylene glycol based oils is used to collect the spheres. The oil is differentially heated so that the droplets are slowed gradually on entering from the gas atmosphere reducing the deforming effects of the liquid. Figures 59 and 60 show an example of spheres jetted by this method using the Nortel laboratory set-up. In this case the alloy SnSb6Cu3. Three phases appear to be present in the microstructure; the primary phase (white needles on the photographs) is thought to be a tin/copper inter-metallic compound (Sn₆Cu₅); the secondary phase is a pseudo-binary eutectic (grey petal shaped areas surrounding white needles) of possibly tin/antimony; and the third phase is the ternary tin/copper/antimony eutectic (darkest areas).

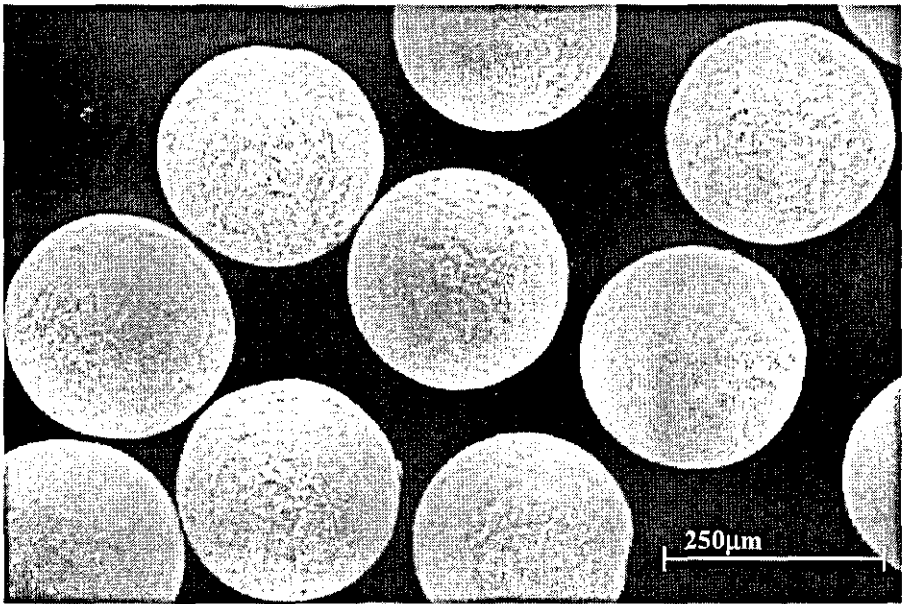


Figure 59 – SnSb6Cu3 solder balls (x40 mag.)

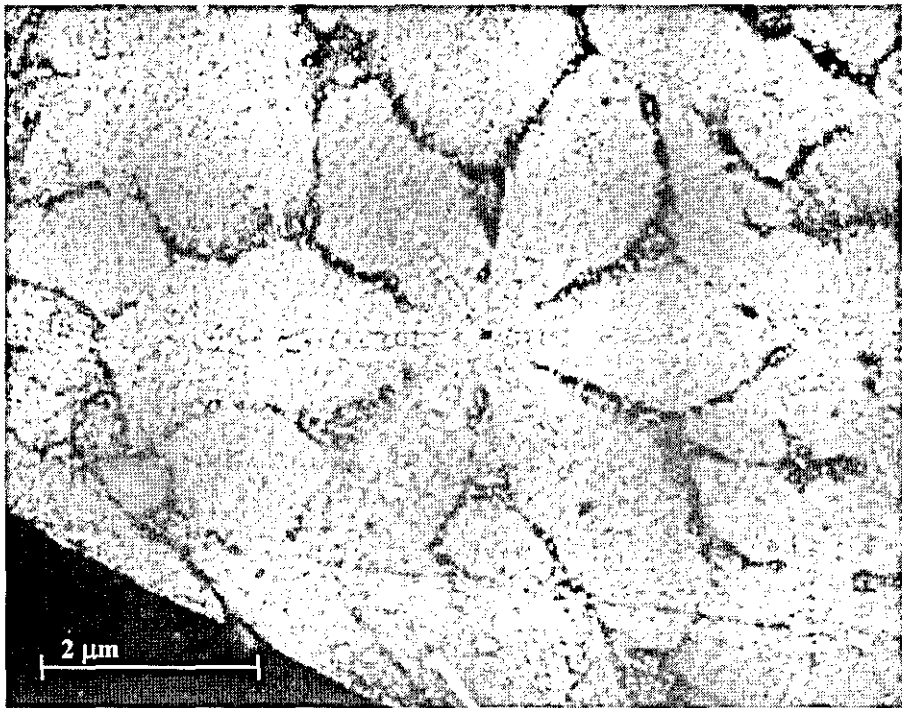


Figure 60 - Cross Section of SnSb6Cu3 solder ball – note the petal-like material structure.

4.2.1 Other Orifice Samples

The Mechanical Engineering department at Loughborough University produced some samples to test the micro-machining capabilities of the tungsten plates using CO₂ lasers, figure 61. These samples allowed the investigation of the importance of jetting through a circular hole.

It was concluded that it was not possible to create uniform droplets using non-circular orifices. Perfectly circular orifices produce very stable jet streams because any liquid stream will naturally form a shape with the lowest surface energy, or area, creating a cylinder. A non-circular orifice initially creates a non-cylindrical shape forcing the stream to adjust itself, until it becomes stable. This additional fluctuation in the stream is predominant over the pressure variations created by the vibrating rod, and the driving frequencies are lost in the noise.

4.3 Stream control

As previously outlined, the success of continuous mode materials jetting is highly dependent on the orifice. The main problem when using a pre-mounted orifice is the inability to predict the stream direction, and this has resulted in the jetting material coating the deflection and focussing plates. To date there are no reports of a highly predictable stream generator. Consequently, it has been necessary to develop a method of altering the direction of the stream and position of the deflection and focussing plates during trials.

The University of California Irving (UCI) has developed a system, figure 62, that has the most impressive control over the continuous mode technique and shown some novel droplet manipulation techniques to overcome the variability in the jet.

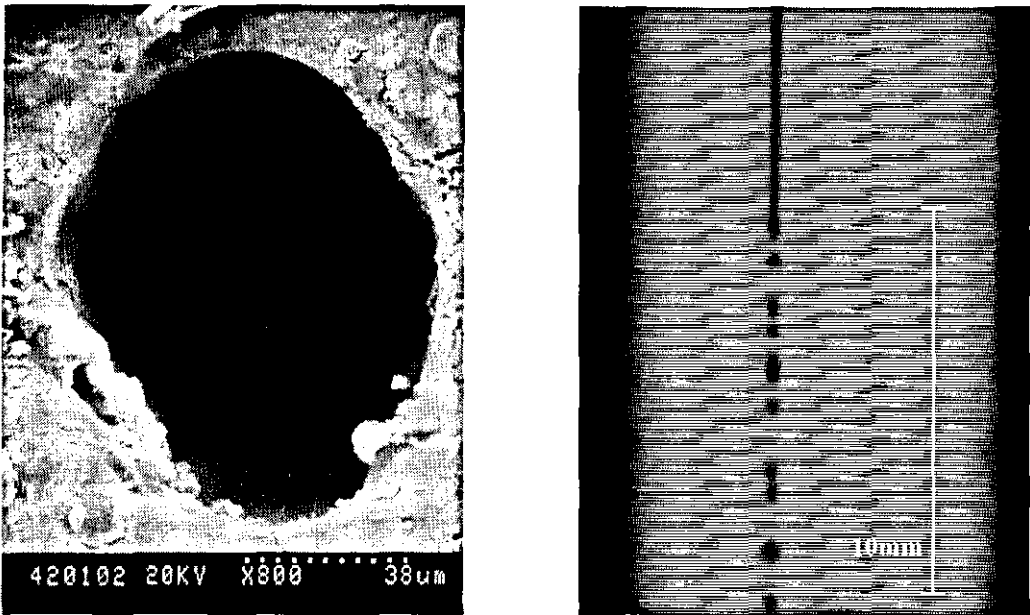


Figure 61 - Excimer ablated hole and non uniform break-up of stream

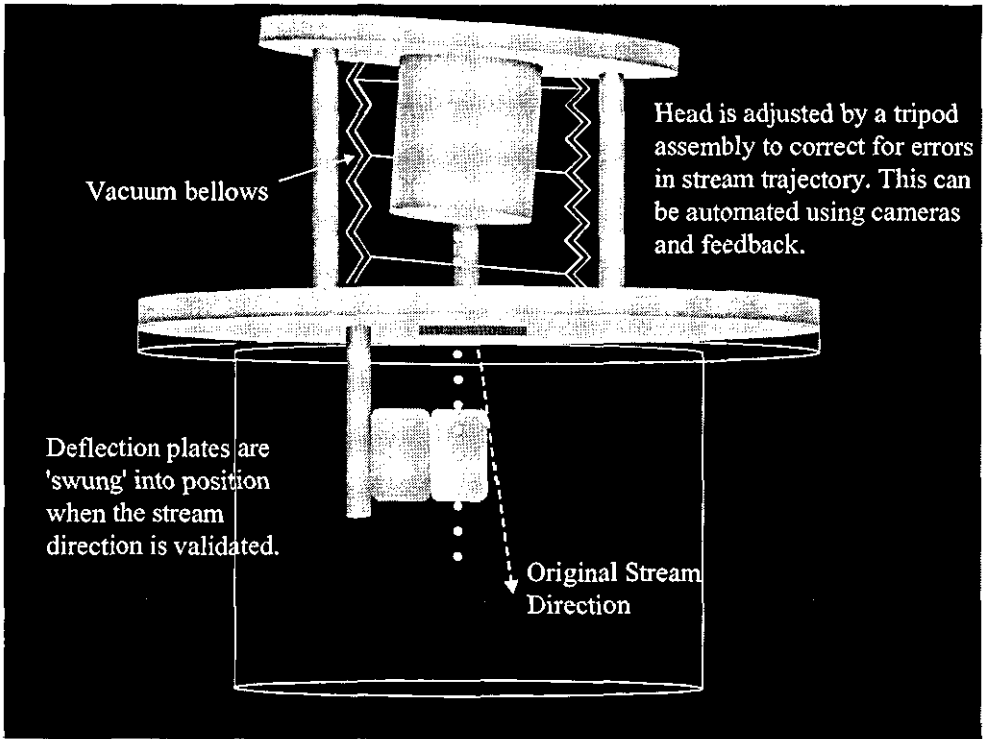


Figure 62 – UCI adjustable head design

The UCI set-up is similar to the MIT equipment in concept but the main distinction is that the droplet control systems implemented by UCI are far more advanced and succinct, enabling automated deflection of the stream. This stream direction is corrected by mounting the jetting head on a tripod-like arrangement and adjusting its position using a computer controlled closed loop feedback system. Stepper motors are used to affect the alignment of the crucible, and therefore orifice, back to a pre determined angle. The charging plates are still attached to the crucible but the adjustable screws allow for any errors in the stream to be corrected and the stream to be aimed through the deflection plates. The stream is constantly monitored during each run to allow for correction of drift in the direction, which could occur due to dross build up or wetting of the orifice. The UCI system uses a 'print-on-the-fly' technique that means that patterns are created by substrate movement in one direction and electrostatic deflection in the other. This greatly improves the pace at which droplets can be deposited. It is previously reported that printing on the fly is susceptible to variations in ball size, and therefore a tight dimensional tolerance is required during the droplet generation. UCI claim that without incorporating closed-loop feedback they can produce droplets using a 100 μ m orifice to within 10 μ m variation. Modelling of this has been validated with experiments.

This section describes the improvements that were made to the Nortel jetting rig in attempt to accommodate the inconsistencies in the jet direction. The aim is to introducing an adjustable crucible arrangement that allows for stream direction to be adjusted from the outside of the chamber. Also, to incorporate two rotating branches into the equipment, one for each side of the stream, which will allow for the addition of focusing and deflection elements.

The method involves separating the jetting flange into two parts, a main flange for the gas and electrical connections, and another to control the stream direction.

Figure 63 illustrates how the arrangement allows for the attachment of various beam deflection elements into the droplet stream. In this configuration only deflection plates have been added for simplicity but the branches give provision for future developments in stream focussing and catching to be added. The charging ring is suspended from the larger flange and is static. The adjustable branches are constructed

out of ½” copper pipe to provide structural stability and also to prevent static build up. The deflection and focusing plates are constructed using stainless steel and insulated using PTFE.

The voltage applied to each pair of plates will determine whether the stream will be deflected or focused. Since the droplets are negatively charged, negative charges must also be applied to parallel plates to focus the stream. If there is a potential difference across the plates then the stream will be deflected towards the anode, as discussed in chapter 2 under “Charging and Deflection”.

The rotating branches allow the deflection and focusing plates to be situated very close to the stream, although problems could still occur if the stream direction becomes greater than 5° off centre. Although this is not relevant to the Cooper-Walker orifices, as the internal dimensions of the hex head component limit the stream direction to a maximum variation of 2°, an additional method of straightening the stream has been implemented to accommodate different orifice mounting methods that may be investigated in the future.

Figure 64 illustrates how three screws aligned in a triangular formation, can be adjusted to control the direction of the jetting crucible flange, by compressing a 12mm diameter rubber O-ring. Adjustments are made to the stream direction by tightening or slacking the relevant screw. Measurements reveal a variation of $\pm 7^\circ$ off the perpendicular is achievable with the current laboratory set-up, figures 65 and 66.

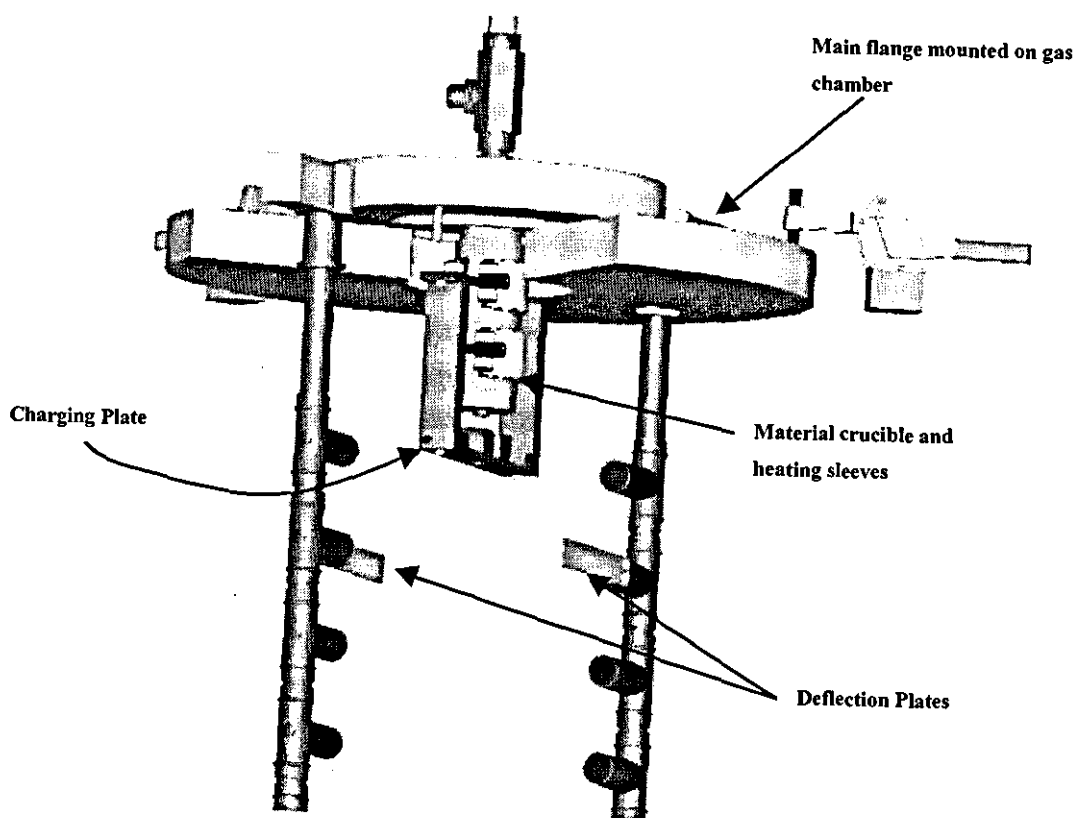


Figure 63 - Branch adjustment of focusing and deflection plates

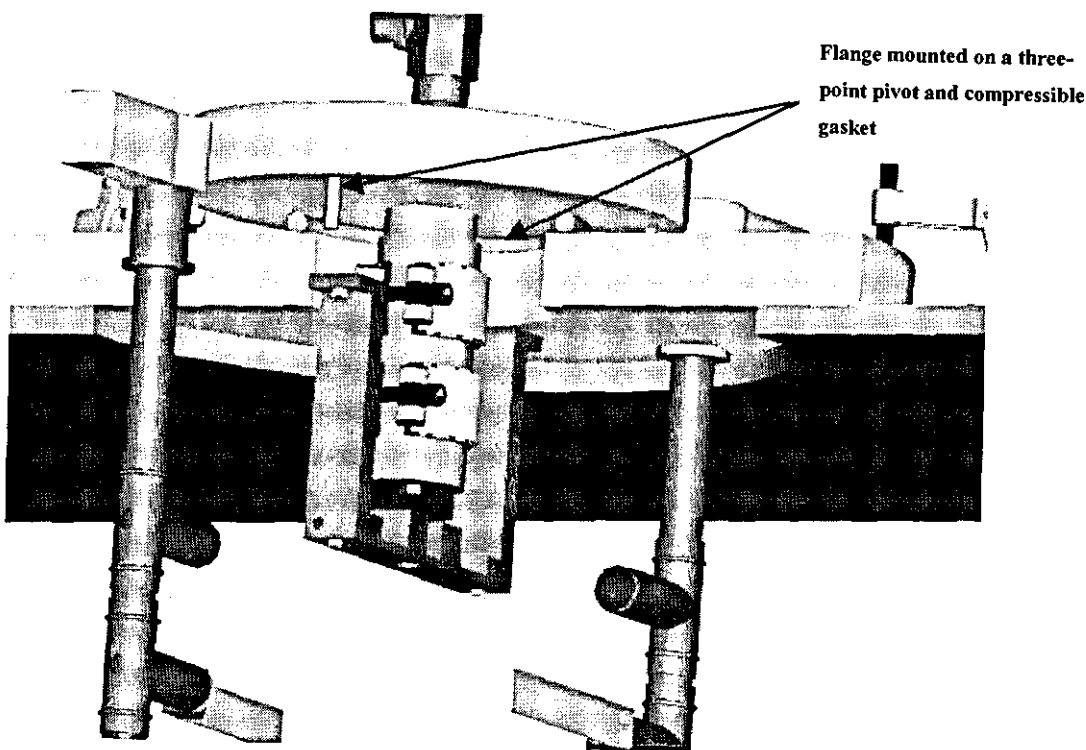


Figure 64 - Adjustable mounting of jetting head

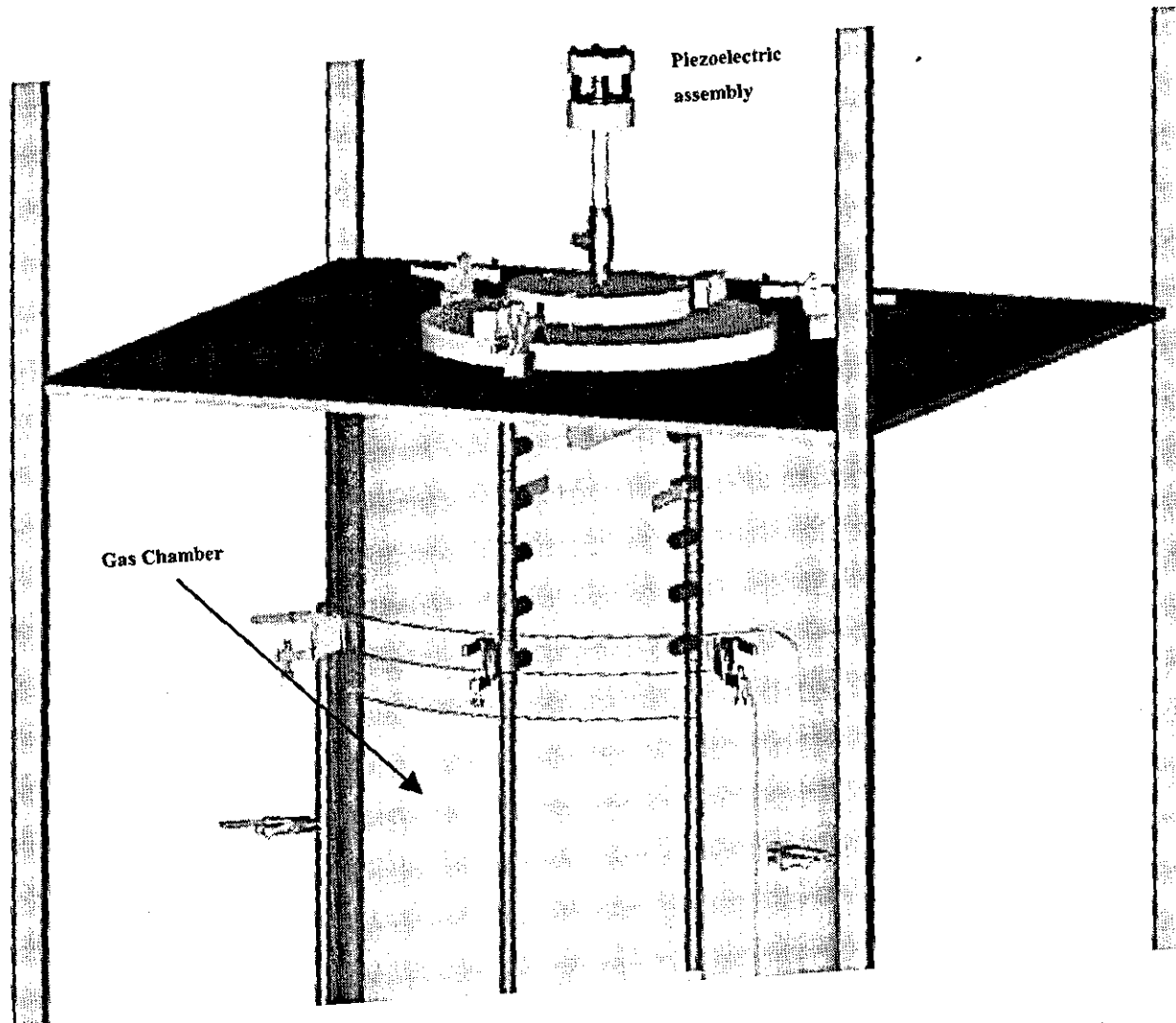


Figure 65 – Current Nortel equipment with adjustable head and rotating 'branches'

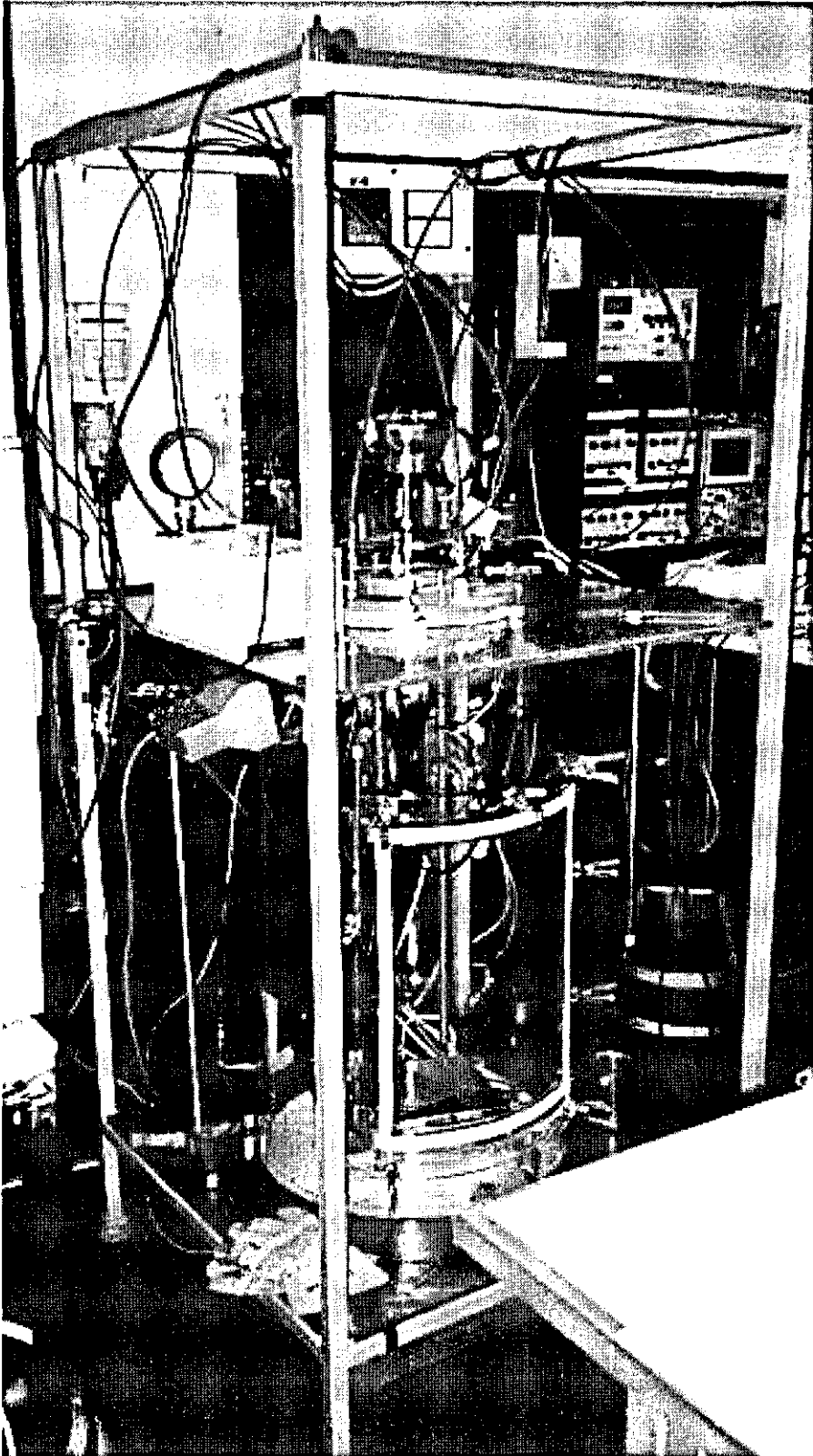


Figure 66 – Nortel laboratory set-up

5 Optoelectronic Demonstrators

“Such is the fashion for data transmission that the world just cannot get enough and the industry is straining to meet demand” [38]. Data and telecommunications are now heavily reliant on optical fibres to carry signals, especially over long distances, and as such optical based products are currently one of the biggest growth business areas. As service providers plan and implement solutions to rapidly expand network capacity, cost containment and network flexibility are critically important issues given today’s very competitive telecommunications arena. Maximum value must be obtained from currently installed fibre infrastructure to avoid or defer the large capital outlays and long lead times associated with new fibre deployment.

Manufacturing of these products face many similar challenges analogous to those faced in the more established electronics-manufacturing environment such as the drive towards increasing volumes of smaller and faster components but with the new challenges of decreased dimensions and the need for optical alignment. Components such as laser diodes and modulators, designed for high-performance applications, are single-mode devices; they must be connected using optical fibres or other types of waveguides with sub-micron alignment accuracies because the mode size of the beam from a single mode fibre can be as small as $9\mu\text{m}$ in diameter. Currently, optoelectronic (OE) packaging is performed by highly skilled technicians looking through microscopes and manually adjusting and fixing the components in place. The labour costs are by far the highest fraction of the total cost of an assembled OE package. The consequences of this low-volume, labour-intensive process of packaging OE devices are readily apparent.

Currently the rapidly rising demand far outstrips the capacity for manufacture, which results in more and more people being employed in a similar manner. At the current rate of growth, with some products experiencing 400% increases in throughput per year, it is not feasible to keep adding more and more people in parallel production lines. Sites already face the simple problem that there are not enough suitable people

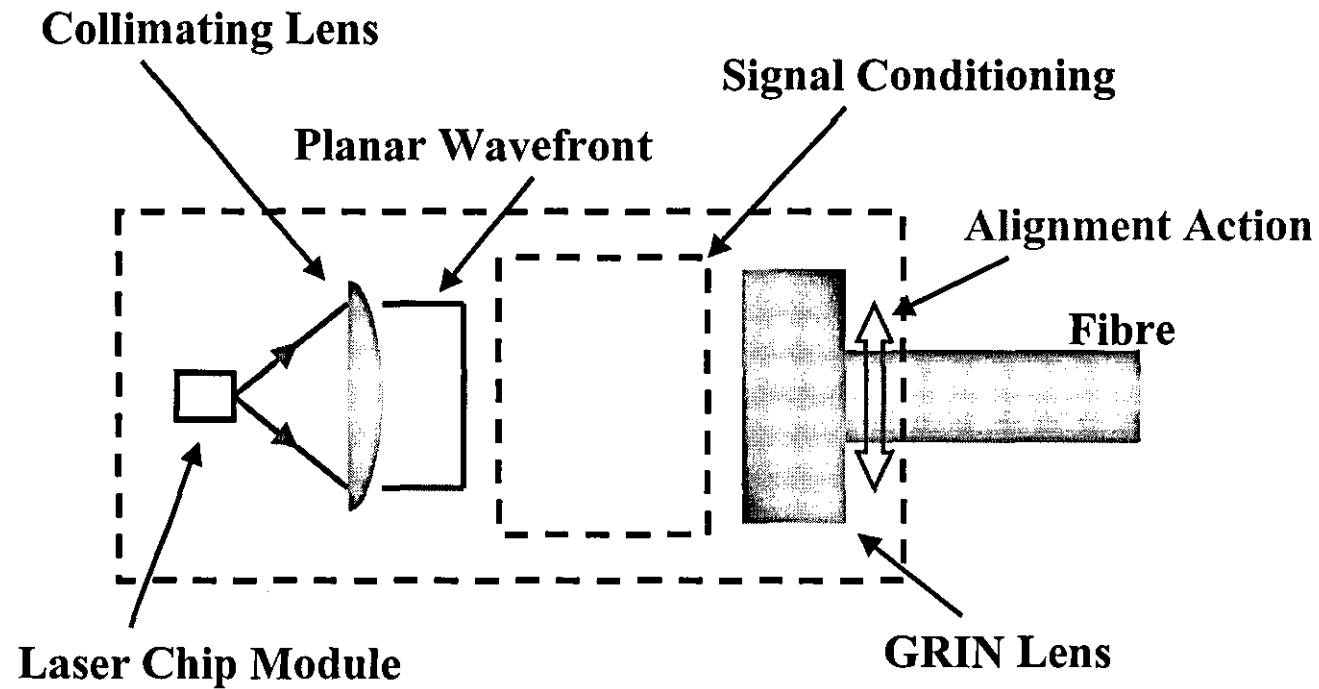
to populate the production lines. The existing method will keep the costs too high to allow the advantages of fibre optics to penetrate such markets as on-chip interconnects, inter-board connections in computers, local area networks, or most importantly fibre to the home. The manual processes must be automated in order for this business to keep fulfilling its potential. Therefore, it is a priority to find fast, repeatable, automated and robust methods of device production.

5.1 What Materials Jetting has to offer

In the following example, figure 67, aligning the fibre with the graded index (GRIN) lens in a generic transmitting package requires an operator to move the fibre in two axes, with micron accuracy, until the optimum coupling is achieved. Although this human intervention allows for high quality and high value added devices it is also open to human error, yield and speed issues. Conversely, the above package can also be considered as a receiver, collecting the light from the fibre.

In considering the above generic optoelectronic package, materials jetting has the potential to address three key areas in its manufacture.

- 1) **(Lead-free) Solder Pre-Form Replacement.** Tin/gold solder is used to mechanically fix items such as the laser module to the optical bench and the bench to the package. Solder pre-forms are costly and require precision human placement – materials jetting is accurate enough to automatically place the correct volume of solder in the package straight from bulk material, taking away the pre-form processing stage.
- 2) **Adhesive Dispensing.** Individual components such as lenses need to be placed with accuracy approaching $\pm 1\mu\text{m}$, this requires the amount of dispensed adhesive to be accurate within the order of picolitres. Materials jetting has the ability to dispense UV curing adhesive in volume multiples of, as little as, $\sim 100\text{ pl}$.



Generic Optical Bench – No Scale

Figure 67 - Example configuration for a transmitting laser module

- 3) **Passive Optical Components.** Current methods of production require the fibre to be aligned in-situ and held in place whilst it is adhered to the lens. If a lens could be fixed directly to the fibre end it would remove the need for in-situ alignment of the fibre and accelerate the overall assembly process. As discussed in chapter 2 polymeric materials have been used to form novel stand-alone components that could be used for low-cost alternatives to the present items.

Microfab Technologies has over fourteen years experience in developing ink-jet / micro-jet printing processes to reduce costs and increase flexibility in a variety of manufacturing applications. They have micro-jet printed a wide range of materials, including liquid metal solders, fluxes, adhesives, epoxies, thermoplastics and UV-curing materials. Of immediate relevance to this area is the ongoing R&D work in developing a new technology for micro-jet printing of liquid solders [3, 39] and micro-optical interconnects [40]. In conjunction with Microfab Technologies Inc, the 3 key areas outlined above have been studied. During a visit to their site in Plano, Texas, 4 key demonstrators have been fabricated, showing their potential for use in automated production.

- 1) Printing various adhesives for bonding optical elements inside package
- 2) Printing Sn/Cu lead-free solder to form a 5mm x 10mm x 100 μm layer onto Nortel substrate (for 980 pump package pre-form);
- 3) Printing MRX-110 polymer (a proprietary compound developed by Microfab) lenslets onto fibres for collimation;
- 4) Printing MRX-110 polymer lenslet arrays on glass for an 8-channel array switch.

5.2 Adhesives

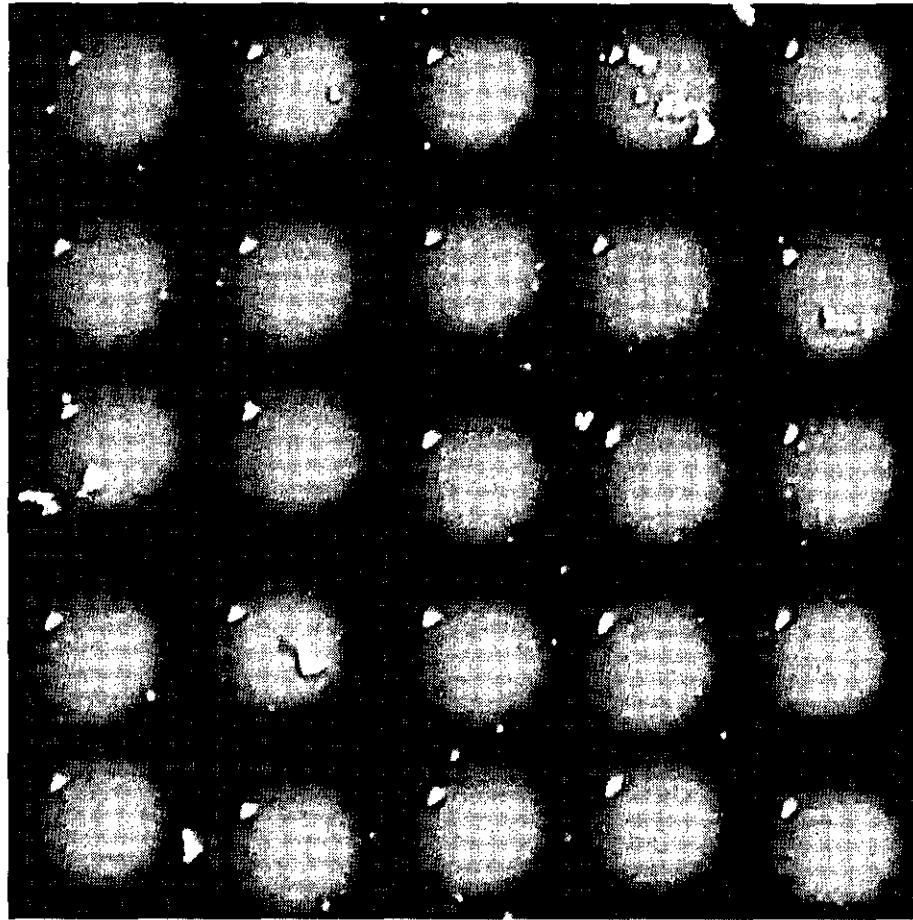
The aim of this investigation was to ascertain whether any of the current optical adhesives, used in optoelectronic production, could be jetted in precise amounts at specific locations. Especially important in optical path component adhesion, the amount of dispensed material must be consistent for each deposition.

The adhesives used in production have the problem of changes in viscosity over time therefore altering the amount dispensed. To address this problem, several optical adhesives have been tested for their suitability in jetting. The specific adhesives tested were two-component thermally curing Epotek 375, Epotek 353 and UV curing Norland 81.

It was found that the Epotek materials quickly set inside the device, because of their low cure temperatures, and hence were unable to be jetted. In order for a material to be jetted its viscosity must be reduced to below 40 cps, since the acoustic waves used to form the drop are severely dampened above this value, although modified devices have operated with materials with a viscosity of nearly 100 cps [28].

For the Epotek materials the reduction of viscosity to below 40 cps occurs only at temperatures above 90°C, which is above the minimum cure temperature, therefore inducing their curing schedule within the jetting device reservoir. Conversely the UV curing Norland 81 adhesive was successfully jetted with little or no issues at a droplet size of 60µm.

An array of single droplets with a spacing of 200µm has been demonstrated, using MRX-110 'yellow', which has similar properties to that of the Norland adhesive, figure 68.



Microfab
proprietary
UV curing
adhesive –
“MRX-110
(yellow)”

—
200 μ m

Figure 68 - Detail from 370x125 array of 60 micron droplets on 200 micron centres

Further to this work, Mike Grove (polymer and adhesives specialist at Microfab) has indicated that several alternatives to the two-component thermally cured adhesives exist. Research regarding jet-able adhesives with the same or improved properties over the Epotek materials will indicate their potential use.

X-ray curing has been performed with the same materials that are jetted to form micro-lenses and glue items together. This would be ideal for components that are highly absorptive in the ultra-violet range of the spectrum, but further research needs to be carried out as to whether the high energy of x-rays would damage materials such as III-V semiconductors. The reaction is relatively fast at room temperature and would negate the need for two component mixing, oven curing, etc. In addition, these adhesives, being polyethers (since the linkages that form, during polymerisation, between the monomeric and oligomeric carbon atoms of the compound are ether (oxygen) links) rather than the alternative polyacrylates, will have better environmental resistance (water vapour) than the alternate ionising radiation curing materials.

5.3 Pre-form replacement

Previous work [3] performed by Microfab had concentrated on tin/lead solders. Here the first reported work on the deposition of lead-free solders is presented, in particular eutectic tin/copper supplied by Multicore Solders, targeted at replacing pre-forms in optoelectronic packaging.

Before inserting it into the device reservoir, the extruded solder, supplied in pellet form, is first filtered, figure 69, using a 2-micron gauze under a vacuum of 10^{-4} Torr. The primary reason for this is to remove any foreign materials that may be present, such as oxides or unwanted inter-metallics, which could have formed during processing and handling. The solder is filtered well above its melting temperature to ensure that the alloy flows freely.

It was found that the lead-free solder jetted with very good droplet characteristics after a few adjustments made to the solder jet station in order to deposit the material. Since

it had not previously been tested, initial problems were encountered, such as the build up of impurities, which inhibited stable break-up and deposition after about 5 days held in the reservoir. This problem was overcome by re-filtering the solder under vacuum.

To demonstrate the control and droplet size consistency of the technique a single layer (i.e. one drop per site) 39x39 array of lead free solder was deposited on a silicon silver substrate, figures 70, 71 and 72.

A direct application to Nortel Networks devices was demonstrated. Lead-free solder was printed on to a 980nm laser pump package, figure 73, used in production. The pre-form presently used, indicated by the blue/grey square, measures 7.5mm x 5.5mm x 0.1mm and is placed in the lowest recess within the package. A heat sink for the optical bench is then placed on this solder and the package is re-flowed to form the joint. This equates to a volume of 4,125 nl. Using a device which droplets with a volume of 113 pl (60µm) are jetted onto the gold substrates. To achieve the necessary volume of solder 36,000 droplets are needed, and with a generation frequency of 600Hz, it would take 60 seconds (with 3 passes) to cover the required area.

The reported droplet generation rate may not be high enough for the amount of material required in this application but optimising the droplet size will decrease the time needed by a power of 3. Droplet diameters of 120µm should be achievable using the current head design albeit with slight imperfections in drop size. Because the shape of each deposition is not critical in this case, the need for perfect droplets is negated. This would reduce the time needed for deposition to 7 seconds. It may be the case that the advantages of drop on demand jetting could negate its own time limitations since pre-forms are costly and the time needed to place the solder is not a bottleneck. A total deposition time of, say, 20 seconds is not unreasonable.

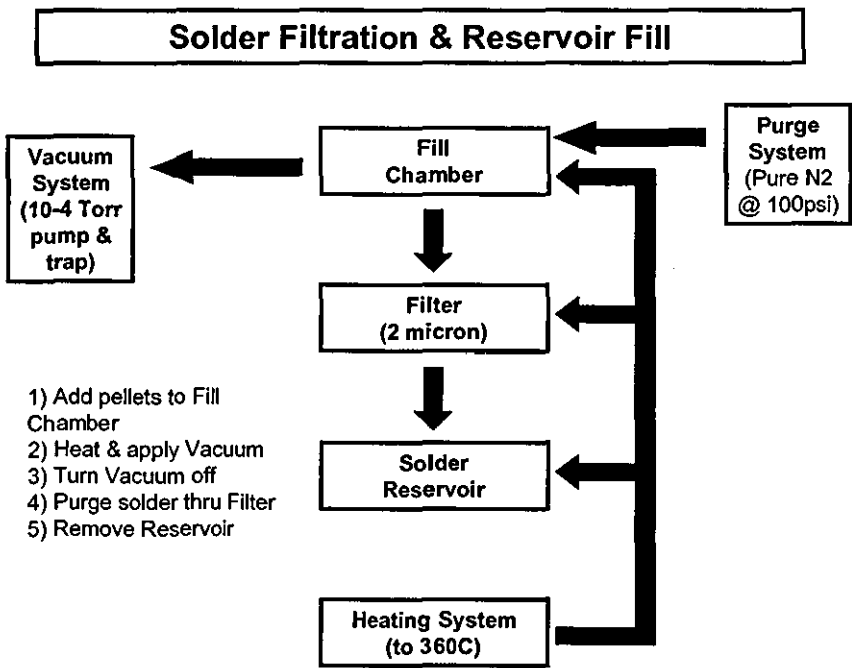


Figure 69 - Filtration method in preparing solders for jetting

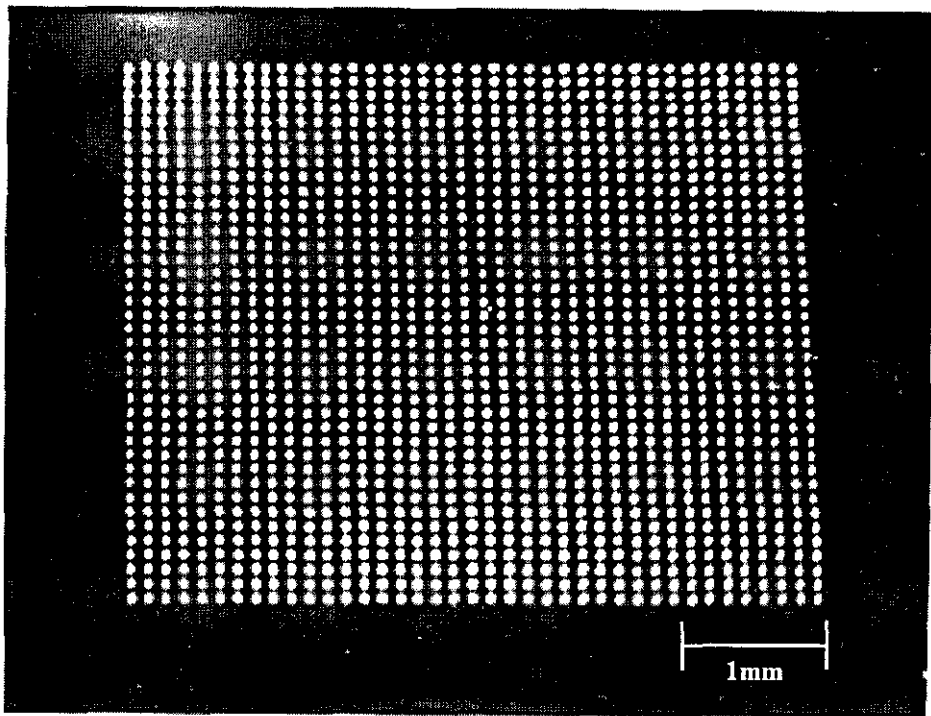


Figure 70 – Array of Multicore lead-free (SnCu) solder on metallised Si wafer.

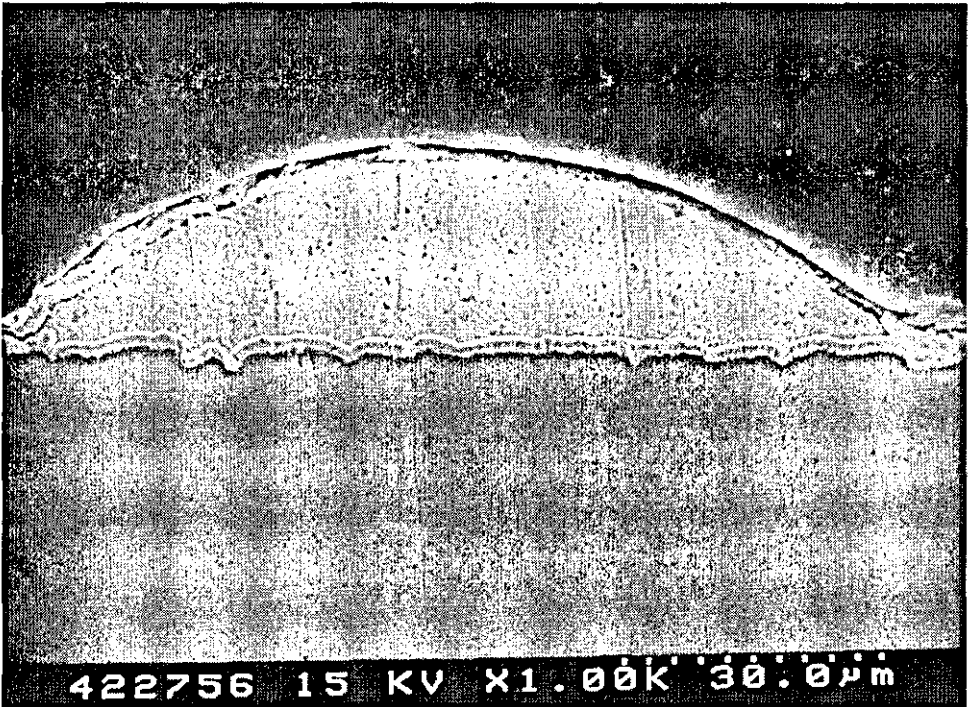


Figure 71 - Detail of Multicore lead-free solder on metallised Si wafer

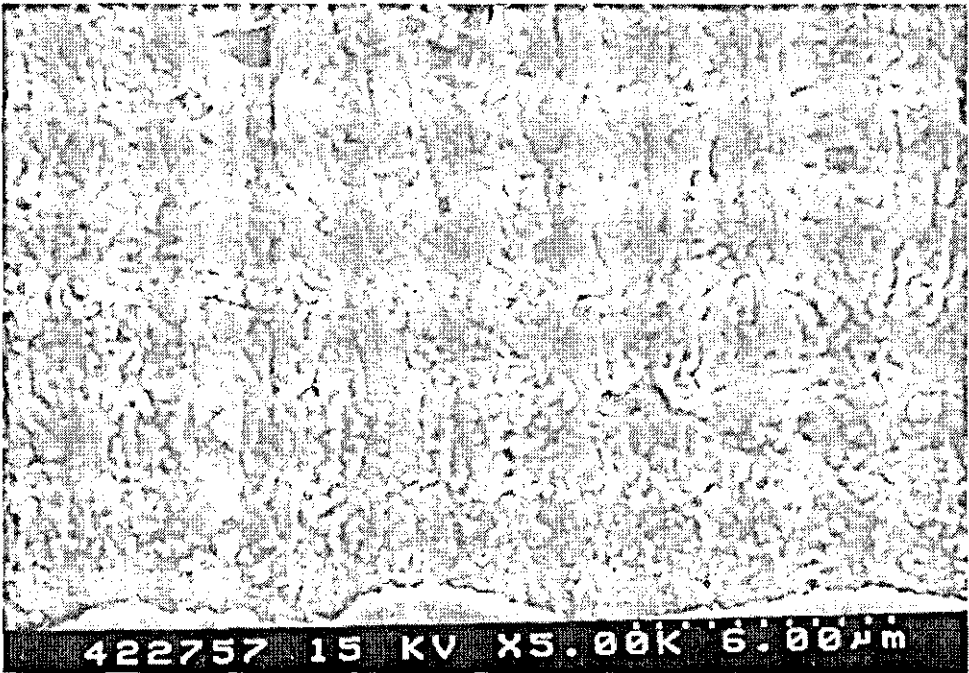


Figure 72 - Detail of Multicore lead-free solder on metallised Si wafer

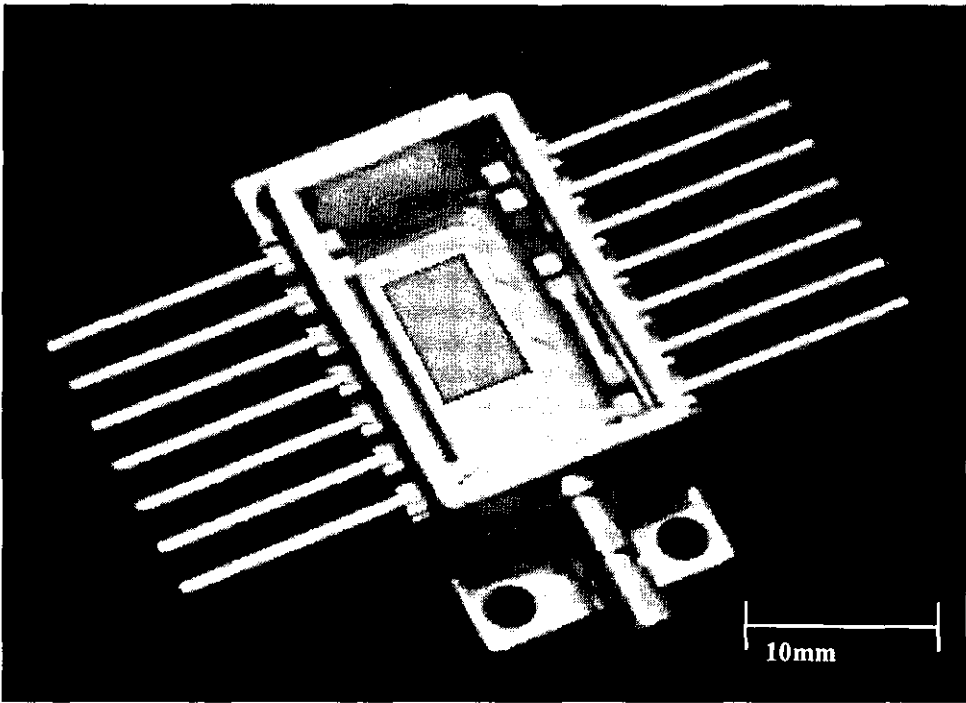
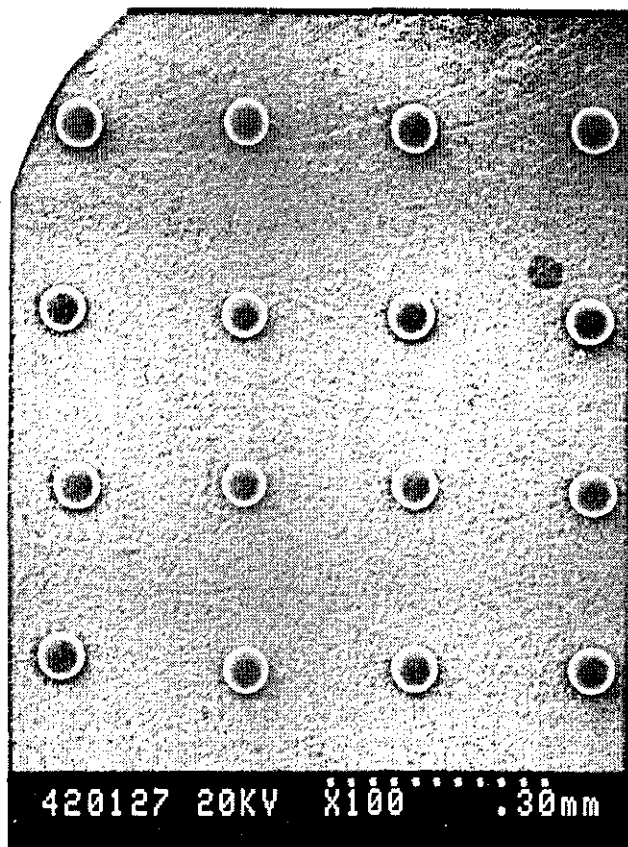


Figure 73 - Nortel Networks 980nm laser pump module case. Position of solder pre-form placement indicated by grey region in the lower recess

Jetting is not limited to flat foil-like pre-form structures, additional solder could be placed in one or more areas of the recess forming shaped joints with a 3 dimensional topography. This may be used in locating and centring components in the recess before reflow. Ideally continuous mode materials jetting should be used for this application but the equipment is much more expensive and less mature. Jetting is also a much more accurate method of solder placement which can be done autonomously. A more detailed costing and feasibility audit therefore needs to be conducted but it is thought that jetting could reduce the cost of solder in each package from \$0.4 to \$0.15.

It is clear that cleaning of the substrate is a necessity, as the droplets do not stick very well to areas of the substrate that are discoloured or contaminated. Droplets do not wet very well until the substrate temperature is raised to about 150°C. One other issue that is raised by this task is the inability of the current head to deposit at distances greater than about 2mm. This is due to the localised nitrogen shroud at the orifice. At distances greater than 2mm, turbulence and oxidation are factors limiting the directional accuracy and wetting characteristics of the droplets. This limits the process application in areas where it is necessary to place solder into a well, such as the laser package or recess, although it is thought that extending the nitrogen shroud could overcome this problem, but would require a slight redesign of the head. Alternatively, the solder could be jetted onto the piece, which is to be placed in the package.

Due to the tiny dimensions involved it has not been possible to perform a full structural analysis on the solder deposits, figure 74. Initial shear tests using a scalpel blade to break the deposited droplets from the substrate, indicating the inter-metallic bond strength, saw the deposits deforming before becoming detached from the substrate, confirming that at least some wetting had occurred prior to solidification.



a



b

Figure 74 - Eutectic SnCu solder deposited onto 980nm pump package gold substrate

5.4 Passive optical components

5.4.1 Design issues

To understand the limitations and issues raised by passive component production the design factors built into fibre communications are outlined. Because of the minute dimensions of long haul optical fibre core (4-6 μm) it is necessary for the light to be expanded and collimated so that it is of a useable geometry. As the guided light emanates from the end of a fibre the circular wave front can be considered to be analogous to Gaussian-spherical beam propagation [41], highlighted by the red line, figure 75.

The development of a Gaussian-spherical beam as it propagates can be followed using the equation

$$\omega^2 = \omega_0^2 \left[1 + \left(\frac{\lambda z}{\pi \omega_0^2} \right)^2 \right] \quad (6.1)$$

where, as shown in figure 75, ω is the beam radius at a distance, z , from the beam waist, or fibre end. For large z , compared to ω_0 , the beam expands at a constant angle, $\theta = \lambda / \pi \omega_0$.

Considering the beam from a single mode step index fibre with numerical aperture (NA) ≈ 0.13 . For use in free space optical applications the beam needs to be expanded to a useable dimension in the order of 200-250 μm . Current art requires the collimating lens to be created away from the fibre and then actively aligned, using 3-axis micro-

positioning stages, whilst passing light through the fibre [42], or etching and laser processing the end of the fibre forming a curved surface.

**Single Mode Step Index Optical Fibre –
diameter 125 μm , core diameter $\sim 5\text{--}6\ \mu\text{m}$**

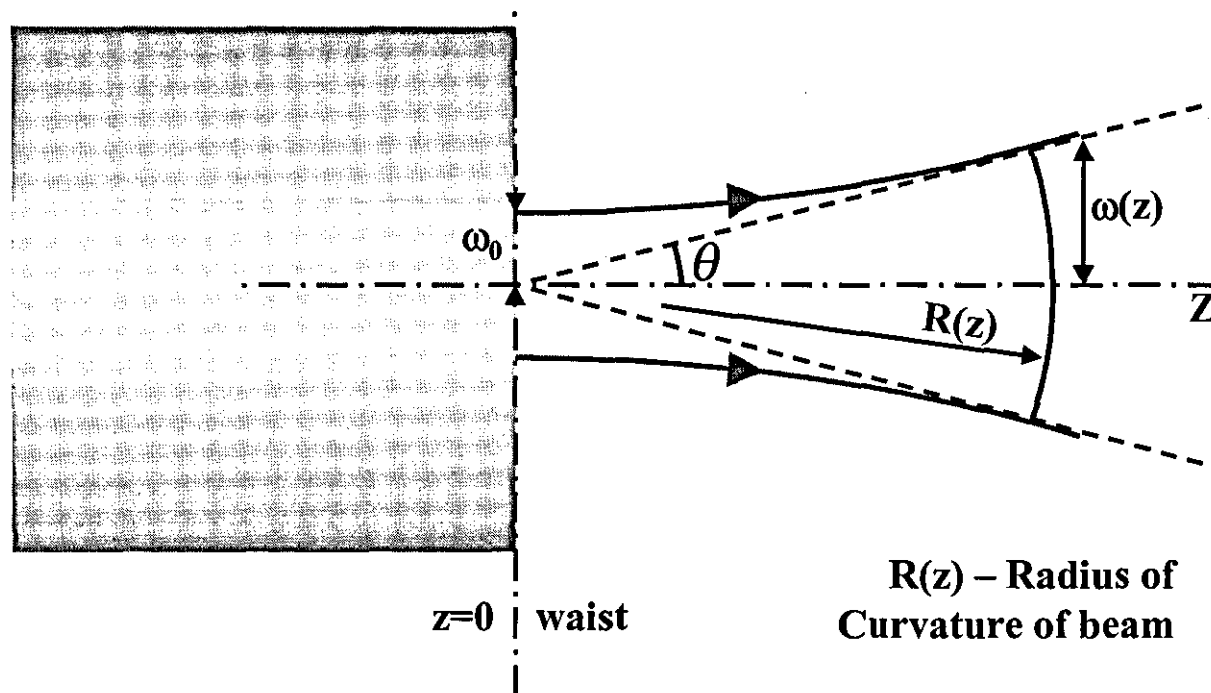


Figure 75 - Beam propagation from the end of a single mode fibre

Etching is a multiple-step process involving masking the end of the optical fibre with a substance that is non-soluble in the reagent. The portion of the coating at the very end of the fibre is then removed and the fibre end immersed. The etching reagent serves to dissolve the uncoated portion of the fibre. By controlling the amount of time that the fibre end is in the reagent, different lens shapes may be formed [43,44]. In a second embodiment, the fibre end is dipped into a liquid epoxy compound whereby a portion of the epoxy is deposited onto the fibre end. The surface tension of the portion deposited thereon draws the liquid epoxy into the desired lens shape. The epoxy is then hardened by UV, or heat, curing to form a permanent lens structure on the fibre end. Neither of these methods allows for accurate placement and geometry of the lens, being highly dependant on macroscopic fluid dynamics, and imposes repeatability problems. In addition, they do not allow for necessary expansion of the beam to a usable diameter.

With micro-jet printing the flow of deposited material stops at the edges of the fibre cladding and surface tension will force lenslet shape symmetry, therefore creating a self-centring geometry and, by use of spacing arrangements, the correct geometries can be formed.

Previous work had only been concerned with multimode fibres. Outlined below is a summary of the questions and issues raised by the optical design group in Nortel Networks optoelectronic manufacturing plant in Paignton. These serve to highlight the issues and design criteria that single mode gaussian beam optics raises with respect to multimode systems. Conventional lens fabrication methods use cutting, grinding and polishing etc to finish specific dimensions and contours on glass materials. Optical material micro-jet printing methods introduce a different set a controllable fabrication factors, which include device orifice, printing temperature, substrate temperature, droplet speed, orifice-substrate distance, number of droplets per lenslet etc. These new factors raise issues that change how systems are designed and as such the method must offer many advantages in order for it to be adopted. Also outlined are some of the burgeoning technologies that Microfab are investigating that could have application in next generation devices such as optical lambda and spatial switches and modulators.

- 1) **When creating a lens it is not desirable for the shape to be governed solely by surface tension as this will lead to aberrations and wave-front inconsistencies, especially when the lens formed is hemispherical. A certain amount of design freedom must be available to allow for the required geometry to be created.**

There are several modes of design freedom for printed microlenses:

- a) *To vary aspect ratio [height(sag)/diameter] at a fixed diameter it is possible to alter the viscosity of the deposited material, and/or the free energy of the substrate surface, in order to control material flow prior to solidification. In this case the lenslet curvature remains spherical.*
- b) *Aspherical performance is obtainable in a printed micro-lens with spherical surface profile by printing it with two materials having different indexes of refraction, in such a way as to produce an axial gradient index of refraction (AGRIN) in the lenslet. Modelling indicates that a 50-fold reduction in focused spot size is achievable in a micro-lens with 50 μ m sag (height) using miscible formulations differing in refractive index by only 0.05, compared to an identically sized micro-lens printed with one material. An R&D Optics-Jet Station is in development at Microfab, which can accommodate two print heads, multiplexed to the drive electronics, in order to investigate AGRIN micro-lens printing.*
- c) *The curvature of a printed micro-lens may be altered to achieve a more hyperbolic shape in two ways: by in-situ spot curing between subsequent depositions of droplets to arrest flow during printing of a lenslet; or by isotropic reactive ion etching (RIE) after printing and curing. The RIE process etches the edges of the lenslets at a slightly faster rate than the top of the lens, since ions striking the edges are at slightly higher velocity (accelerating longer prior to impact) than those striking the top of the lenslet. RIE is a macro-machining process, which may be used to reduce spherical aberrations in large numbers of micro-lenses simultaneously by altering their curvatures away from spherical.*

d) To achieve a non-spherical curvature matching a design equation would require micro-machining of individual lenslets after printing and curing, a comparatively expensive process.

- 2) For the light emergent from a fibre it must be collimated to be of use for signal processing. Divergence is limited by forming a collimated beam of the maximum useable diameter.**

For a fibre with an NA of 0.3, an optical printing material of index 1.55, and a microlens of same diameter as the fibre it is expected to be able to obtain a collimated beam width of 70 μm . By extending the diameter of the printed lenslet well beyond that of the fibre to the limit of mechanical stability, it can achieve collimated beam widths of at least 140 μm . In all cases the micro-lenses would be printed onto a previously printed pedestal of the same material to obtain the appropriate offset of the lenslet from the fibre tip.

- 3) For use in communication devices the beam direction error from the lens is required to be $<1/20^\circ$ off the z-axis of the fibre / optical train.**

Beam direction error is determined primarily by the axial alignment error of the printed microlens relative to the fiber axis. The flow of deposited material stops at the edges of the fiber cladding and surface tension will force lenslet shape symmetry.

- 4) How mechanically unstable, if possible to manufacture, is a lens that is created bigger than the 125 μm fibre diameter? Can these lenses still accurately collimate the beam to width of, say, 200 μm ?**

The most mechanically stable and accurately aligned microlenses that can be printed are ones which extend to the edge of a fibre cladding. In these cases flow of deposited material stops at the fibre edge and surface tension allows the building up of a nearly spherical lenslet, as shown in figure 76, indicating how lenslets of differing radii of curvature may be printed onto the tip of 140 μm diameter fibres.

Number of 50 micron droplets:

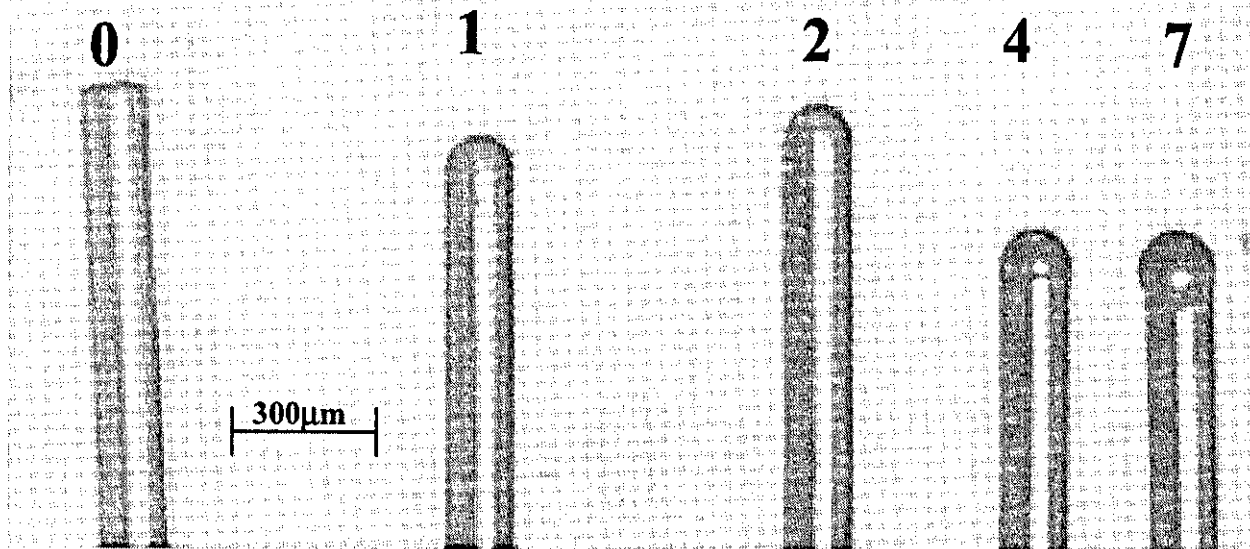


Figure 76 – Polymer lenses printed directly onto multimode fibres, of diameter 140µm

- 5) Optical flatness requires the surface of a component to be smooth to a precision of $0.1\mu\text{m}$.**

Surface smoothness of much better than $0.1\mu\text{m}$ is readily achievable, as evidenced by Zygo interferometric lenslet profile data and work performed in replicating printed microlenses into silicon wafers. For spherical microlenses the reproducibility of radius of curvature, which is governed by the volumetric precision of droplet formation (typically better than 2%) and by substrate surface uniformity and cleanliness, varies in absolute value with lenslet size and is typically better than 1%, e.g., $2\mu\text{m}$ for a lenslet with $200\mu\text{m}$ curvature radius.

- 6) Along with values for spherical aberration, astigmatism and coma etc, what are the achievable values for wave-front planarity?**

The only data available to address this question are point spread power distribution curves and modulation transfer functions measured for printed micro-lenses of varying diameters, which show aberrations increasing with lenslet diameter, with near-diffraction-limited performance for $100\mu\text{m}$ diameter lenslets. These values have been obtained by modelling.

- 7) How much variation on the mechanical properties and refractive index do the effects of temperature have on the polymers they use for these lenses?**

The changes in focal length measured for printed & cured micro-lenses after baking for several hours at 200°C have been less than 1%, which is at or below Microfabs current measurement resolution. Currently these temperature ageing experiments are being extended to longer bake times and are putting together a set up which will enabling measurement of focal length at temperatures up to 150°C .

8) How possible is it to deposit optically flat thin films of, for example, liquid crystals?

Liquid crystal formulations have been printed. Achieving an optically flat surface (thickness variation less than $\lambda/4 - \lambda/2$) over an area of interest with printed droplets should be possible by diluting the formulation with solvent and by pre-treating the substrate surface with a high-wetting agent. (surface free-energy of agent matched to that of the liquid crystal). Printing into appropriately treated wells, or onto locally defined areas which are surrounded by a less wettable surface, would control the flow of deposited materials and promote formation of a very flat meniscus.

9) What is the potential of the technique to jet a passive structure such as prism? Is it possible to jet into a mould or to post process the polymer?

For a 90° turning prism printing into a release-coated slab of material with micro-machined V-grooves would seem to be the most straightforward approach. This approach has been used in printing multimode waveguides for a customer. Titanium-oxide coated grooves in a silicon wafer have been used to provide a mould for the jetted polymer. After UV-curing from above, the polymer waveguides were lifted out of the grooves and used successfully in a demonstration interconnect system. Here dilute HF, which does not attack the optical epoxy, was used to achieve release of the polymer waveguides from the TiO₂. Issues to be addressed here include release and physical removal of the cured optical element from the mould and achieving flat and optically smooth surfaces, especially on the deposition side of the prism.

10) Does the technique, either with or without post processing, have the potential to create single mode fibres?

Single mode fibres/waveguides could be created by the ink-jet printing method, but only with pre- and/or post- processing, as the minimum printable feature size on a flat surface is on the order of 25 μm . Approaches might

include: (a) printing of droplets into excimer-laser micro-machined grooves in a sheet of lower index material, then removing any over flow prior to curing; (b) printing 50-80 μ m wide lines of an optical material which is formulated to solidify by driving out a solvent or heating and then selectively polymerised by a narrowly focussed beam of UV-illumination.

5.4.2 Lens on single-mode fibre for beam collimation

The challenge from Nortel Networks point of view is to produce a highly collimated beam from a 125 μ m diameter single mode communications grade fibre. A lens cannot be deposited directly on the end of the fibre, since the optical geometry is too small and the refractive index of the polymer is too low to allow for the collimation of the divergent light into a beam of necessary dimensions. In order to achieve collimation of the beam, the lenses must be placed at some distance away from the tip of the fibre.

Two ways are currently being investigated to achieve the necessary physical dimensions. If a lens is first deposited on to the fibre tip a section of the fibre can then be removed using in-situ post processing.

For these trials MRX-110 polymer, developed by Microfab, was used to form these lenses. This family of pre-polymers was originally selected for its high temperature durability (200 deg. C.) for military applications. It is thought that some improvements and alterations need to be made to better meet the needs of data communications.

For jetting, approximately 30-40ml of the material is held in the reservoir of the device under a back vacuum of approximately 15 torr. The heating of the device, for MRX110, holds the reservoir at 156°C, whilst the actual print head is held at 133°C. Lenses are printed with varying aspect ratios directly onto the end of the fibre to ascertain the achievable lens sizes, quality and centring with respect to the central fibre axis. This will serve to identify the geometric limits for post processing in order to achieve a collimated beam. Jetting MRX-110 polymer on to each fibre of a stripped

and cleaved end of a single-mode ribbon showed how the process inherently creates a self-centring lens. Figures 77 and 78 show a 125 μm fibre ribbon with hemi-spherical polymer lenses printed with a target height / diameter aspect ratio of 1:2. If the fibre end is clean and free from defects, when the droplet impinges on the end of the fibre the spreading and wetting of the material extends equally in all directions reaching the edge of the cleaved end.

Lenses with a discrete number (n) of polymer droplets up to $n=7$, have previously been reported on 140 μm diameter multimode fibres. The conditions during these trials limited the maximum number of depositions to $n=4$, as shown by the right-most lens in figure 77. The left-most lens was deposited by subsequently printing ($n=3$) 50 μm droplets at rate of 1Hz. The SEM picture of the lens, figure 78, from the top shows how a smaller number of droplets potentially do not produce a smooth conformal finish. The reduced n in these trials was due to the smaller dimensions of the fibres along with a non-optimised process. The fibres towards the middle of the bundle show the result of the polymer sliding down the edge of the fibre due to condensation or out-gassing effects from the print head, which is held 1-2mm away from the deposition site. These effects decrease the surface tension of the material allowing it to flow more freely on the substrate. As subsequent droplets are deposited they again, are controlled by the edge and consequent surface tension effects, until a critical mass is reached where the weight of the material exceeds the surface tension forces. This can be overcome by care being taken during the printing and allowing the fibre to cool slightly.

5.4.3 Lens on collar

As previously stated, to provide the beam geometry, allowing for necessary divergence, the lens must be positioned a distance away from the fibre end. A second approach is to micro machine a glass pellet to form a collar, which is slid onto the fibre end and fixed with optical polymer at the correct distance allowing for the light to be collimated by the deposited lens, figure 79. The feasibility of the approach has been demonstrated by creating a lens with the correct radius of curvature as calculated using the ZEMAX Optical CAD (O-CAD) package.

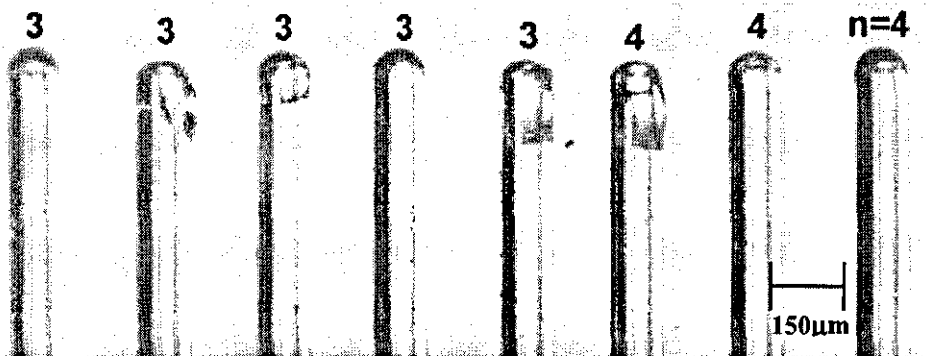


Figure 77 - MRX-110 Polymer lenses printed on 8-strand Nortel Networks single mode (125µm diameter) fibre ribbon



Figure 78 - End view of single mode fibre having printed lens with 3 droplets

The optical system is modelled to yield the required lens height/diameter aspect ratio and fibre position in the collar. Now consider the bound variables to be the collar diameter and the numerical aperture of the fibre (object plane). The variables used to optimise the system are the lens height and fibre position. Using the O-CAD package automatic optimisation is performed on the system until the best value for the image plane NA, at infinity, is obtained. For a collar of diameter 900µm it is found that the fibre position needs to be 1090µm from the top end of the collar for a lens with a radius of curvature of 488µm, of height of 300µm.

The relationship between the number of droplets, n , needed to form a lens with radius of curvature, R , and diameter, d , is given by [45]

$$nV_d = \frac{2}{3}\pi R^3 - \frac{\pi}{3}\left(2R^2 + \frac{d^2}{4}\right)\sqrt{R^2 - \frac{d^2}{4}} \quad (6.2)$$

where V_d = volume of each droplet, R and d the radius of curvature and diameter of the lens respectively. Once the well is filled to the top of the collar, a lens with a diameter of 900µm and radius of curvature 488µm requires ≥ 900 60µm diameter droplets; figure 80 shows the relationship in graphical form for a lens diameter of 900 µm. To form this lens using the jetting technique the deposition is monitored using a CCD camera. In practice lenses are formed with respect to the required height /diameter aspect ratio, in this case 1:3. The polymer is jetted in bursts of a number of discrete droplets, which can be altered when more precision is required or depending on the total amount needed.

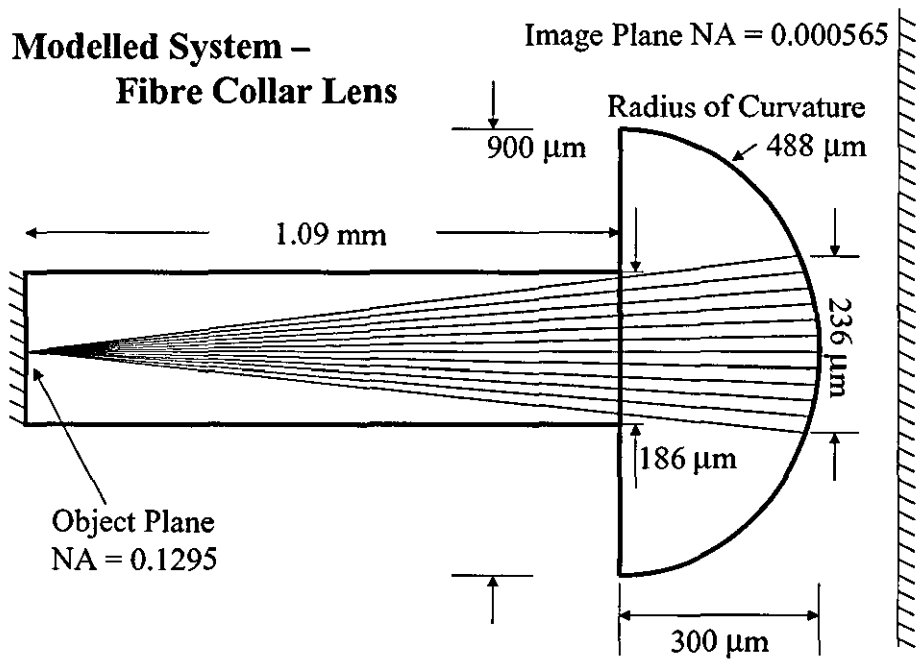


Figure 79 - Modelled optical system for deposition into glass collar / fibre arrangement

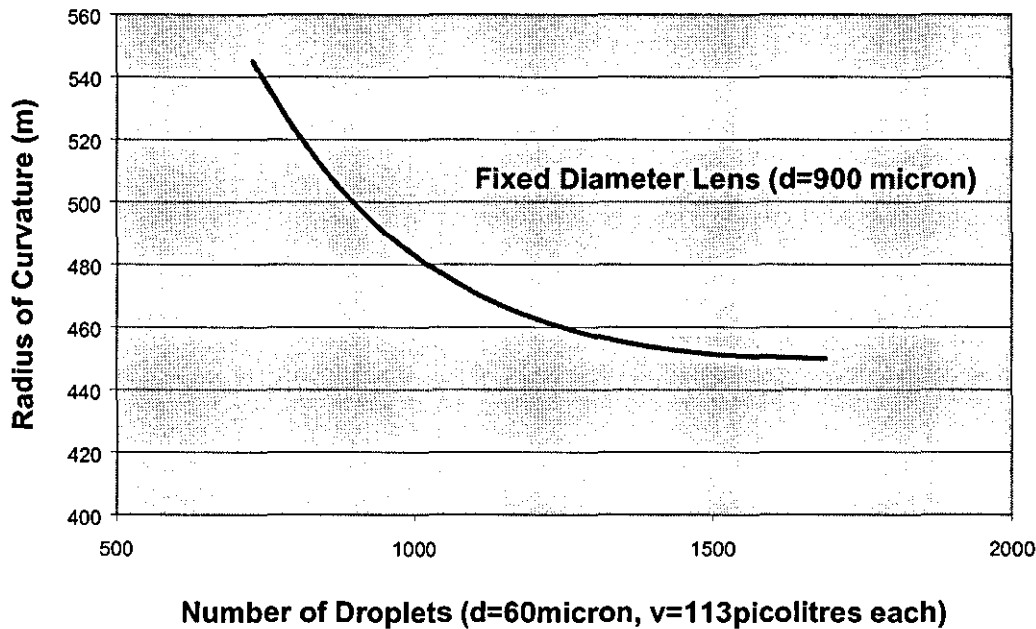


Figure 80 - Relationship between amount of deposited droplets and lens radius of curvature

5.4.4 Collar evolution

The collars were initially machined with a single 125 μm diameter central hole the whole length of the collar, figure 81a. The polymer used to form the lens was jetted into the well created by the fibre and collar arrangement. This configuration causes a problem in two respects. Firstly, the deposition of droplets into the well is approaching the positional accuracy limits of the system. As they enter the well some deposits may wet to the walls before they reach the lowest point. This build-up then results in the trapping of air, figure 82a, forming a second material interface and additional refraction of the beam. Secondly, and most limiting, the modelling of the optical system revealed that the divergence of the beam would cause it to hit the walls of the well, creating reflection and possible waveguide effects. In an attempt to solve these problems the glass collar was further recessed, figure 81b and 82b. This arrangement allows for the expansion of the beam but in practice it was found that the jetting of polymer into the lower cavity of the well was inhibited even after one droplet deposition, again caused by the droplet size being of the order well entrance, because even if one droplet is not jetted all the way to the bottom of the well and wets to the side walls the subsequent droplets cannot make it past producing an air pocket.

There is no optical nor mechanical reason why the wider well cannot be extended to the fibre position. Hence the micro machining in the latest configuration, figure 81c, extends the well down to the position of the fibre. Indicated by the dashed white line, figure 82b. This allows for the successful deposition of polymer and divergence of the light, figures 83 and 84. Further trials may reveal this design allows for the fibre to be adjusted so that the beam can be made even bigger, potentially allowing for the required lens power to be reduced.

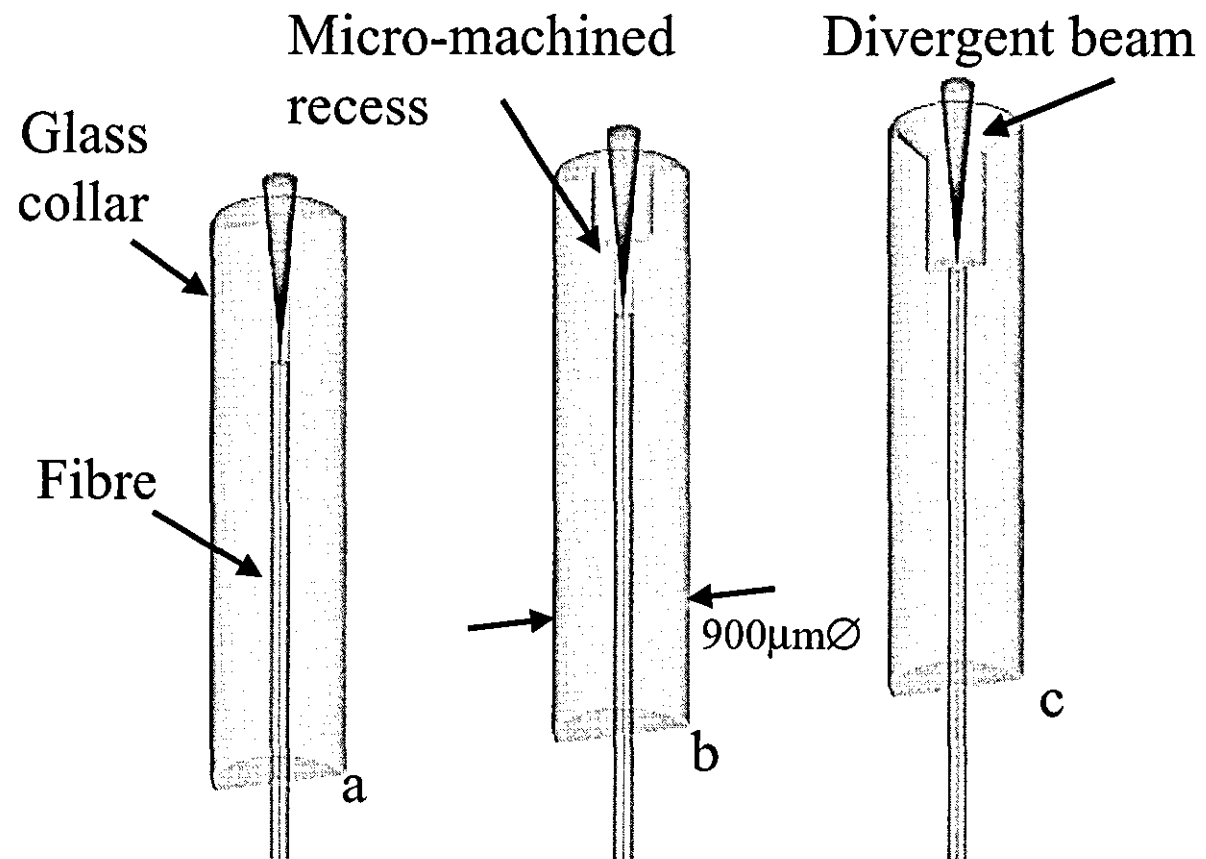


Figure 81 - Design iterations of glass collar. Red cone indicating the expansion of the beam from the fibre

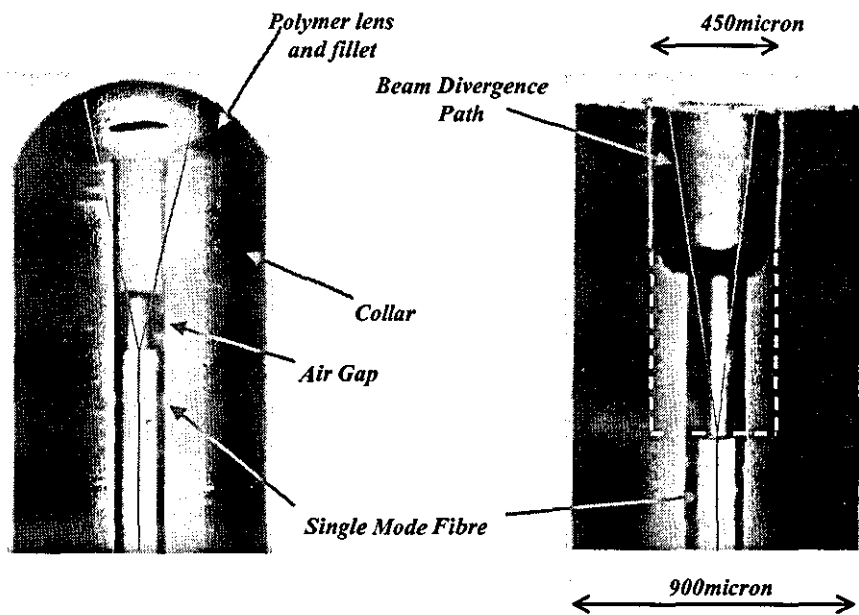


Figure 82 - a) Initial trials using a collar on the fibre led to air being trapped between the fibre and the polymer. b) A recessed collar (unfilled) to allow for divergence of the beam.

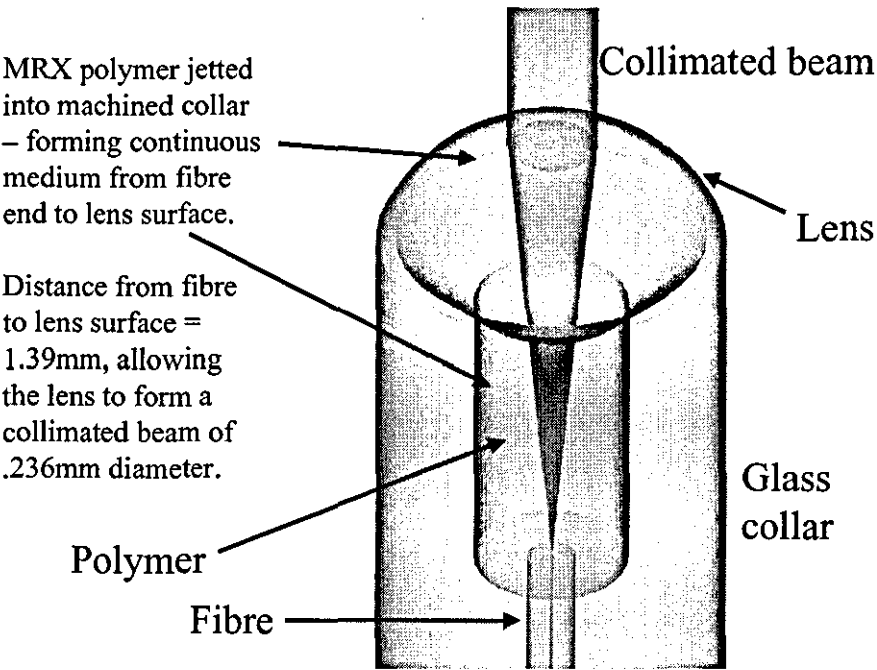


Figure 83 - Optimum design of glass collar, for ease of machining, beam divergence and droplet deposition

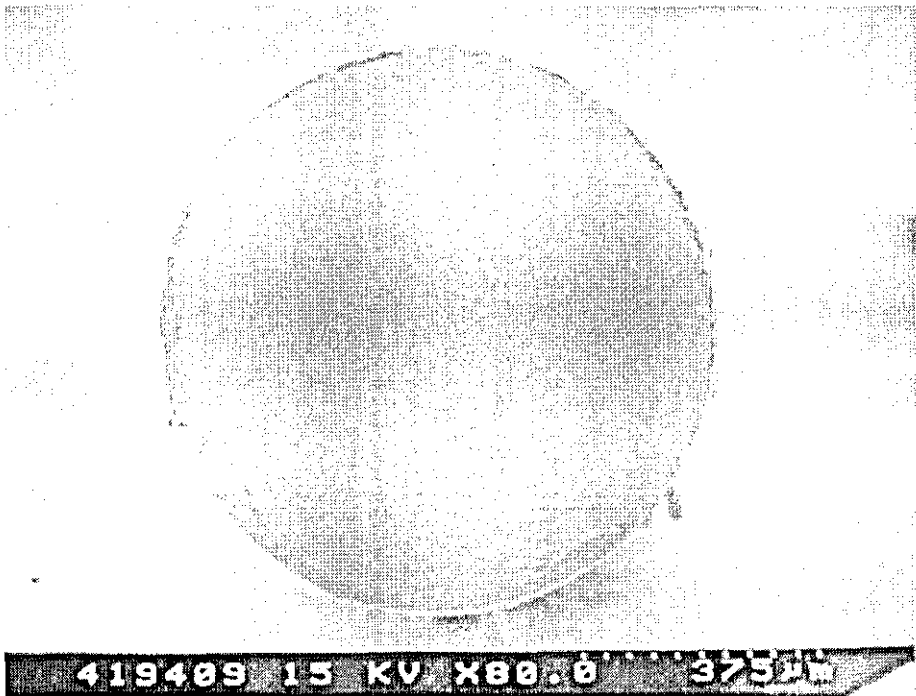
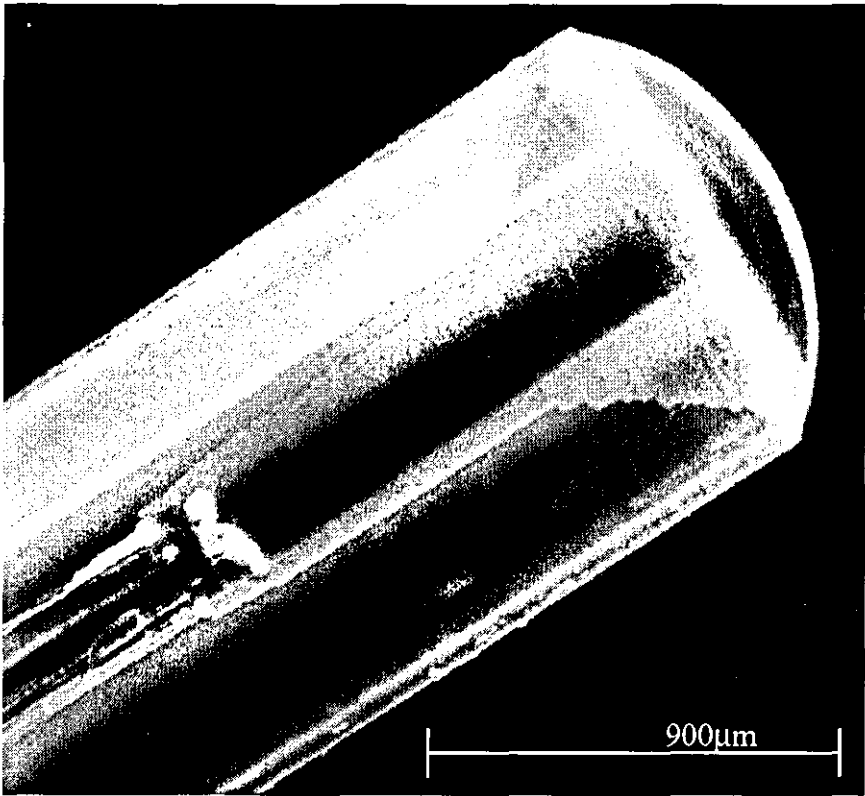


Figure 84 - 1:3 aspect ratio lens, MRX110 polymer deposited on glass collar

5.4.5 Lens on glass slide

In line with current development of optical routing devices based on Micro Electro Mechanical Systems (MEMS), figure 85, a 1D array of micro-lenses was printed on a 2mm thick borosilicate optical flat from UQG Optics, Cambridge, figure 86. The array is designed to accept, and collimate, the beam from 8 input fibres. The dimensions of the proposed switch will demand a beam width of approximately 400µm in order for the necessary processing to be performed without losing the required energy density of the beam before it is inserted into the exit channels. Currently expensive GRIN lenses are used in the proposed assembly, mounted individually, requiring difficult alignment. Using jetting it is possible to first butt the fibres to the glass slide with a centre-centre spacing of 800µm and, then, target the lenses at the fibre centres.

If a glass slide, of 2mm thickness, is used to house the lenses, the required aspect ratio (height/diameter) is again modelled with ZEMAX and is calculated to be 1:8.2 for a lens diameter of 700µm. Micro-lenses with this diameter and aspect ratio had not previously been reported so several new process parameters had to be considered. This application calls for the use of a polymer formulation to encourage the reduced wetting necessary to produce lenses with smaller f -numbers. Using a wetting agent on the glass, to control of the spread of the polymer as it impacts, governs the aspect ratio of the lens. A series of pre-deposition baking steps were used to degrade the low-wet coating of each slide. The back focal lengths of the lens were measured at 100x adjusting the baking steps accordingly, from slide to slide, to get them within 50µm of the backsides of the slides.

This film is not monomolecular and is attached to the glass by absorption forces. Because the mass of the drop is much more than the thin wetting layer it is thought that a small fraction may partition into the interface, since it is reactive with the printed polymer, although the process is not completely understood. This non-ionic layer should not cause a reliability issue over say, 20 years, should the normal protection for telecom equipment from the environment be employed.

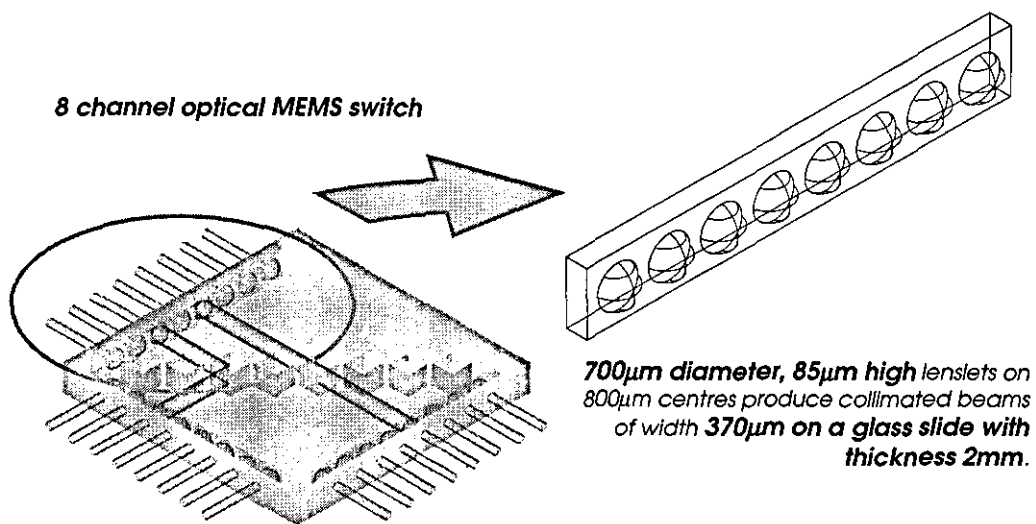


Figure 85 - Schematic of 8 channel MEMS switch currently in development

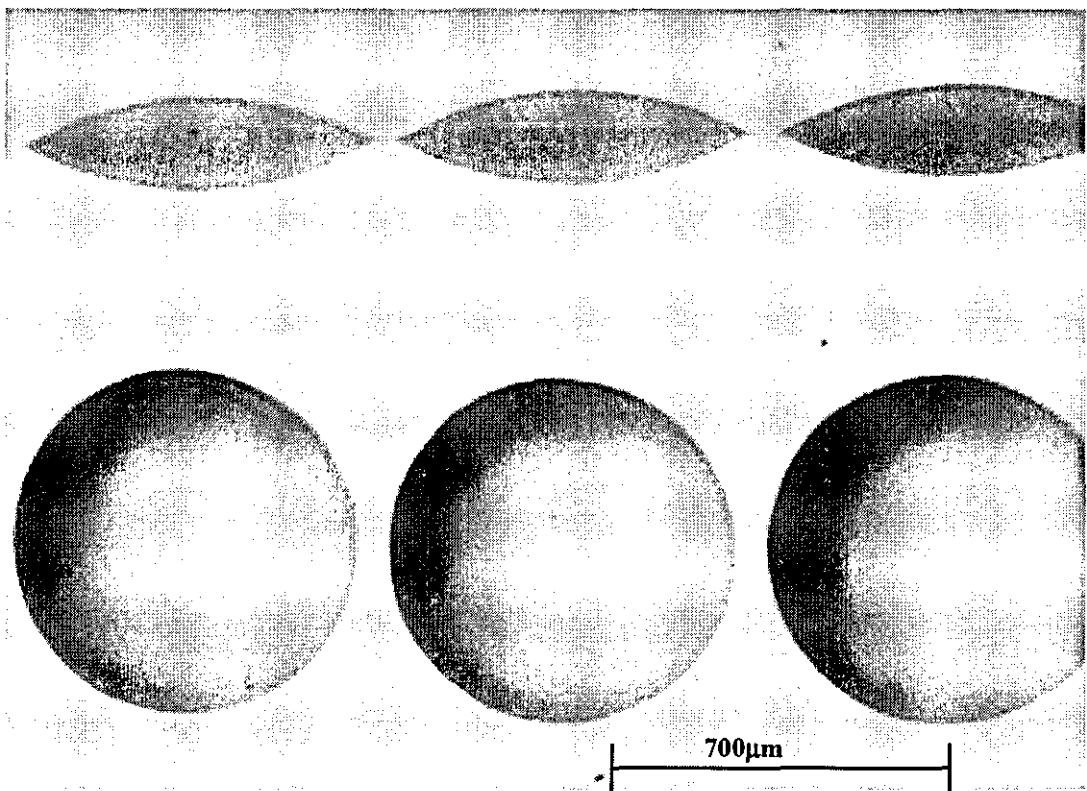


Figure 86 - 3 (of 8) 1:8 aspect ratio lens printed on boron silicate optical flat

Coatings applied to glass or silica (or silicon) surfaces are in the nature of a conversion coating rather than a true (thick film) coating. There are three types, which are used in these applications:

- 1) *A thin film coating that is a low-solids lacquer is fixed in place by solvent evaporation. The solids are usually acrylic polymers or copolymers. For low surface energy of the final coating, which will be much less than a micron, the acrylic polymer is usually fluorinated.*
- 2) **Organosilane coatings.** *This is the largest class of glass surface modifiers. Several dozen of these compounds are in regular commercial production, and there are literally hundreds of them available. Monomolecular layers can be made with proper treatment. The compounds basically have two natures, the inorganic part attaches to the glass and the organic part forms the surface to the external environment. Depending on the nature of the organic part, a variety of surfaces can be made available for micro-lens depositions with varying surface energies.*
- 3) **Self-assembled layers.** *This usually starts out with an organosilane being attached to a glass or silica surface as a monolayer. The organo portion of the compound is going to react with a functional group on the next compound to be applied so that an ordered set of layers is created. The external surface will have the desired surface energy properties. #3 is more complicated than #2, and Microfab are just starting to examine its utility.*

During these trials several variations of the organosilane coatings were tried. These gave a large variation in results where the aspect ratio could be 'tuned' from 1:5 to 1:14. This is promising as the required aspect ratio, 1:8.2, sits in the middle of these limits. More work needs to be carried out to optimise the process to make it repeatable.

During these trials several issues were highlighted

- 1) **Jet inconsistency.** *The first droplet of each batch is prone to variation, this is not a problem for lenses with high n , but for small arrays the first deposited lens can be offset slightly*
- 2) **Wettability** *becomes an issue as the droplet n increases - surface tension effects are over taken by impurities on the surface of the glass*
- 3) **Condensation and/or out gassing?** *During several deposition runs a fogging of the glass is observed, this is accompanied by increased difficulty in creating uniform lenses. Initially this was thought to be condensation caused by the proximity of the heated jetting device. Considering the dew point of the surroundings it is also thought that the polymer surrounding the orifice could be out-gassing, evaporating onto the substrate.*

Again, the key to successful deposition is care. The process is very capable of depositing lenses with the correct dimensions but particular attention must be paid to the deposition atmosphere, head out-gassing effects and slide contamination. Several 8x1 lens arrays have successfully been deposited by this method showing physical values close to those modelled.

5.4.6 Lens array characterisation

Lens diameter, roundness and centre-to-centre spacing are found using an optical system with automated edge detection. In this method, deviation from perfect lenslet circularity contributes significantly to the location of its centre, and hence the centre-to-centre distance. Taking the results from one example slide (N5) it shows the obtained geometries were approaching those targeted by the modelling, table 4. These results, as a first attempt, show how promising the technique is and its potential to yield lenses with dimensions close to the modelled values with further development time. The measurements for all the size lens arrays are given in Appendix 5.

	Mean	Std. Dev.	Std. Error	Minimum	Maximum	Range
Distance	0.7994	0.0193	0.0073	0.7730	0.8279	0.549
Diameter	0.7134	0.0071	0.0025	0.6991	0.7215	0.0224
Roundness	0.0024	0.0007	0.0003	0.0017	0.0040	0.0023

Table 4 - Measurement of centre-centre distance, diameter and roundness of lenses printed on glass slide

5.4.7 Microscope measurements of focal length

The centre for Basic, Thermal and Length Metrology at the National Physical Laboratory (UK) has established measurement facilities dedicated to micro-optical components [NPL]. A selection of the printed lenses were characterised using their specialist equipment.

A test chart was used as an object and placed 80mm from the lens array with the convex lens surfaces facing the object. Images were formed close to the rear surface of the substrate and viewed with a microscope. The microscope was equipped with a split field focusing attachment that enabled the test surface / focal point to be precisely located. By focusing on the substrate and measuring the displacement, necessary to focus on the image of the test chart, the position of each image with respect to the substrate was deduced, table 5.

Sample N5 lens number	Distance (in air above surface) μm
1	109
2	105
3	108
4	89
5	82
6	64
7	62
8	32

Table 5 - Focal length error, in microns above rear surface of optical flat, for 8x1 lens array

The lenses are referred to as 1 to 8, where no. 8 was the first lens to have been printed. As can be seen from the above table, the error in focal length increases with each subsequent deposition. The error in focal length is defined as the difference between the target focal length (nominally the depth of the glass slide) for each lens and the interferometrically measured focal length. This could be due to the substrate being heated up and / or contaminated with the out gassing effects from the print head.

Note: White light illumination was used and because of the physical limitations of the apparatus the object was not truly at infinity. A very small correction should be applied. The focal length may well be different when using wavelengths (λ) in the infrared region of 980, 1300 and 1550 nm of the spectrum that is of most interest for optical communications.

5.4.8 Interferometry measurements of curvature

If the lens surfaces are close to spherical the measurement of radius of curvature can be carried out on a Zygo interferometer of the Fizeau type. A reference wave-front is created from a 1mm sapphire sphere, figure 87.

An image of the graticule can be seen when focussed on the lens surface and when positioned at the centre of curvature of the surface, that is, at the confocal position. Measuring the radius of curvature by this method is similar for that of the measurement of the focal length except that, rather than move the lens back so that the focussed spot coincides with the focal point, it is moved forwards until it coincides with the centre of curvature. Under this condition all light is normal to the surface and is retro reflected into the interferometer to give a fringe field. The difference in the number of fringes through the lens compared with the reference wave gives the value of the radius of curvature, table 6. The convergence of the lines in the interference pattern show a difference in the radius of curvature in the x and y direction. Any imperfections in the smoothness of the lens surface are highlighted as inconsistencies across the fringe pattern. The interferometric images for sample N5 are shown in Appendix 6.

Sample N5 lens number	Radius of Curvature (µm)
1	475
2	475
3	478
4	463
5	462
6	457
7	453
8	439

Table 6 - Radius of curvature measurements for each lens in array

5.5 Further Drop on Demand Work

The performance of lead-free solder and adhesives deposition illustrate the potential for drop on demand printing to be included in the production environment in the near future. It has also been demonstrated that the technique will be incorporated into optoelectronic production. Further testing of the real applications and problems in manufacturing will allow for specific devices and solutions to be provided. It is also desirable to follow up the x-ray curing materials, which may enable this disruptive technology solution to pre-determine the materials used instead of providing a solution to an old problem.

The initial trials and deposition of micro-lens arrays and collimating lens for single-mode fibres, shows promise for incorporation into the production environment. This work demonstrates a major step forward in the control of fibre lens geometries. The experimental results have, so far, yielded values for lens curvature and focal length, which are very close to those highlighted by the modelling. A Mach-Zender interferometer was used to examine the wave fronts transmitted by the lenses. The test lens was mounted with the unexpanded beam from a helium-neon laser ($\lambda=632.8\text{nm}$) incident on the convex lens surface forming a focused spot near to the rear surface of the slide. The beam was then re-collimated by a high quality microscope objective.

An image of the transmitted wave front from a source placed at the backside of the slide was taken at several distances moving away from lens surface, figure 88.

Transmission of light through the lens gave rise to multimode patterns using the white light source. It was found that the transmitted wave front was only collimated over a small aperture of the light due to the aberration from the lens being too severe. Since the application of these lenses would require only the central part of the lens to be used further study needs to be made with a reduced aperture and light of the required wavelength.

Further work will investigate the etching of the slide, before deposition, to inhibit the flow of the polymer over the surface, fixing the diameter of the lens. This method, which has analogies with the collar deposition, would improve the lens radius of curvature variation in the x and y direction. Work is currently underway to optimise the coatings and process conditions to produce lenses with the required performance. A second attempt at micro-lens printing will incorporate recent improvements, such as software that utilizes XY-stage linearity and temperature corrections for improved placement accuracy. The mechanical stability of the material over extended times at high power densities and their optical performance at wavelengths of 1300nm, 1550nm and 980nm need evaluation.

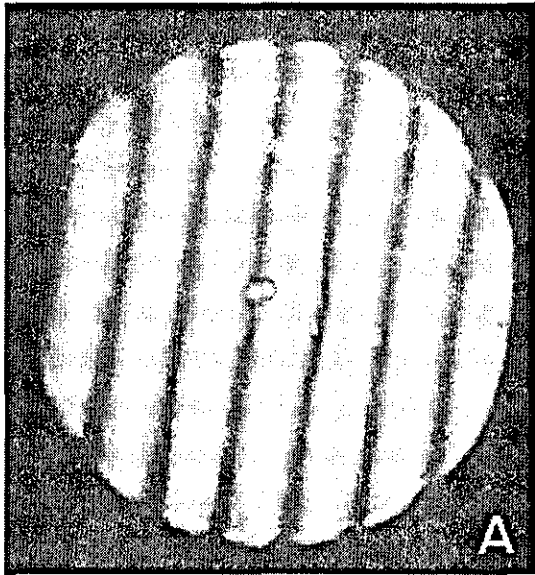


Figure 87 - Sapphire sphere reference wave

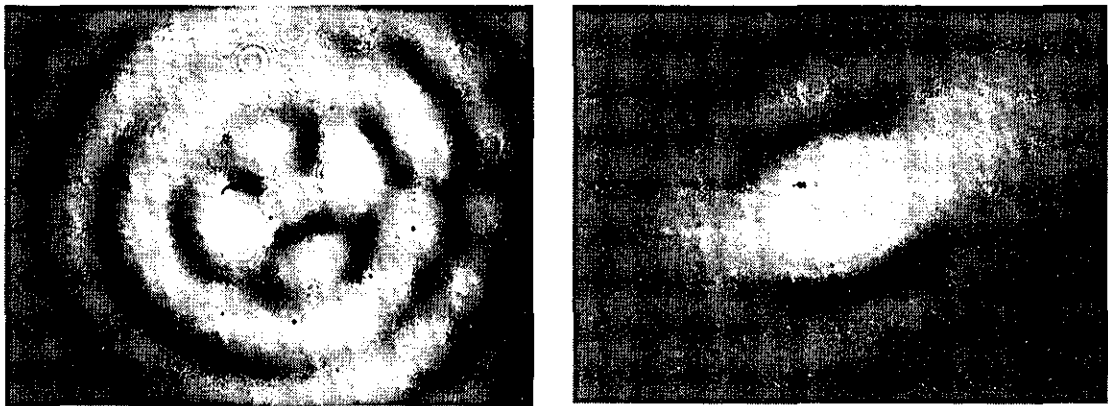


Figure 88 - Transmitted wave fronts using white light illumination across entire aperture of the lens

6 Discussion and Specifications

Materials Jetting is still very much a maturing technology and, as such, several issues must be addressed before it is widely accepted in the industry.

The MIT system does highlight the current issues that surround the acceptance of materials jetting in commercial production. The issue with most concern is the orifice and stream instability. Experiments at Nortel Networks have highlighted and tried to improve upon the cemented orifice gem volatility and although two promising techniques have been identified a more involved study and development program needs to be conducted.

The system used at the University of California does show impressive control of solders with individual spheres being deposited at precise locations at high speed. However, since all continuous mode systems create a lot of waste material a satisfactory method of recycling either in-line or separate must be devised before it can be considered economically sound for manufacture.

The limits of the current piezoelectric materials used in the drop on demand system to create the mechanical vibrations inhibit certain desirable materials such as low softening point glasses to be deposited. Although continuous mode goes some way in solving the problem by distancing the piezo-electric material from the highest temperature in the systems, it is limited by the in-consistencies in the stream control after production and the inability to control dielectric materials. Therefore the most commercially acceptable technology is drop on demand, due to its wider ranging material possibilities and it looks as if the temperature barrier will be broken before the recycling and consistency issues of continuous mode.

Aside from the limitations of the separate technologies, materials jetting shows promise as a new technology that may be able to address the desires of optoelectronic production such as the precise and controllable deposition of discrete volumes of material down to a volume of a few picolitres. It has been shown that the technique is

capable of depositing adhesives in a very controllable fashion that is essential for fixing components that lie in the optical path. This is a problem that was not an issue in electronics manufacture and is one that device reliability depends upon. Since most of the products used in long haul communications have to have a lifetime of up to 25 years any quasi-static creep in the post cure regime of the adhesives is almost unacceptable. However it is impossible to completely eliminate this settling so making sure that exactly the right amount of material is placed down in the initial construction of the device.

Both variations on the technology have the capability to produce discrete volumes of lead free solder. It is noted that the drop on demand technique has produced a world first in the deposition of tin/copper solder into an optoelectronic package. This is a small but important step in the process of eliminating lead from electronic and optoelectronic devices by 2004, which will be necessary by legislation. It not only shows compatibility with legislation but the deposition of solders directly into the package from the bulk material removes the need for pre-form production, a costly step in the manufacturing process.

Due to the currently unprecedented rise in demand for optical communications equipment, the capacity of manufacturing sites cannot cope with demand. One solution to this would be the automation of the device manufacture, but this, as outlined previously, is limited by the need for sub micron precision in the alignment of the optical components in single mode long haul devices and the handling of the 'fibre-tail' (the short length of optical fibre that is used to incorporate the device into a system). It is thought that the demonstrators outlined in this report show promise for adding low cost to device manufacture. Presently the polymeric lens examples produced are not refined enough to be considered for single mode components but may provide a route to be implemented primarily in the lower power multimode devices. Since polymers are not considered a suitable material for single mode high-added-value optical components, it may be that as the technology matures, along with the development of low softening point glasses, an avenue may open up where materials jetting can compliment the current technologies, reducing processing steps and cost.

The costs for purchase of the hardware for the differing technologies differs by a factor of 3 in favour of the continuous mode system (based on a license from MIT) but again it is essential to consider the maturity of the techniques and therefore it is not possible to perform a direct cost comparison. The drop on demand mode system comes all but complete for \$200k and will allow for development of applications against the development of the continuous mode technique.

It is believed that the technique of materials jetting is potentially a cost effective stepping stone in the development of automated manufacture of optoelectronic devices, albeit with several questions to be resolved before it can be considered for a specific application.

7 Acknowledgements

Jim Watts with whom I carried out the project for his patience and experimental dexterity!

Chris Tanner, Ken Snowdon and Ian Abraham of Nortel Networks for application knowledge and technical assistance.

Paul Conway and David Whalley of Loughborough University for project and technical support.

Paul Watson and Ken Bishop of CEMCO, Waterloo for invaluable assistance in solder handling techniques and the XY motion control table.

Royall Cox, Mike Grove and Rick Hoenigman for their assistance and input into the development of micro-lens printing.

Thanks to Dr Richard Stevens, NPL, for his assistance, and speed, in testing the lens arrays.

8 References

- [1] D.B.Wallace, "A Method of Characteristics Model of a Drop-On-Demand Ink-Jet Device Using an Integral Method Drop Formation Model," *American Society for Mechanical Engineers (ASME) publication 89-WA/FE-4*, December 1989.
- [2] J.S.Aden, J.H.Bohorquez, D.M.Collins, M.D.Crook, A.Garcia, and U.E.Hess, "The Third Generation HP Thermal InkJet Printhead," *Hewlett-Packard Journal*, 45(1), Feb 1994.
- [3] D.J.Hayes, D.B.Wallace, M.T.Boldman, and R.E.Marusak, "Picoliter Solder Droplet Dispensing", *Int. J. Microcircuits and Electronics Packaging*, 16(3), pp 173-180, 1993.
- [4] J.Priest, E.Jacobs, B.Holt, and B.Hammerschlag, "Liquid Metal-Jetting Technology: Application Issues for Hybrid Technology", *Int. J. Microcircuits and Electronics Packaging*, 17(3), pages 219-227, 1994.
- [5] Essien, M. et al., "Computational Modeling of On-Demand Solder Delivery for Fluxless Multi Chip Module Packaging Applications", *International Society for Hybrid Microcircuits (ISHM) '96 Proceedings*, pp 414-419, 1996.
- [6] Waldvogel, J. M., Poulikakos, D., "Solidification phenomena in picoliter size solder droplet deposition on a composite substrate", *Int. J. Heat Mass Transfer*, 40(2), pp 295-309, 1997.
- [7] M.Orme, C.Huang, J.Courter, "Deposition Strategies for Control of Microstructure, Microporosity and Surface Roughness in Droplet-Based Solid Free Fabrication of Structural Materials", *Proceeding of The Minerals, Metals and Materials Society*, 1996.
- [8] J. W. Strutt (Lord Rayleigh), "On the Instability of Jets", *Proc. London Math Soc.*, 10(4), 1878.
- [9] J.-H. Chun et al, "Production of charged uniformly sized metal droplets", *US Patent 5,266,098*.
- [10] Hoang Hoang and R. Godin, "Developments of Chip Scale Packaging (CSP) Solder Ball Attach Utilizing Metal Jet Technology", *CSP Related*

- Technologies Conference, Semiconductor Equipment and Materials International (SEMI) 1997.*
- [11] Alvarez, J. C. R., **"Control of the Uniform Droplet Spray Process for the Production of Solder Balls for Ball Grid Array Electronics Packaging"**, *MSc Thesis (unpublished)*, Massachusetts Institute of Technology, 1997.
 - [12] MPM Corporation , **"Materials Jetting Technology leaflet"**, MPM World Headquarters, Franklin, MA, 02038-3137, USA, printed 1996.
 - [13] D.J.Hayes and D.B.Wallace, **"Solder Jet printing for low cost wafer bumping"**, *Proceedings 1996 International Symposium on Microelectronics (International Society for Optical Engineering (SPIE) Vol. 2920)*, pp. 296-301.
 - [14] R. Godin, **"Application of Eutectic Solder Using Solder Jetting Technology"**, *Proceedings of Surface Mount International*, 2, pp. 739-744, 1996.
 - [15] D. Schwarzbach, A. Baggerman, N. van Veen., **"A solderjetting process for maskless waferbumping"**, *12th European Microelectronics & Packaging Conference*, pp. 291-297, 1999.
 - [16] Passow, C. H., **"A Study of Spray Forming Using Uniform Droplet Sprays"**, *MSc Thesis (unpublished)*, Massachusetts Institute of Technology, 1992.
 - [17] Cox, W. R. et al., **"Fabrication of micro-optics by microjet printing"**, *International Society for Optical Engineering (SPIE)*, 2383, pp. 110-115.
 - [18] Cox, W. R. et al., **"Microjet printing of anamorphic microlens arrays"**, *International Society for Optical Engineering (SPIE)*, 2687, pp. 89-98, 1996.
 - [19] F. Savart, **"Memoire sur la Constitution des Veines Liquides Lancées par des Orifices Circulaires en Mince Paroi"**, *Annales de Chimie et de Physique*, 53, pp. 337-386, 1833.
 - [20] Wallace, D. B., **"Capillary Instability of a Jet of Liquid Metal"**, *J. Fluids Eng.*, 115, pp. 529-532, 1993.
 - [21] M. Essien, D. R. Frear, D. T. Schmale, **"Direct Molten Solder Delivery for Ball Grid Array Applications: Comparison of Computational and Experimental Results"**, *Int. J. Microcircuits and Electronic Packaging*, 20(2), pp. 155-161, 1997.

- [22] J. M. Schneider, C. D. Hendricks, **"Source of Uniform-Sized Liquid Droplets"**, *Review of Sci. Inst.*, **35**(10), pp. 1349, 1964.
- [23] E. A. Avallone, T. Baumeister, eds, **"Marks Standard Handbook for Mechanical Engineers"**, McGraw-Hill Book Company, New York, 1987.
- [24] Metals Handbook, 9th Edition, American Society for Metals, 1979.
- [25] G. K. Abel, **"Characterisation of Droplet Flight Path and Mass Flux in Droplet-Based Manufacturing"**, *MSc thesis* (unpublished), Massachusetts Institute of Technology, 1993.
- [26] Microfab Technologies, **"Seminar on Ink-Jet Technology"**, Unpublished, 1999.
- [27] Smith, T. M., **"Electrodynamic Pump for Dispensing Molten Solder"**, U.S. Patent 5,377,961, January 3, 1995.
- [28] D. B. Wallace, D. J. Hayes, **"Solder Jet Technology Update"**, *Proceedings International Society for Hybrid Microelectronics (ISHM) '97*, Oct 1997.
- [29] D.B. Bogy and F.E. Talke, **"Experimental and Theoretical Study of Wave Propagation Phenomena in Drop-On-Demand Ink Jet Devices,"** *IBM Journ. Res. Develop.*, Vol. 29, pp. 314-321, 1984.
- [30] H-Y. Kim, **"Spreading Behaviour of Molten Metal Microdroplets"**, *PhD Thesis*, Massachusetts Institute of Technology, unpublished, 1999.
- [31] B. Xiong et al., **"An Investigation of Key Factors Affecting Solder Microdroplet Deposition"**, *J. Heat Transfer*, **120**, pp 259-270, 1998.
- [32] W. H. Press et al., **"Numerical Recipes in C - The Art of Scientific Computing (2nd Edition)"**, Cambridge University Press, pp 504-510, 1992.
- [33] Jennifer Shin, **"Feasibility study of rapid prototyping using the uniform droplet spray process"** *BSc thesis* (unpublished), Massachusetts Institute of Technology, 1998.
- [34] **"Handbook of Chemistry and Physics"**, *CRC Press*, 60th Edition, 1979.
- [35] G. Baker, AEA Technology, **"Laser Micro-hole Drilling"**, *Pulsed Laser Micro-machining Workshop*, SPIE **2639**, 1998.
- [36] J Lister, Exitech, **"Nozzle Drilling Techniques"**, *Pulsed Laser Micro-machining Workshop*, SPIE **2639**, 1998.

- [37] J. D. Watts, **"The production of lead-free solder spheres for the electronics industry using materials jetting"**, *MPhil Thesis, University of Loughborough, Unpublished*, 2001.
- [38] A. Langmaid, **"The Right Place at the Right Time"**, Northern Lights, Nortel Networks Internal Publication, Sept 1999.
- [39] D.J. Hayes, D.B. Wallace and W.R. Cox, **"MicroJet Printing of Solder and Polymers for Multi-Chip Modules (MCM) and Chip-Scale Packages"**, *Proceedings, International Microelectronics and Packaging Society (IMAPS) - International Conference on High Density Packaging and MCMs*, Denver, April 1999.
- [40] W.R. Cox, D.J. Hayes, T. Chen, H-J. Trost, M.E. Grove, R.F. Hoenigman and D.L. MacFarlane, **"Low Cost Optical Interconnects by Micro-jet Printing"**, *ISHM 29th International Symposium on Microelectronics*, Minneapolis, MN, Oct., 1996; also *International Microelectronics and Packaging Society (IMAPS) - International Journal of Microcircuits & Electronic Packaging*, Vol. 20, No. 2, pp.89-95, 1997.
- [41] P. E. Dyer, **"Laser Properties and Beam Characteristics"**, Book Chapter – *Laser Applications in Physical Chemistry*, D. K. Evans Ed., Marcel Dekker, 1989.
- [42] M. P. Buchin, **"Method for attaching a gradient index lens to an optical fibre in the course of making an optical instrument"**, US Patent 5299272.
- [43] C. A. Frelief, **"Fiber optical laser collimating device"**, US Patent 5937123.
- [44] J. J. Pan et al., **"Micro lens formation at optical fiber ends"**, US Patent 4118270.
- [45] T. Chen, **"Design Guide-line of Printed Hemi-Spherical Microlenses"**, unpublished, Microfab, 1996.
- [46] C. W. Hansell, **"Jet Sprayer Actuated by Supersonic Waves"**, US Patent 2512743, 1950.

9 Appendix 1 - Listing A

Video and Image Metrics Display Thread

Visual C++ Listing – Part of the Display Video Class, which is used to display and analyse the image of the droplet stream.

```

int CDisplayVideo::Run()
{
    ASSERT(m_pOwner != NULL);    //if thread does not return a valid owner exit
10    if (m_pOwner == NULL)
        return -1;

    //Metrics Value
    int arraycount;
    DWORD timestart=NULL, timeend=NULL, cyclestart=NULL, cycleend=NULL;
    double m_CurrentBSRatio, elapsedtime=NULL;
    double m_AverageBSRatio[AVERAGING_MAX], rationew[AVERAGING_MAX], ratiototal;
    double terma, termb, currentsize, ChangeFactor, ChangeVoltage;
    char* charbuf;
20    CString infostr = "";

    //Open Data File and Write Headings
    CStdioFile datafile;
    if( !datafile.Open( m_pOwner->m_LogFileName, CFile::modeCreate
        | CFile::modeWrite | CFile::typeText ) )
    {
        #ifdef _DEBUG
        AfxMessageBox("Cannot Create "+ m_pOwner->m_LogFileName);
        #endif
30        exit( 1 );
    }

    if (m_pOwner->m_bSaveLogFile)
    {
        SYSTEMTIME ctime;
        GetLocalTime(&ctime);
        char* datestr = new char [20];
        char* timestr = new char [20];
        sprintf(datestr, "%02d/%02d/%02d", (int)ctime.wDay, (int)ctime.wMonth,
40        (int)ctime.wYear);
        sprintf(timestr, "%02d:%02d", (int)ctime.wHour, (int)ctime.wMinute);
        infostr = "File " + m_pOwner->m_LogFileName + "\nCreated on " + datestr
        + " at " + timestr + "\n";
        delete [] timestr;
        delete [] datestr;
        datafile.WriteString( infostr );
        infostr = "Target Ratio : ";
        charbuf = new char[10];
        sprintf(charbuf, "%.2lf", (float)m_pOwner->m_TargetBSRatio);
50        infostr += charbuf;
        infostr += "\n";
        infostr += "Material : ";
        infostr += "\n";
        infostr += "Initial Pressure :";
        infostr += "\n";
        infostr += "Initial Frequency :";
        infostr += "\n";
    }
}

```

```

        infostr += "Voltage Set Point : ";
        m_pOwner->GetDlgItemText(IDC_FLOWVOLTAGE, charbuf, 10 );
        infostr += charbuf;
60      infostr += "\n";
        datafile.WriteString( infostr );
        infostr = "BS\\tR\\tCF\\tAV\\tET\\tCT\\tVO\\n";
        datafile.WriteString( infostr );
    }

    for (arraycount=0;arraycount<AVERAGING_MAX;arraycount++)
    {
        rationew[arraycount] = m_AverageBSRatio[arraycount] = 0.0;
    }
70

CSingleLock sLock(&(m_pOwner->m_mutex));    //syncornise the thread with the owner
cyclestart = GetTickCount();

//Do the camera stuff

    CPen aPen;
    aPen.CreatePen(PS_DOT, 2, RGB(0, 0, 0));
    CCamera* m_pCamera = &m_pOwner->m_Camera;
80    m_pCamera->ifexist = 0; //Need to do soft reset frame and grab window
    Mv1GrabWindow GrabAreaCtl;
    CBitmap* pNewBitmap = new CBitmap;
    CClientDC* pDC = (CClientDC*)m_pOwner->m_CameraView.GetDC();
    CDC* pMemDC = new CDC;
    pMemDC->CreateCompatibleDC(pDC);
    pNewBitmap->CreateBitmap(m_pCamera->dx, m_pCamera->dy, 1, 8, NULL);
    pMemDC->SelectObject(pNewBitmap);
    if (m_pCamera->ifexist == 0)

90    // Set grabbing window
    Mv1SetGrabWindow(0L, 0, 0, m_pCamera->dx, m_pCamera->dy, &GrabAreaCtl);
    // Create frame structure using the same size of the grab window
    Mv1CreateFrame(&(m_pCamera->frame), 0, 0, (long)m_pCamera->dx, (long)m_pCamera-
>dy, &GrabAreaCtl);
    m_pCamera->ifexist = 1;
}

// Start grabbing live video

100    if (Mv1StartGrab(Mv1_Cont_Grab, Mv1_Grab_Even) != Mv1_OK)
        AfxMessageBox("Having trouble starting the grabbing!");
    Mv1WaitFrameEnd();
    //Array of bits for the 8bit image
    byte* buffer = new byte[(long)m_pCamera->dx * (long)m_pCamera->dy];

    while (!m_bDone)
    {
        //Get cycle start time in milliseconds
        timestart = GetTickCount();
        infostr = "";
110        // read a frame to the buffer
        Mv1FrameRead(&(m_pCamera->frame), 0, 0, (long)m_pCamera->dx, (long)m_pCamera-
>dy, buffer);

        //Ball Space Ratio Routine
        //Average over the last AVERAGING_MAX entries
        //pop the last value from the array (must be a better way to do this)
        for (arraycount=0;arraycount<AVERAGING_MAX-1;arraycount++)
            rationew[arraycount+1] = m_AverageBSRatio[arraycount];
120        //get current ratio and push it onto the array
        rationew[0] = ::GetBallSpaceRatio(buffer, m_pOwner-
>m_CameraView.m_FeedbackRect, m_pOwner->m_ThresholdLevel * 2, m_pCamera->dx);
        ratiototal = 0.0;
        for (arraycount=0;arraycount<AVERAGING_MAX;arraycount++)
        {
            m_AverageBSRatio[arraycount] = rationew[arraycount];
            ratiototal += m_AverageBSRatio[arraycount];
        }
        m_CurrentBSRatio = ratiototal / AVERAGING_MAX;
130        //Workout current size from m_CurrentBSRatio
        terma = (3.0/2.0) * (float)pow(m_pOwner->m_OrificeSize,2);

```

```

        termb = (1.0 / m_CurrentBSRatio) + 1;
        currentsize = (float)sqrt( terma * termb );

        // Control the Output to the Variable Valve
        if ( (m_CurrentBSRatio > m_pOwner->m_TargetBSRatio * 1.02)
            || (m_CurrentBSRatio < m_pOwner->m_TargetBSRatio * 0.98) )
        {
            ChangeFactor = (m_CurrentBSRatio - m_pOwner->m_TargetBSRatio ) /
140    m_pOwner->m_TargetBSRatio;
        }
        else
        {
            ChangeFactor = 0.0;
        }

        /* Affect Valve if Feedback if selected */
        cycleend = GetTickCount();
        if ( m_bFeedback
            && (cycleend > (cyclestart + m_pOwner-
150    >GetDlgItemInt(IDC_VALVETIMEDELAY, NULL, FALSE)))
        {
            ChangeVoltage = m_pOwner-
            >GetDlgItemInt(IDC_FLOWVOLTAGECHNG, NULL, FALSE);
            ChangeVoltage = (ChangeVoltage / 1000) * ChangeFactor;
            m_pOwner->m_FlowVoltage += ChangeVoltage;
            if (m_pOwner->m_FlowVoltage > 9.500) m_pOwner-
            >m_FlowVoltage = 9.500;
            if (m_pOwner->m_FlowVoltage < 8.500) m_pOwner-
            >m_FlowVoltage = 8.500;
160    m_pOwner->m_DIO.PutAnalogValue(0, 1.0, m_pOwner-
            >m_FlowVoltage);

            cyclestart = GetTickCount();
        }
        /* Display Values in Metrics Window */
        if (m_pOwner != NULL)
        {
            charbuf = new char[10];
            sprintf(charbuf, "%.2lf", (float)m_AverageBSRatio[0]);
170    m_pOwner->m_ImageMetrics.SetDlgItemText(IDC_LASTVALUE, charbuf);
            sprintf(charbuf, "%.2lf", (float)currentsize);
            m_pOwner->m_ImageMetrics.SetDlgItemText(IDC_DIAMETER, charbuf);
            infostr+=charbuf;
            infostr+="\t";
            sprintf(charbuf, "%.2lf", (float)(m_CurrentBSRatio));
            m_pOwner->m_ImageMetrics.SetDlgItemText(IDC_BSRATIO, charbuf);
            infostr+=charbuf;
            infostr+="\t";
            sprintf(charbuf, "%.2lf", (float)(ChangeFactor));
180    m_pOwner->m_ImageMetrics.SetDlgItemText(IDC_CHANGEFACTOR, charbuf);
            infostr+=charbuf;
            infostr+="\t";
            m_pOwner->GetDlgItemText(IDC_FLOWVOLTAGEACT, charbuf, 10);
            infostr+=charbuf;
            infostr+="\t";
            sprintf(charbuf, "%.2lf", (float)m_pOwner->m_TargetBSRatio);
            m_pOwner->m_ImageMetrics.SetDlgItemText(IDC_TARGETRATIO, charbuf);
            delete [] charbuf;
190    }

        // transfer data from buffer to bitmap and display
        pNewBitmap->SetBitmapBits((long)m_pCamera->dx * (long)m_pCamera->dy, (LPSTR)
buffer);
        // display grab rectangle
        pMemDC->SelectObject(&aPen);
        pMemDC->SetROP2(R2_NOTXORPEN);
        pMemDC->SelectStockObject(NULL_BRUSH);
        pMemDC->Rectangle(    m_pOwner->m_CameraView.m_FirstPoint.x,
            m_pOwner->m_CameraView.m_FirstPoint.y,
200    m_pOwner->m_CameraView.m_SecondPoint.x,
            m_pOwner->m_CameraView.m_SecondPoint.y);
        pDC=(CClientDC*)m_pOwner->m_CameraView.GetDC();
        pDC->BitBlt( 0, 0, (WORD)m_pCamera->dx, (WORD)m_pCamera->dy, pMemDC, 0, 0,
SRCCOPY);
        //Display Time Taken to Analyse and Display Image
        timeend = GetTickCount();

```

```

elapsedtime += ((float)timeend-(float)timestart)/(float)1000.0;
charbuf = new char[10];
sprintf(charbuf, "%.2lf", (float)elapsedtime);
210   infostr+=charbuf;
      if (m_pOwner != NULL)
          m_pOwner->m_ImageMetrics.SetDlgItemText(IDC_CYCLETIME, charbuf);
      infostr+="\t";
      sprintf(charbuf, "%d", (int)(timeend - timestart));
      infostr+=charbuf;
      delete [] charbuf;
      infostr+="\n";
//Output Data to File
      //May need to be entered into an array if disk access isn't fast enough
220   if (m_pOwner->m_bSaveLogFile)
          datafile.WriteString( infostr );
      //Pick up any waiting messages
          Sleep(1);
  }
  // Clean Up
      datafile.Close();

      charbuf = NULL;
      Mv1StopGrab();
230   delete [] buffer;
      delete pNewBitmap;
      delete pMemDC;

      return 0;
}

```

10 Appendix 2 - Listing B

Image Processing Algorithms

```

float WINAPI GetBallSpaceRatio(      byte data [ ], CRect grabrect, int mag, int
camwidth)
{
    int BallTotal = 0;
    int xpos, ypos, MagthisPos;
10    BOOL *p_bTemp = NULL;
    BOOL LeadingEdgeFound, TrailingEdgeFound = FALSE;
    BOOL *p_bRowHasBall = new BOOL[grabrect.Height()];
    p_bTemp = p_bRowHasBall;
    // Deflate roiRect As we are passing 3*3 Matrix over the area
    // therefore starting one pixel up and one pixel back
    grabrect.DeflateRect(1,1);
    // Move the data pointer to the beginning of the roi
    data += grabrect.TopLeft().y * camwidth;
    data += grabrect.TopLeft().x;
20    ypos = 1;
    //Iterator over the roi looking for maximum and minimum edges in the same row
    while (ypos < grabrect.Height())
    {
        xpos = 1;
        LeadingEdgeFound = TrailingEdgeFound = FALSE;
        while (xpos < grabrect.Width())
        {
30            MagthisPos = Sobel(data, S_VERTICAL, camwidth);
            if ( abs ( MagthisPos ) > mag)
            {
                if (MagthisPos < 0)
                {
                    LeadingEdgeFound = TRUE;
                    *(data - (2*camwidth)) = 250;
                }
                else
                {
40                    TrailingEdgeFound = TRUE;
                    *(data - (2*camwidth)) = 252;
                }
            }
            data++;
            xpos++;
        }
        ypos++;

        if (LeadingEdgeFound && TrailingEdgeFound)
        {
50            *p_bRowHasBall++ = TRUE;
            BallTotal++;
        }
        else
        {
            *p_bRowHasBall++ = FALSE;
        }
        data ++;
        data += (camwidth - grabrect.Width());
60    }

    p_bRowHasBall = p_bTemp;
    delete [] p_bRowHasBall;
    return ( (float)BallTotal / (float)(grabrect.Height() - BallTotal) );
}

```

```

}

void WINAPI fourl(float data [ ], unsigned long nn, int isign)
//From "Numerical Recipes in C Second Edition
//Replaces data [1..2*nn] by its discrete Fourier transform, if isign is input as 1; or
70 //replaces data [1..2*nn] by nn times its inverse discrete Fourier transform, if isign
//is input as -1. data is a complex array of length nn or, equivalently, a real array
//of length 2*nn. nn MUST be an integer power of 2 (this is not checked for!). Set up
//for arrays with zeroth order value at 1 need "data-1" for use with arrays in C
{
    unsigned long n, mmax,m,j,istep,i;
    double wtemp, wr, wpr, wi, wpi, theta;          //Double precision for
    trigonometric recurrences.
    float tempr, tempi;
    n=(nn<<1);
80
    j=1;

    for (i=1;i<n;i+=2) {
        if (j>i) {
            //This is the bit reversal section of the routine
            SWAP (data[j],data[i]);
            SWAP (data[j+1],data[i+1]);
            //Exchange the two complex numbers
90 m=(n>>1);
            while (m>=2 && j>m) {
                j -= m;
                (m >= 1);
            }
            j += m;
        }
        //Here begins the Danielson-Lanczos section of the routine
        mmax=2;
        while (n>mmax){
100 //Outer loop executed log2nn times
            istep=(mmax<<1);
            theta=isign*(6.28318530717959/mmax);
            //Initialise the
            trigonometric recurrence
            wtemp=sin(0.5*theta);
            wpr = -2.0*wtemp*wtemp;
            wpi=sin(theta);
            wr=1.0;
            wi=0.0;
            for (m=1;m<mmax;m+=2) {
110 //The two nested inner loops
                for (i=m;i<=n;i+=istep) {
                    j=i+mmax;
                    //This is the Danielson-Lanczos formula;
                    tempr=(float)wr*data[j]-(float)wi*data[j+1];
                    tempi=(float)wr*data[j+1]+(float)wi*data[j];
                    data[j]=data[i]-tempr;
                    data[j+1]=data[i+1]-tempi;
                    data[i]+=tempr;
                    data[i+1]+=tempi;
120
                }
                wr=(wtemp=wr)*wpr-wi*wpi+wr;
                //Trigonometric recurrence
                wi=wi*wpr+wtemp*wpi+wi;
            }
            mmax=istep;
        }
    }

int WINAPI FindNOP(float data [ ], unsigned long nn, int isign)
130 {
    unsigned int count = 0, maxpos = 0;
    float maxvalue = 0;
    fourl(data-1, nn, isign);
    float* pdata = &data[2];
    count = 2;
    while (count<(nn/4))
    {
        if (fabs(*pdata)>maxvalue)

```

```

140         {
            maxpos = count;
            maxvalue = *pdata;
        }
        pdata+=2;
        count+=2;
    }
    return (maxpos);
}

int Sobel(byte* pData, int direction, const int& CamWidth)
150 {
    int p[9];
    int hmag, vmag = 0;
    switch (direction)
    {
        case S_HORIZONTAL:
            {
                p[0] = *(pData - (CamWidth + 1));
                p[1] = *(pData - CamWidth);
                p[1] *= 2;
                p[2] = *(pData - (CamWidth - 1));
                p[6] = *(pData + (CamWidth - 1));
                p[7] = *(pData + CamWidth);
                p[7] *= 2;
                p[8] = *(pData + (CamWidth + 1));
                hmag = (p[0]+p[1]+p[2])-(p[6]+p[7]+p[8]);
                vmag = 0;
                break;
            }
        case S_VERTICAL:
170         {
            p[0] = *(pData - (CamWidth + 1));
            p[2] = *(pData - (CamWidth - 1));
            p[3] = *(pData - 1);
            p[3] *= 2;
            p[5] = *(pData + 1);
            p[5] *= 2;
            p[6] = *(pData + (CamWidth - 1));
            p[8] = *(pData + (CamWidth + 1));
            hmag = 0;
            vmag = (p[2]+p[5]+p[8])-(p[0]+p[3]+p[6]);
            break;
        }
        case S_BOTH:
        default:
190         {
            p[0] = *(pData - (CamWidth + 1));
            p[1] = *(pData - CamWidth);
            p[1] *= 2;
            p[2] = *(pData - (CamWidth - 1));
            p[3] = *(pData - 1);
            p[3] *= 2;
            p[5] = *(pData + 1);
            p[5] *= 2;
            p[6] = *(pData + (CamWidth - 1));
            p[7] = *(pData + CamWidth);
            p[7] *= 2;
            p[8] = *(pData + (CamWidth + 1));
            hmag = abs( (p[0]+p[1]+p[2])-(p[6]+p[7]+p[8]) );
            vmag = abs( (p[2]+p[5]+p[8])-(p[0]+p[3]+p[6]) );
200         break;
        }
    }
    return (hmag+vmag);
}

```

11 Appendix 3 – Lenslet arrays data

Data for 6 each Slides with 8 each lenslets per slide shipped to Nortel (Units – mm)

Part: N5,N6,N7,N8,N9 and N12

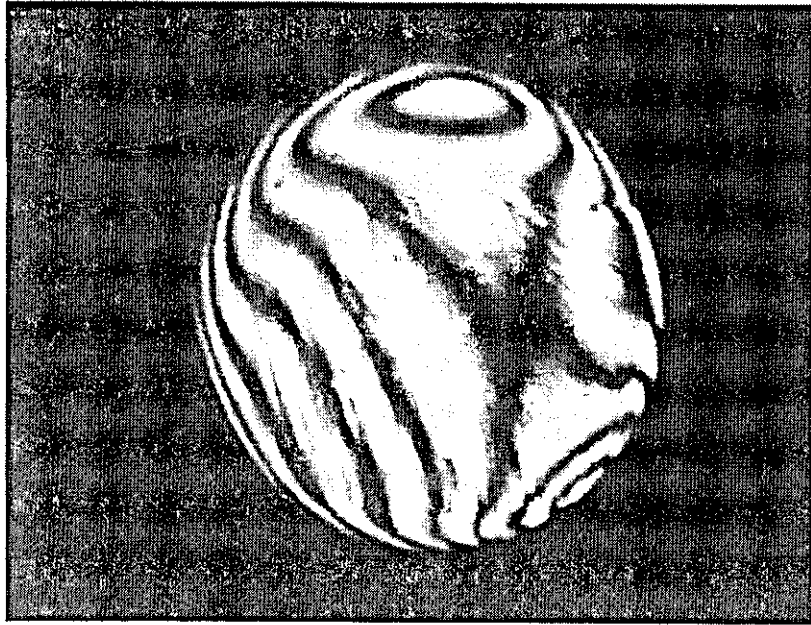
Descriptive Statistics

	Mean	Std. Dev.	Std. Error	Minimum	Maximum	Range
N5 Dist.	.7994	.0193	.0073	.7730	.8279	.0549
N5 Dia.	.7134	.0071	.0025	.6991	.7215	.0224
N5 Roundness	.0024	.0007	.0003	.0017	.0040	.0023
N6 Dist.	.7989	.0086	.0033	.7885	.8098	.0213
N6 Dia.	.7165	.0161	.0057	.6985	.7509	.0524
N6 Roundness	.0037	.0012	.0004	.0020	.0058	.0038
N7 Dist.	.7991	.0079	.0030	.7865	.8079	.0215
N7 Dia.	.7002	.0044	.0016	.6948	.7065	.0117
N7 Roundness	.0030	.0020	.0007	.0010	.0071	.0061
N8 Dist.	.8014	.0073	.0028	.7902	.8113	.0211
N8 Dia.	.6845	.0042	.0015	.6782	.6925	.0143
N8 Roundness	.0034	.0021	.0007	.0014	.0079	.0065
N9 Dist.	.8007	.0090	.0034	.7928	.8169	.0241
N9 Dia.	.7252	.0040	.0014	.7171	.7291	.0120
N9 Roundness	.0041	.0017	.0006	.0019	.0066	.0047
N12 Dist.	.7987	.0217	.0082	.7755	.8322	.0567
N12 Dia.	.7060	.0092	.0033	.6952	.7221	.0269
N12 Roundness	.0044	.0014	.0005	.0022	.0064	.0042

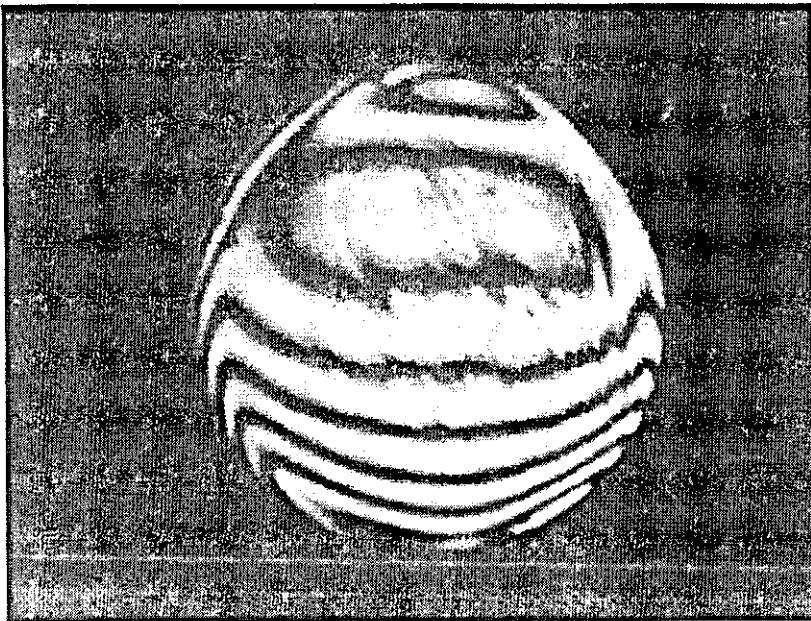
"Dist." = center-to-center distance between lenslets
"Dia." = diameter of a lenslet
"Roundness" = degree of out-of-roundness = (max diameter) - (min diameter) of a lenslet

12Appendix 4 – Interferometer Images

Lens Array N5 – Interferometer Measurements



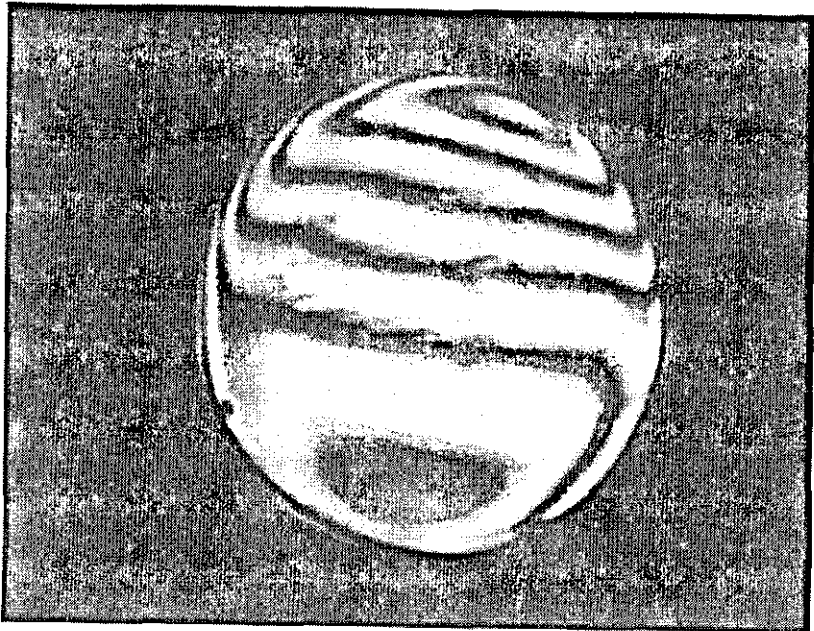
1 – Radius of Curvature (ROC) = 0.475



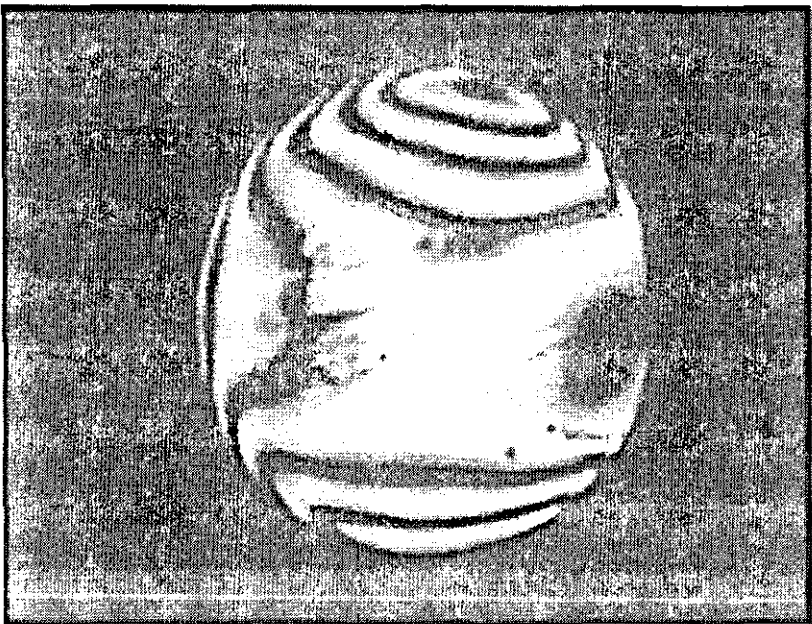
2 – ROC = 0.475

Appendix 4 – Interferometer Images

Lens Array N5 – Interferometer Measurements



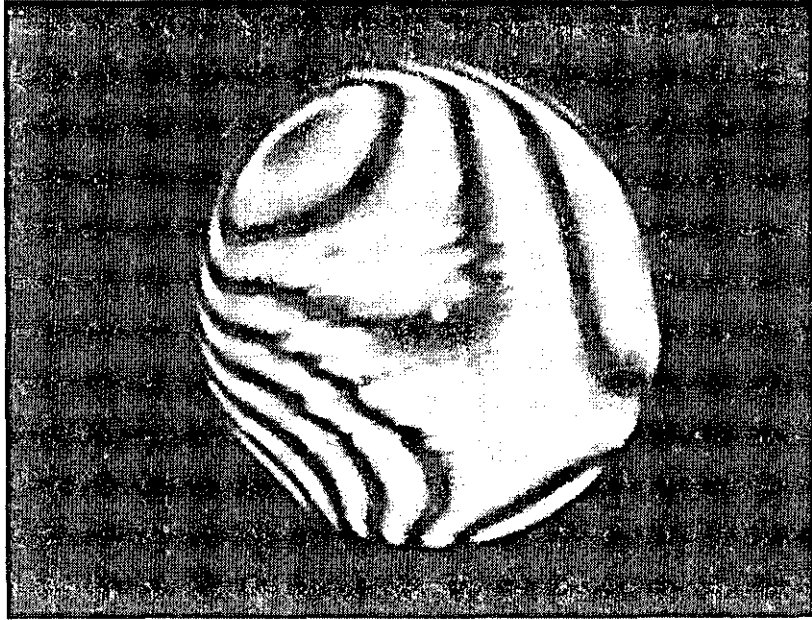
3 – ROC = 0.478



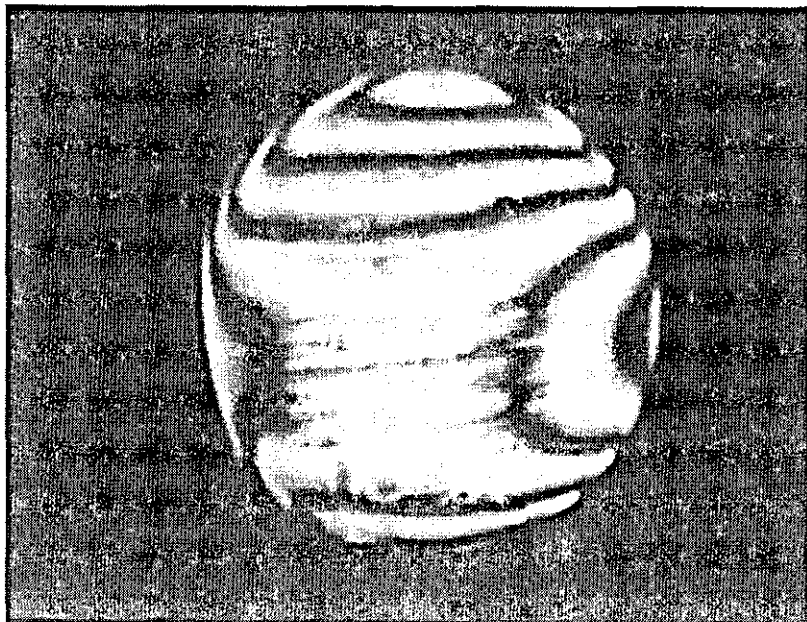
4 – ROC = 0.463

Appendix 4 – Interferometer Images

Lens Array N5 – Interferometer Measurements



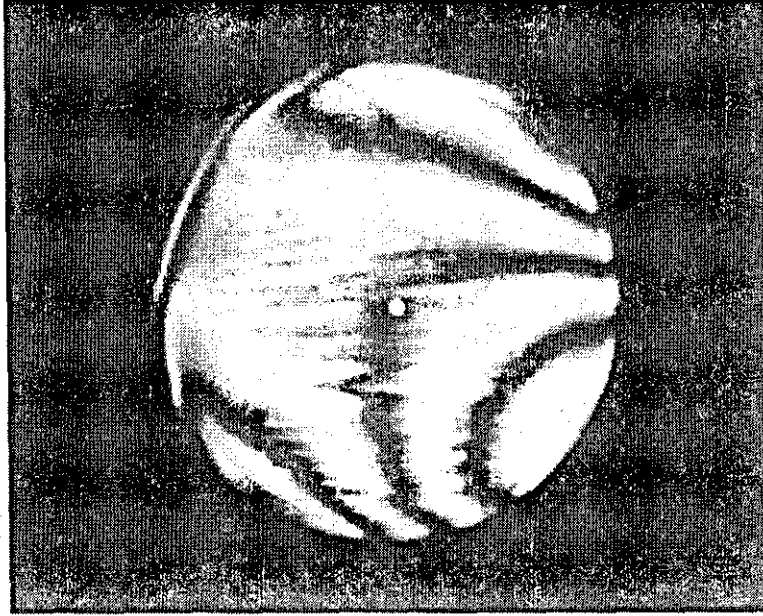
5 – ROC = 0.462



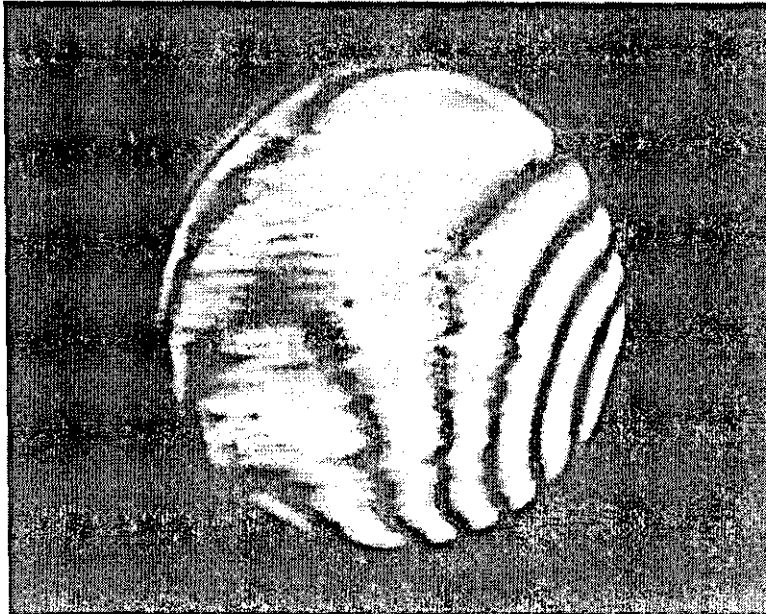
6 – ROC = 0.457

Appendix 4 – Interferometer Images

Lens Array N5 – Interferometer Measurements



7 – ROC = 0.453



8 – ROC = 0.439

